CHEMICAL AND ISOTOPIC (LI, H, O, C) COMPOSITION OF SURFACE WATERS AND SEDIMENTS – IMPLICATIONS ON WEATHERING, EROSION, AND PALEOENVIRONMENTAL RECONSTRUCTIONS ON THE TIBETAN PLATEAU

Dissertation submitted in partial fulfilment of the requirements for the academic degree

DOKTOR DER NATURWISSENSCHAFTEN (DR. RER. NAT.)

FACHBEREICH GEOWISSENSCHAFTEN
FREIE UNIVERSITÄT BERLIN

vorgelegt von
MARC WEYNELL

Freie Universität Berlin

May, 2018 – Berlin, Germany

Date of disputation: July 19th, 2018

Supervisor:

Dr. Uwe Wiechert

Institut für Geologische Wissenschaften
Freie Universität Berlin
Malteser Straße 74-100
12249 Berlin
Germany

Referees:

1. *Prof. Dr. Harry Becker*

Institut für Geologische Wissenschaften
Freie Universität Berlin
Malteser Straße 74-100
12249 Berlin
Germany

2. *Prof. Dr. Bernhard Diekmann*

Alfred Wegener Institut – Helmholtz Zentrum für Polar- und Meeresforschung
Telgrafenberg A43
14473 Potsdam
Germany

Institut für Erd- und Umweltwissenschaften
Universität Potsdam
Karl Liebeknecht Straße 24/25
14476 Potsdam-Golm
Germany

Selbständigkeitserklärung

Hiermit versichere ich, die vorliegende Dissertation eigenständig und ausschließlich unter Verwendung der angegebenen Hilfsmittel, angefertigt zu haben. Alle Aussagen innerhalb der vorliegenden Arbeit, welche dem Wortlaut oder dem Sinne nach aus anderen Quellen entnommen wurden, einschließlich solcher aus elektronischer Medien, sind im Text kenntlich gemacht und befinden sich in einem vollständigen Verzeichnis.

Die vorliegende Arbeit ist in dieser oder anderer Form zuvor nicht als Prüfungsarbeit zur Begutachtung vorgelegt worden.

Unterschrift   Berlin, May 11, 2018

SUMMARY

Understanding the natural controls on atmospheric carbon dioxide concentrations (pCO_2) is a major goal of climate research, as anthropogenic carbon dioxide (CO_2) emissions continue to rise pCO_2. Those controls can be partially revealed by investigating the reason for a substantial pCO_2 decline throughout the Cenozoic (from 65.5 Ma on), which resulted in a massive climate change. Atmospheric CO_2 is mainly balanced by degassing from Earth's interior and removal during weathering of silicate rocks. Increased silicate weathering rates, mainly triggered by Himalayan and Tibetan Plateau formation, are proposed as reason for the Cenozoic pCO_2 decline. This assumption is in opposition to stable CO_2 degassing during this era as imbalances result in complete removal of atmospheric CO_2.

Lithium (Li) is an element, which is almost exclusively hosted in silicate minerals and its two isotopes ($^7Li/^6Li$) fractionate during silicate weathering reactions. Thus, studying Li isotope variations are ideal to investigate silicate weathering processes. Coeval to the Cenozoic pCO_2 decline, oceanic Li isotope ratios (δ^7Li) rose. Identifying a potential connection between both events possibly clarifies some controls behind the Cenozoic climate change. Several studies attributed an uplift-driven increase of the global riverine δ^7Li value as causal for the rise of seawater δ^7Li.

The objective of this thesis is to understand the controls on Li isotope fractionation during weathering on the Tibetan Plateau and to use Li isotope variations in rivers and sediments as a silicate weathering tracer across the plateau. Further, the impact of Tibetan Plateau formation on the average global riverine Li isotope composition is considered. For this reason, field work was performed in the catchment of Lake Donggi Cona, located on the semi-humid northeastern Tibetan Plateau and Lake Bangong, located on the hyper-arid western plateau. Bedrock, different types of sediments (loess, fluvial, limnic), and surface waters (lake, stream, spring, and thermal waters) were analyzed. Additionally, the upper Huang He (Yellow River), Yarlung Tsangpo (upper Brahmaputra), and the upper Indus were investigated as these rivers drain large areas with different climate and geomorphic conditions on the eastern, southern, and western plateau. The limited anthropogenic activity on the plateau is ideal to study nearly undisturbed climate and weathering patterns. In contrast, the widespread occurrence of hydrothermal activity has to be considered as this may disturb weathering or climate induced geochemical variations.

Average δ^7Li values for the bedrock, soil solutions, and secondary weathering products in the catchment of Lake Donggi Cona were deduced from local loess, streams, and lake sediments

and are around +1.9 ‰, +16.6 ‰, and -0.8 ‰, respectively. The hydrochemistry of the major inflow, small streams, and the lake is determined by weathering of carbonates. In contrast, the hydrochemistry of a small inflow is dominated by hydrothermally supplied Na, Cl, Ca, HCO$_3$. Thermal waters have δ^7Li values around +10.5 ‰ but the small inflow has values around +20.5 ‰, although the major proportion of Li likewise is of hydrothermal origin. A model reproduces Li concentrations and isotope compositions of the small inflow. Li from thermal waters mixes with Li that was solubilized from bedrock minerals within the weathering zone. Subsequent around 70 % of dissolved Li is removed during incorporation into secondary minerals. This resembles removal of around 85 % of Li in parts of the catchment without hydrothermal activity. The fractionation factor used in the model is empirically deduced from hydrothermally undisturbed areas. Hence, hydrothermally provided Li does not overprint weathering induced Li variations. Carbon isotopes in the stream and spring waters identify microbial respiration as dominant source for dissolved inorganic carbon. This highlights substantial organic processes in the weathering zone despite low annual temperatures and discontinuous permafrost conditions. Oxygen and hydrogen isotopes as well as major element compositions highlight that the major inflow (Dongqu River) supplies around 90 % and thermal waters (direct or indirect via the small inflow) around 10 % to the water budget of Lake Donggi Cona. Applying Li concentrations and isotope compositions to this lake water balance reproduces the Li lake composition within 4 %. Thus, Li isotopes are not fractionated within the lake water and integrate the weathering solutions of the catchment. A simple steady-state mass balance model for Li in the weathering zone highlights an at least five times larger export of Li in secondary minerals and rock detritus compared to the export as dissolved Li form the weathering zone. Thus, the relative large difference between δ^7Li in streams and drained bedrock but low offset between bedrock and eroded sediments is the result of an erosion-dominated, kinetically-limited weathering regime.

δ^7Li values of the two major inflows to Lake Bangong are on average low between +6 ‰ and +9 ‰. River sediments of both inflows display δ^7Li values down to -4.3 ‰. Major and trace element compositions in the river sediments follow a mixing trend between shale and igneous rock fragments, which may identifies a source control on the low δ^7Li values. However, Li isotope compositions in the river beds of the two large inflows strongly correlate with chemical weathering intensity proxies (e.g. CIA; Na/Ti). δ^7Li values of river beds decrease and weathering intensity increases downstream in the sub-catchment of the southern major inflow. This identifies multiple processing and intense weathering of sediments in the small floodplains where scarce moisture concentrates. δ^{18}O and δD values identify strong evaporation in the

smallest inflow and the lake basins (69 to 86 % water loss), which results in Li isotope fractionation within the water bodies. However, Li in the two large inflows is unaffected by evaporation. High dissolved Li/Na ratios in both inflows identify an impact of thermal waters but the hydrochemistry of streams in the catchment and nearby geothermal fields differ. This is explained with processing of thermal waters in the weathering zone, similar to processes in the catchment of Lake Donggi Cona. The low riverine δ^7Li values are the result of little net-incorporation (25 % and 40 %) of Li into clays during silicate weathering. The mass balance model highlights roughly balanced export of Li via chemical weathering or physical erosion, characteristic for supply limited weathering. The considerably low erosion rates allow chemical weathering to overcome the limitation by water.

The major rivers across the Tibetan Plateau display low δ^7Li values around +6 ‰ in the upper Indus in the west and +5 ‰ in the Yarlung Tsangpo in the south, but high values around +17 ‰ in the Huang He in the northeast of the plateau. These values resemble those from the two lake catchments and are explained by a change from supply limited weathering on the western and southern plateau to kinetically-limited weathering in the northeast. Silicate weathering rates are low around 1 t/km^2/a across the Tibetan Plateau but riverine δ^7Li vary substantially. Thus, silicate weathering rates have no first order control on riverine Li isotope ratios and Li isotope are controlled by the weathering regime.

Rivers that drain the Tibetan Plateau display no distinct δ^7Li signal and are not causal for the increase of the global riverine δ^7Li value during the Cenozoic. However, this study supports a dominant control of the weathering regime on Li isotopes. Uplift of the plateau resulted in kinetically-limited weathering in the mountain belts that border the plateau and are characterized by high dissolved δ^7Li. Hence, a change of the global topography is able to explain a global riverine and maybe seawater δ^7Li increase throughout the Cenozoic, which does not require a change in silicate weathering rates.

ZUSAMMENFASSUNG

Das Verstehen der natürlichen Prozesse, die die Kohlendioxidkonzentration der Atmosphäre (pCO_2) steuern, ist ein Hauptziel der Klimaforschung, da der durch anthropogene Kohlendioxid (CO_2)-emissionen verursachte pCO_2-Anstieg andauert. Diese Prozesse können durch Erforschung der Ursachen einer erheblichen pCO_2-Abnahme im Känozoikum (seit 65,5 Ma), welche zu einem massiven Klimawandel führte, teilweise aufgedeckt werden. CO_2-Entgasung aus dem Erdinneren sowie Entfernung von CO_2 während der Verwitterung von Silikatgesteinen bestimmen die atmosphärische Kohlendioxidkonzentration. Die Entstehung des Himalayas und des Tibet-Plateaus sollen zum Anstieg von Silikatverwitterungsraten und somit der Abnahme des pCO_2 geführt haben. Dies steht im Widerspruch zu der Annahme konstanter CO_2-Entgasungsraten innerhalb dieser Ära, da ein Ungleichgewicht zum vollständigen Abbau des atmosphärischen CO_2 führen würde.

Lithium (Li) ist ein Element, das fast ausschließlich in Silikaten vorkommt. Seine beiden Isotope ($^7Li/^6Li$) fraktionieren während der Silikatverwitterung. Daher ist das Untersuchen von Li-Isotopenvariationen ideal, um Silikatverwitterungsprozesse zu erforschen. Zeitgleich zum pCO_2-Rückgang im Känozoikum stiegen die Lithiumisotopenverhältnisse (δ^7Li) in den Ozeanen an. Das Aufdecken einer möglichen Verbindung zwischen beiden Ereignissen verdeutlicht möglicherweise einige Steuerungen hinter dem känozoischen Klimawandel. Mehrere Studien nannten einen hebungsgesteuerten Anstieg der globalen δ^7Li-Werte in Flüssen als Hauptgrund für den Anstieg der δ^7Li-Werte in den Ozeanen.

Das Ziel dieser Dissertation ist es, Prozesse, die die Li-Isotopenfraktionierung während Verwitterungsprozessen auf dem Tibet-Plateau steuern, zu verstehen und Li-Isotopenvariationen in Flüssen und Sedimenten als Tracer für die Silikatverwitterung auf dem Plateau zu verwenden. Zusätzlich ermöglicht dies, den Einfluss der Hebung des Tibet-Plateaus auf die durchschnittliche globale Li-Isotopenzusammensetzung der Flüsse zu beleuchten. Aus diesem Grund wurde die Geländearbeit im Einzugsgebiet des Donggi Cona, einem See, der im semi-humiden Nordosten des Plateaus liegt und dem Einzugsgebiets des Bangong Co, einem See, welcher im hyper-ariden Westen des Plateaus liegt, durchgeführt. Gesteine, Löss, fluviale und limnische Sedimente sowie Oberflächenwässer (Seen, Flüsse, Quellwässer, Thermalwässer) wurden analysiert. Zusätzlich wurden der Oberlauf des Huang He (Gelber Fluss), der Yarlung Tsangpo (Oberlauf des Brahmaputra) und der Oberlauf des Indus untersucht, da diese Flüsse große Bereiche mit unterschiedlichem Klima und unterschiedlicher Geomorphologie auf dem östlichen, südlichen und westlichen Plateau entwässern. Die

begrenzte anthropogene Aktivität auf dem Plateau ist ideal, um ursprüngliche Klima- und Verwitterungsmuster zu untersuchen. Im Gegensatz dazu muss das weitverbreitete Auftauchen von hydrothermaler Aktivität berücksichtigt werden, da diese womöglich die von Verwitterungsprozessen oder Klima verursachten geochemischen Schwankungen überdeckt.

Die durchschnittlichen δ^7Li-Werte des Grundgesteins, der Bodenlösungen und der sekundären Verwitterungsprodukte im Einzugsgebiet des Donggi Cona wurden über lokalen Löss, Flüsse und Seesedimente ermittelt und sind +1,9 ‰, +16,6 ‰ und -0,8 ‰. Die Hydrochemie des Hauptzuflusses, der kleinen Bäche und des Sees wird von der Karbonatverwitterung bestimmt. Im Gegensatz dazu wird die Hydrochemie eines kleinen Zuflusses aus dem Norden von hydrothermal zugeführtem Natrium, Chlor, Calcium und Hydrogenkarbonat dominiert. Thermalwässer haben δ^7Li-Werte um +10,5 ‰, der kleine Zufluss dagegen Werte um +20,5 ‰, obwohl der Großteil des Li hydrothermalen Ursprungs ist. Ein Modell reproduziert die Li-Konzentrationen und -Isotopenverhältnisse des kleinen Zuflusses. Von Thermalwässern geliefertes Li mischt sich mit Li, das in der Verwitterungszone gelöst wurde. Nachfolgend werden ungefähr 70 % des gelösten Li in Sekundärminerale eingebaut. Dies ähnelt dem Einbau von 85 % Li in hydrothermal unbeeinflussten Bereichen des Einzugsgebiets. Der im Modell angewandte Fraktionierungsfaktor wurde empirisch in hydrothermal unbeeinträchtigten Bereichen des Einzugsgebiets ermittelt. Somit werden Li-Variationen, die von Verwitterungsreaktionen hervorgerufen wurden nicht von hydrothermalem Li überdeckt. Kohlenstoffisotope in den Flüssen und Quellen identifizieren mikrobielle Atmung als Hauptquelle für den gelösten anorganischen Kohlenstoff. Dies zeigt beträchtliche organische Prozesse in der Verwitterungszone an, die trotz der niedrigen Temperaturen und dem diskontinuierlichen Permafrost auftreten. Sauerstoff- und Wasserstoffisotope, sowie Hauptelemente zeigen, dass der Hauptzufluss (Dongqu Fluss) ungefähr 90 % und Thermalwässer (direkt oder indirekt über den kleinen Zufluss) ungefähr 10 % zum Wasserbudget des Donggi Cona beitragen. Die Li-Konzentration und die Li-Isotopenzusammensetzung des Sees können innerhalb von 4 % reproduziert werden, wenn die Li-Konzentrationen und Li-Isotopenzusammensetzungen der Zuflüsse und Thermalwässer auf die Seewasserbilanz angewendet werden. Somit werden Li-Isotope nicht innerhalb des Sees fraktioniert und integrieren über die Verwitterungslösungen des Einzugsgebietes. Ein einfaches stationäres Massenbilanzmodell zeigt, dass mindestens fünfmal mehr Li in Sekundärmineralen und Gesteinsdetritus als als gelöstes Li aus der Verwitterungszone exportiert wird. Somit ist der relativ große Unterschied zwischen δ^7Li in Flüssen und Grundgestein im Gegensatz zum

kleinen Unterschied zwischen Li im Grundgestein und in erodierten Sedimenten das Resultat eines erosions-dominiertem, kinetisch-limitiertem Verwitterungsregimes.

Die durchschnittlichen δ^7Li-Werte der beiden großen Hauptzuflüsse des Bangong Co betragen +6 ‰ und +9 ‰. Die Flusssedimente der beiden Zuflüsse zeigen niedrige δ^7Li-Werte bis -4.3 ‰. Haupt- und Spurenelementzusammensetzungen in den Flusssedimenten können einerseits durch Mischung von Tonsteinen und magmatischen Gesteinen erklärt werden, was möglicherweise eine Kontrolle der niedrigen δ^7Li-Werte durch die Lithologie anzeigt. Andererseits korrelieren Li-Isotopenzusammensetzungen stark mit Elementverhältnissen, welche die Verwitterungsintensität anzeigen (z.B. CIA, Na/Ti). Im Einzugsgebiet des südlichen Zuflusses nehmen δ^7Li-Werte in den Flussbettsedimenten flussabwärts ab und die Verwitterungsintensität zu. Dies wird mit multiplem Prozessieren und intensivem Verwittern von Sedimenten in den kleinen Flussauen, in denen sich die spärliche Feuchtigkeit konzentriert, erklärt. δ^{18}O- und δD-Werte identifizieren starke Evaporation im kleinsten Zufluss und den Seebecken (Wasserverlust von 69 % bis 86 %), welche zu Li-Isotopenfraktionierung innerhalb der Wasserkörper führt. Lithium in den beiden großen Hauptzuflüssen ist nicht von Evaporation beeinträchtigt. Hohe Li/Na-Verhältnisse in den beiden Zuflüssen zeigen einen hydrothermalen Einfluss an. Allerdings unterscheidet sich die Hydrochemie von den Flüssen im Einzugsgebiet deutlich von nahegelegenen Geothermalfeldern. Ähnlich den Prozessen im Einzugsgebiet des Donggi Cona wird dies ebenfalls mit dem Prozessieren von Thermalwässern in der Verwitterungszone erklärt. Die niedrigen δ^7Li-Werte in beiden Flüssen sind das Resultat eines kleinen Anteils (~25 % und ~40 %) von Li, der während der Silikatverwitterung in Tonminerale eingebaut wird. Das Li-Massenbilanzmodell zeigt annähernd ausgeglichene chemische Verwitterungs- und Erosionsflüsse, charakteristisch für eine Limitation der silikatischen Verwitterung durch mangelnde Zufuhr von frischen Mineralen von der Verwitterungsfront (supply-limited). Die äußerst niedrigen Erosionsraten ermöglichen es der chemischen Verwitterung, die Wasserlimitation zu überwinden.

Die großen Ströme auf dem Tibet-Plateau haben niedrige δ^7Li-Werte um +6 ‰ im oberen Indus im Westen und um +5 ‰ im Yarlung Tsangpo im Süden, aber hohe Werte um +17 ‰ im Gelben Fluss im Nordosten des Plateaus. Diese Werte ähneln denen der Einzugsgebiete der beiden Seen und spiegeln eine Änderung von einem Zufuhr-limitierten Verwitterungsregime im Westen und Süden des Plateaus zu einem kinetisch-limitierten im Nordosten wieder. Silikatverwitterungsraten auf dem Tibet-Plateau sind niedrig (um 1 t/km^2/a), wogegen die δ^7Li-Werte der Flüsse beträchtlich variieren. Somit kontrollieren Silikatverwitterungsraten nicht

direkt die Lithiumisotopenverhältnisse der Flüsse. Diese werden vom vorherrschenden Verwitterungsregime kontrolliert.

Flüsse, die das Tibet-Plateau entwässern, haben keine eindeutige δ^7Li-Signatur und sind nicht der Grund für den globalen δ^7Li-Anstieg in Flüssen während des Känozoikums. Allerdings zeigt diese Studie einen dominierenden Einfluss des Verwitterungsregimes auf Li-Isotope auf. Die Hebung des Tibet-Plateaus erzeugte kinetisch-limitierte Verwitterung in den Gebirgsgürteln, die das Plateau begrenzen und durch hohe δ^7Li-Werte in den Flüssen charakterisiert sind. Daher kann eine Änderung der globalen Topographie durchaus einen Anstieg der globalen δ^7Li-Werte in den Flüssen und vielleicht im Meerwasser erklären, was wiederum keine Änderungen der Silikatverwitterungsraten erfordert.

ACKNOWLEDGEMENTS

difficult times and, especially, gave me so much fun and nice moments. Thank you Alexandra, Rieke, Frank, Linda, Steffen, Marf, Rike, Manu, Simon, Christian, Zaicong, Chunhui, Timo, Yogita, Marie, Uwe, Matthias, Elis, Franzi, Kathrin, Dennis, Philipp, Lena, Frau Feth, Herr Hammerschmidt, Harry, Alexander, Oliver, Linus, Tim, Elfrun, Felix…

Finally, I would like to thank my family for her long lasting support.

Contents

CHAPTER 1

INTRODUCTION

Until the year 2400 humans will emit 5000 gigatons (Gt) of carbon to the atmosphere (Caldeira and Wickett, 2003) substantially raising the partial pressure of atmospheric CO_2 (Zachos et al., 2008). Possible consequences of this sharp rise attract considerable attention. Carbon dioxide is a major greenhouse gas in Earth's atmosphere, thus, strongly influencing global climate and maintaining habitable conditions for life on Earth. A comprehensive understanding of the carbon cycle and its feedback mechanisms are crucial to predict climate responses on anthropogenic CO_2 emissions and related global warming. The current geological era, the Cenozoic, covers the transition from Early Cenozoic hothouse conditions to the Oligocene cooling period, induced by variations in the carbon cycle, which result in a substantial decline of atmospheric carbon dioxide (Beerling and Royer, 2011). Several studies explained the decline with changes in silicate weathering as it represents the major sink for atmospheric carbon dioxide (e.g. Raymo and Ruddiman, 1992; Maher and Chamberlain, 2014; Caves et al., 2016). Lithium isotopes are ideal to track silicate weathering (Huh et al., 2001; Kisakürek et al., 2005; Dellinger et al., 2017). Seawater lithium isotope ratios ($^7Li/^6Li$) rose during the Cenozoic potentially allowing to identify the controls behind those changes of the carbon cycle (Misra and Froelich, 2012). The change of Cenozoic silicate weathering and seawater δ^7Li was attributed to the uplift of the Tibetan Plateau and Himalayas (e.g. Raymo and Ruddiman, 1992; Misra and Froelich, 2012). For this reason, an investigation of Li isotope variations during silicate weathering reactions on the Tibetan Plateau are focus of this thesis.
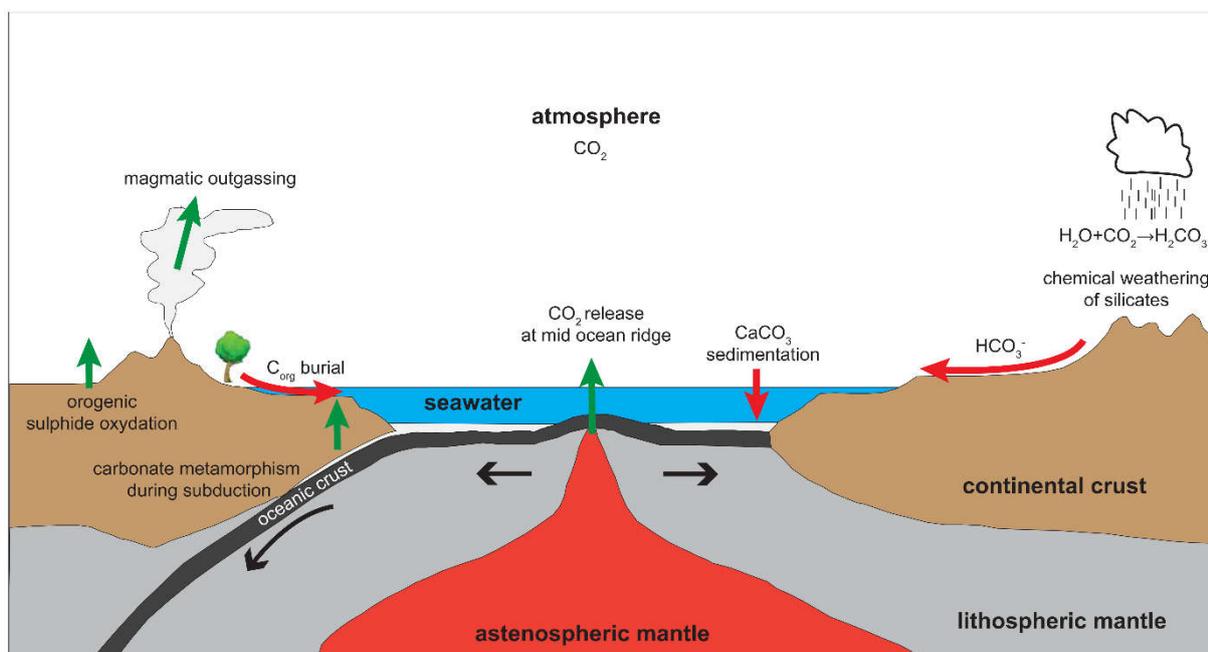
Figure 1-1

Carbon cycle and atmospheric carbon dioxide sources and sinks

1.1 THE CARBON CYCLE AND ATMOSPHERIC CO_2

The earth is the only planet where life is known to exist. Today the average Earth surface temperature is about +15 °C (Kump et al., 2003). Solar radiation, continent distribution, and the atmospheric partial pressure of CO_2 (pCO_2) control Earth's surface temperature (Royer et al., 2004). Earth's atmosphere is build-up of several trace gases that absorb and re-emit much of the infrared radiation emitted from Earth's surface. The resulting greenhouse effect warms the Earth's surface by 33 °C, keeps water liquid, and makes it habitable for life (Kump et al., 2003). Water vapor and carbon dioxide are the two major greenhouse gases. The atmospheric level of carbon dioxide is controlled by the interaction of its sources and sinks over geological timescales (Fig. 1-1). Plate tectonics governs CO_2 sources such as degassing from Earth's interior, carbonate dissolution during subduction, and orogenic sulphide oxidation (Berner et al., 1983; Pearson and Palmer, 2000; Kerrick, 2001; Rowley, 2002; Torres et al., 2014; Van Der Meer et al., 2014). In turn, chemical weathering and physical erosion regulate the major sinks of atmospheric CO_2, precipitation as marine carbonates after conversion to hydrogen-carbonate during silicate weathering (Zeebe, 2012) as well as burial as organic carbon (France-Lanord and Derry, 1997). Proposed pCO_2 between around 200 ppm and a few thousands ppm throughout the Phanerozoic reveal nearly balanced source and sink fluxes over million years (Royer et al., 2004). This prevents the atmosphere from complete depletion in CO_2 or running away in permanent greenhouse conditions, keeping water at Earth's surface liquid, and maintaining habitable conditions for life. This thesis focusses on the silicate weathering sink.

1.2 WEATHERING AND EROSION

Besides plate tectonics, weathering and erosion are the two dominant processes that control Earth's morphology and the chemical composition of the oceanic and upper continental crust, regolith, hydrosphere, and partly bio- and atmosphere. Comminution and chemical alteration of bedrock generates a thin, porous layer at Earth surface, the regolith. It divides into rock fragments (primary minerals), minerals formed by weathering reactions (secondary minerals), and the soil, the portion of the regolith that contains organic material and supports life (Bouchez
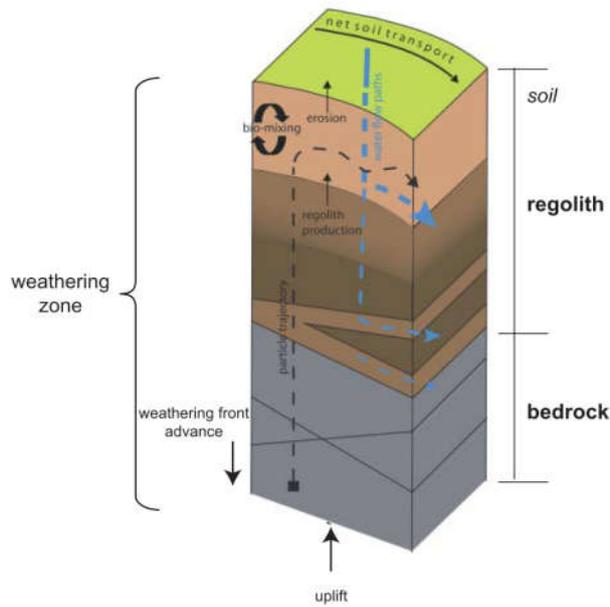
Figure 1-2

Schematic diagram of the weathering zone (also described as weathering reactor). Figure modified from Anderson et al. (2007)

et al., 2013). Rock fragments, soil, water, atmospheric gases, and living organisms interact within the Regolith. For this reason, this zone is defined as weathering reactor (Fig. 1-2; Anderson et al., 2007).

Weathering comprises physical and chemical processes. Both lead to breakdown of bedrock and sediments, which in turn are the result of preceding bedrock comminution. Physical weathering comminutes bedrock by mechanical stress as pressure (e.g. freezing water, root infiltration, etc.) or heat (e.g. solar radiation, day-night-cycles, etc.). Chemical weathering (W) is the (partial) dissolution of thermodynamically unstable minerals and formation of new, at surface conditions stable, minerals (Babechuk et al., 2014). Secondary minerals form. Some elements are retained in the mineral and some are released to the involved solution. Exemplary, the transformation of potassium feldspar to illite (1-I) and kaolinite (1-II) is shown.

$$3\ KAlSi_3O_8 + 2\ CO_2 + 14\ H_2O \rightarrow 2\ K^+ + KAl_3Si_3O_8(OH)_2 + 2\ HCO_3^- + 6\ Si(OH)_{4\ (aq)} \quad (1\text{-}I)$$

$$2\ KAlSi_3O_8 + 2\ CO_2 + 11\ H_2O \rightarrow 2\ K^+ + Al_2Si_2O_5(OH)_4 + 2\ HCO_3^- + 4\ Si(OH)_{4\ (aq)} \quad (1\text{-}II)$$

Ions are solubilized from minerals by hydrolysis, the reaction of slightly acidic solutions with the mineral bondings. Carbonic acid is the dominant involved acid as it forms by the reaction of water (precipitation, groundwater) and atmospheric or soil CO_2. Hence, chemical weathering removes atmospheric CO_2. Weathering of carbonates results in no CO_2 net drawdown (see equation 1-III and 1-IV) but during silicate weathering two moles of CO_2 are removed from the atmosphere but only one mole is released during precipitation as carbonate in the ocean (see equation 1-V and 1-VI).

$$CaCO_3 + \mathbf{1\ CO_2} + H_2O \rightarrow Ca^{2+} + 2\ HCO_3^- \quad\quad\quad (1\text{-}III)$$

$$Ca^{2+} + 2\ HCO_3^- \rightarrow CaCO_3 + H_2O + \mathbf{1\ CO_2} \quad\quad\quad (1\text{-}IV)$$

$$CaSiO_3 + \mathbf{2\ CO_2} + 3\ H_2O \rightarrow Ca^{2+} + 2\ HCO_3^- + Si(OH)_4 \qquad (1\text{-}V)$$

$$Ca^{2+} + 2\ HCO_3^- \rightarrow CaCO_3 + H_2O + \mathbf{1\ CO_2} \qquad (1\text{-}VI)$$
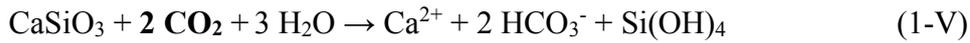
Dissolved (earth)alkali ions and hydrogen carbonate are transported to groundwater, rivers, and the ocean (Babechuk et al., 2014). Transport of dissolved ions to the oceans alters ocean alkalinity, which changes pH and subsequent atmospheric pCO$_2$ on a millennial timescale by ocean-atmosphere gas exchange (e.g. Gislason et al., 2009; Beaulieu et al., 2012). Precipitation of hydrogen carbonate as carbonates in the oceans removes CO_2 from the ocean-atmosphere system on a million-year timescale (e.g. Berner, 1992) until partial re-activation during subduction of oceanic sediments (Fig. 1-1). Thus, chemical weathering has a substantial impact on the overall supply of metals to surface systems, nutrients to ecosystems, and ocean alkalinity, and silicate weathering specifically on atmospheric pCO$_2$.

Continental silicate weathering is largely dependent on physical erosion (Li and Elderfield, 2013). The bottom-up supply of fresh material from the rock-regolith interface or lateral transport to the regolith is balanced by erosion (E) due to removing material at the top (Fig. 1-2). Thus, erosion sustains chemical weathering by continuously refreshing mineral surfaces and impeding thick soils, which cover bedrock from chemical weathering (e.g. Gaillardet et al., 1999b).

The sum of weathering and erosion is defined as denudation (D = W+E). Weathering and erosion are controlled by the availability of weatherable material and involved reaction kinetics (Stallard and Edmond, 1983; West et al., 2005). A limitation of silicate weathering by the supply of fresh minerals from the weathering front defines a supply-limited (also termed transport limited) geomorphic regime (Riebe et al., 2004; West et al., 2005). Minerals are completely weathered and the corresponding weathering intensity is high. Weathering intensity is defined as the loss of mobile elements relative to immobile elements in sediments or in other words, as the fraction of cations transported in dissolved form versus total denudation. The supply-limited regime is characterized by low chemical weathering and erosion rates (hence, low denudation rates) and a linear relationship between weathering and erosion (West et al., 2005). The other geomorphic regime (also termed weathering regime) is characterized by high relative erosion rates compared to chemical weathering rates resulting and a low weathering intensity. There is abundant fresh material but weathering is limited by mineral kinetics, thus, climatic parameters as temperature, runoff, and vegetation (Riebe et al., 2004). This regime is defined as kinetically-limited (formerly defined as weathering limited). Morphology, climate

(defined as temperature and precipitation), and substrate (bedrock composition) determine the dominant limiting parameters on weathering in a distinct area, hence, define the prevalent weathering regime.

1.3 THE CENOZOIC CLIMATE

The Cenozoic spans the time from 65.5 million years (Ma) to the present. The Cenozoic climate includes the transition from hothouse to modern icehouse conditions, controlled by a pCO_2 decline from more than 1000 ppm to ~260 ppm (Fig. 1-3; Pearson and Palmer, 2000; Royer et al., 2004; Beerling and Royer, 2011; Lefebvre et al., 2013; Van Der Meer et al., 2014). It has not yet been finally understood if variations of CO_2 sources or sinks were primarily responsible.

Degassing of CO_2 from Earth's interior deduced from ocean ridge production is assumed to be constant throughout the Cenozoic (Rowley, 2002; Van Der Meer et al., 2014). In contrast, Lefebvre et al. (2013) proposed increased carbonate subduction and related CO_2 degassing as main reason for high pCO_2 in the Early Cenozoic. Destabilization of methane hydrates (Zachos et al., 2008) and/or carbon provided by an impact (Schaller et al., 2016) perhaps resulted in further short-term CO_2 addition to the atmosphere, which lead to CO_2 peaks and hyperthermals in the Paleocene (66 to 56 Ma) and Early Eocene (from 56 Ma on). All these processes are proposed to create high short- and long-term $pCO2$ and accompanied hothouse climate in the Early Cenozoic.

Most investigations focus on the CO_2 sinks to explain varying Cenozoic pCO_2. The marine isotope proxies $^{87/86}Sr$ and $^{187/186}Os$ increased throughout the Cenozoic, which was explained by increasing silicate weathering fluxes due to uplift of the Himalayas and Tibetan Plateau (Raymo and Ruddiman, 1992; Peucker-Ehrenbrink and Ravizza, 2000). The formation of the Himalayas and Tibetan Plateau intensified the Asian monsoon (An et al., 2001), in turn also increasing erosion and silicate weathering (Raymo and Ruddiman, 1992; Garzione, 2008; Lefebvre et al., 2013) and/or organic carbon burial (France-Lanord and Derry, 1997). This possibly increased CO_2 removal and cooling from around 40 million years on (Garzione, 2008). A reversal of the theory that uplift lowered pCO_2 is the "absence of a CO_2 sink hypothesis". Chemical weathering is low in tectonically inactive regions (Edmond et al., 1995; von Blanckenburg et al., 2004) and climate regulation by silicate weathering is lowest when global topography is subdued (Edmond et al., 1995; Maher and Chamberlain, 2014). A low relief topography impedes erosion, resulting in a thick regolith cover. Silicate weathering is inhibited by the supply of fresh, weatherable, minerals to the weathering reactor and shielding of the

bedrock from weathering agents (Edmond et al., 1995). This allows global temperature to vary between distinct levels depending on the global topography and the distribution of mountain belts (Maher and Chamberlain, 2014). In the Early Cenozoic topography levels were assumed to be relatively flat (Herold et al., 2014). Thick, intensively weathered laterites constituted around 85 % of the pedogenic cover (Nahon, 2003). Therefore, silicate weathering is assumed as almost dormant, thus, pCO$_2$ and global temperatures were high (Froelich and Misra, 2014).

Explaining pCO$_2$ variations by changes of the CO$_2$ source or sink fluxes lack on the fact that lasting imbalances in the release and removal of atmospheric carbon dioxide would result in runaway ice- or hothouse climate within several million years (e.g. Li and Elderfield, 2013; Torres et al., 2014). A negative feedback is assumed to balance release and removal rates of CO$_2$ over several million years (Berner et al., 1983; Caves et al., 2016). Increased plate tectonics and volcanic activity increase pCO$_2$ and cause uplift and orogenesis. A higher atmospheric CO$_2$ level increases the average surface temperature leading to an intensified hydrological cycle and enhanced dissolution kinetics of (silicate) minerals. Thus, increased CO$_2$ degassing is balanced by promoted CO$_2$ removal during silicate chemical weathering. This assumed weathering-climate feedback is challenged by a proposed strong coupling of modern silicate weathering to tectonic activity but a weak coupling to climate (Gaillardet et al., 1999b; West et al., 2005). A control of enhanced continental silicate weathering and related CO$_2$ drawdown during tectonic active periods is explained by decreased basalt weathering on ocean islands (Li and Elderfield, 2013), CO$_2$ release due to orogenic induced sulphide oxidation and subsequent sulphuric acid dissolution of carbonate rocks (Torres et al., 2014), and/or nearly diminished biotic-driven rock weathering in upland regions of active orogens (Pagani et al., 2009).

The proposed fluctuations in silicate chemical weathering rates are at odds with a nearly stable global runoff throughout the Cenozoic (variations around ±10 %; Otto-Bliesner, 1995) and stable weathering fluxes throughout the last 12 Ma (Willenbring and von Blanckenburg, 2010; von Blanckenburg et al., 2015). Kump and Arthur (1997) and Li and Elderfield (2013) explain stable denudation rates but declining pCO$_2$ by a change in the weatherability of minerals throughout the Cenozoic.
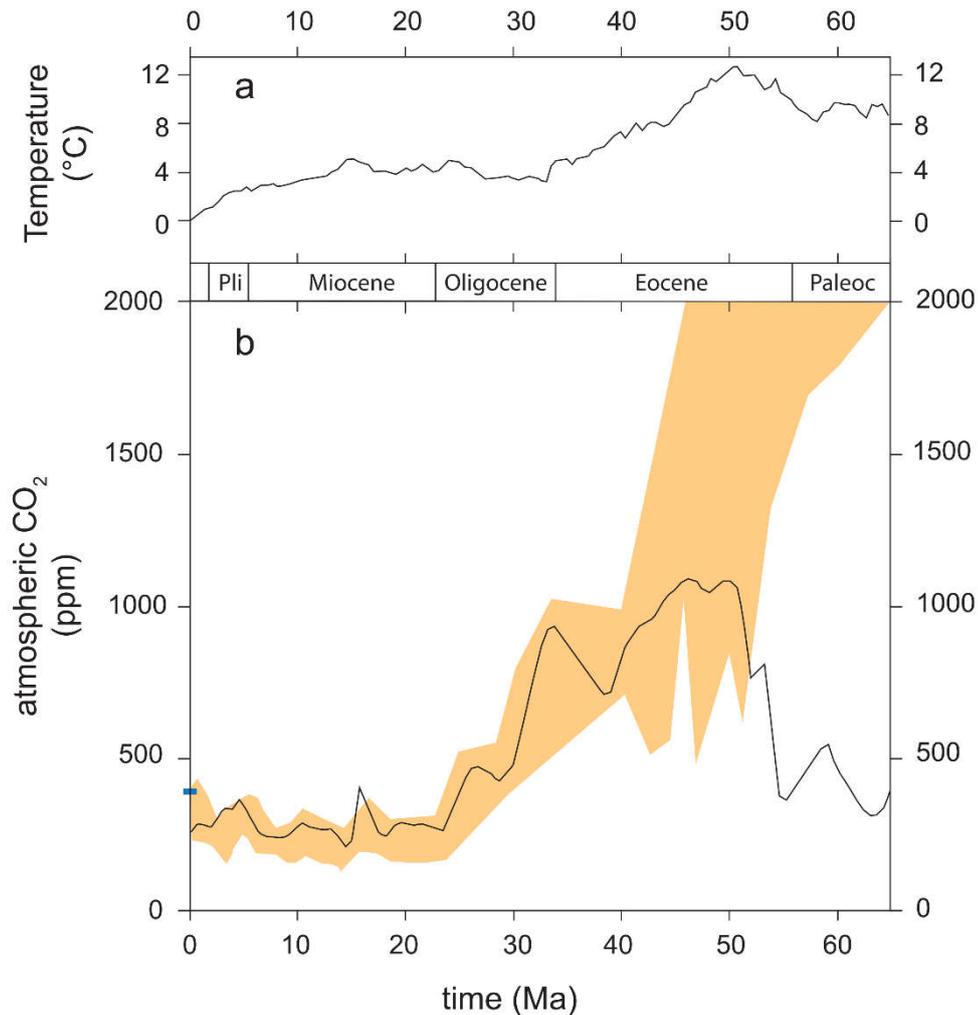
Figure 1-3

Earth's Cenozoic atmospheric CO_2 and temperature history by proxy. (**a**) Deep-sea temperatures generally track the estimates of atmospheric CO_2 (based on black line). (**b**) black line reconstructed from terrestrial and marine proxies (Beerling et al., 2011). Dark yellow shaded area based on surface ocean pH modelling (Pearson et al., 2000). Blue horizontal line indicates the present-day atmospheric CO_2 concentration (390 ppm). Figure modified from Beerling et al. (2011).

1.4 LITHIUM

Weathering proxies used in the past, i.e. the isotope composition of radiogenic Strontium (Sr) of marine carbonates (e.g. Raymo and Ruddiman, 1992) and marine sedimentary Osmium (Os) mainly record changes in the dominant weathered lithology, thus, do not exclusively track silicate weathering reactions or rates (Peucker-Ehrenbrink and Ravizza, 2000; Oliver et al., 2003). Lithium (Li) is almost exclusively hosted in silicate minerals and Li isotopes fractionate during water-mineral exchange (e.g. Huh et al., 1998; Huh et al., 2001; Kisakurek et al., 2005). This makes Li ideal to trace silicate weathering and initiated numerous studies in the last 20 years to focus on Li isotope variations in and between different reservoirs in the weathering

zone, including bedrock, minerals, bulk soil, fluvial sediments, soil solutions, river water, etc. (e.g. Huh et al., 1998; Tomascak, 2004; Pogge von Strandmann et al., 2006; Vigier et al., 2009; Lemarchand et al., 2010; Millot et al., 2010c; Wimpenny et al., 2010; Dellinger et al., 2014; Pogge von Strandmann et al., 2014; Wanner et al., 2014; Bagard et al., 2015; Dellinger et al., 2015; Liu et al., 2015; Pogge von Strandmann and Henderson, 2015; Wang et al., 2015; Henchiri et al., 2016; Dellinger et al., 2017; Pogge von Strandmann et al., 2017). This dissertation focusses on lithium isotope variations in the weathering zone to trace silicate weathering.

1.4.1 Isotope fractionation

This section gives a brief summary on stable isotope fractionation as the fractionation of stable Li and partly carbon (C), oxygen (O), and hydrogen (H) isotope variations are tools applied in this dissertation.

An atom is built up of protons and neutrons in the nucleus and electrons in the outer shell(s). The number of protons in the nucleus defines the specific element and the electron distribution in the outer shells defines its chemical properties. Isotopes are atoms with the same number of protons and electrons but different number of neutrons. Thus, isotopes vary in their atomic weights but not in their chemical properties. Stable isotope fractionation describes the disproportional transfer of isotopes of a given element between different reservoirs. The ratio between stable isotopes of one element alters during transfer from one reservoir to another. The disproportional transfer is caused by the mass difference between the isotopes that results in differences of the related bonding strength, which in turn is related to resulting differences in translational, vibrational, and rotational motions (Sharp, 2007).

Two types of isotope fractionations are distinguished:

1) Equilibrium isotope fractionation: equilibrium isotope fractionation occurs in equilibrium reactions, thus, forward and backward reactions proceed under the same rate in a closed system. Different bond energies resulting from the different atomic masses control the equilibrium fractionation, which is caused by the aim of a system to distribute isotopes until total energy is minimized. The process varies as a function of temperature.

2) Kinetic isotope fractionation: Kinetic isotope effects are either related to transport effects or chemical reactions. The reactions have to be unidirectional, thus, irreversible or incomplete; and chemical equilibrium could not be attained. Kinetic fractionation is related to the speed of the atoms as the lighter atom moves and reacts faster. Differences in the zero-point energy result in a higher energy barrier for the heavier isotopes to react.

Isotopic fractionation between two substances or reservoirs is expressed with the isotope fractionation factor α.

$$\alpha = \frac{R_A}{R_B} \qquad\qquad\qquad (1\text{-VII})$$

R_A and R_B stand for the ratios of two isotopes of a given element in the substances or reservoirs A and B.

The ratio that defines α usually differs at the third or fourth decimal scale, for this reason, it often is expressed in the term $1000 \cdot \ln \alpha$. The measured ratios are calibrated against a standard because relative differences in isotope ratios can be measured much more precisely than absolute ratios and to ensure intra-laboratory comparability. The difference between the measured ratios of a sample and the reference standard is expressed by the delta value

$$\delta = \left(\frac{R_x - R_{standard}}{R_{standard}}\right) * 1000 \qquad\qquad (1\text{-VIII})$$

R_x is the isotopic ratio of the sample and $R_{standard}$ is the ratio of the reference standard. δ values are expressed in permil (‰).

Details on lab procedure and measurements regarding determined and reported δ values in this thesis are given in section 2.4.3 and 3.4.2.

1.4.2 Lithium as tracer for (silicate) weathering and erosion processes

Several sources contribute to the Li mass balance in the weathering zone and Earth surface environments. Silicates are the dominant type of mineral that host Li. Most of dissolved Li in soil solutions, rivers and, finally, lakes or the ocean are solubilized from silicates (Kisakurek et al., 2005; Millot et al., 2010c; Dellinger et al., 2015; Wang et al., 2015). Carbonates contain low amounts of Li (Hoefs and Sywall, 1997). Even in rivers draining mostly carbonates, Li in solution is almost exclusively derived from silicate weathering (e.g. Kisakurek et al., 2005). Lithium mass fractions in marine and most continental evaporites are low, thus, dissolution of them does not substantially provide Li (Dellinger et al., 2015). However, at some locations, continental evaporites contain large amounts of Li and dissolution of them substantially contributes to the dissolved Li mass balance (e.g. Araoka et al., 2014; Wang et al., 2015). Hydrothermal fluids usually have several orders of magnitude higher Li concentrations compared to soil solutions, rivers, or the ocean. For this reason, they have a substantial impact on the oceanic Li budget (Chan et al., 1993; Elderfield and Schultz, 1996) and on solutions (soil

or stream water) in continental watersheds where hydrothermal activity occurs (Tomascak et al., 2003; Millot and Négrel, 2007; Millot et al., 2007; Millot et al., 2010b; Millot et al., 2011; Rad et al., 2013; Henchiri et al., 2014; Pogge von Strandmann et al., 2016). Anthropogenic sources can have a considerable effect on Li budgets of soil solutions, groundwater, and rivers. Lithium is common in batteries, medicine, and fertilizers, which are proposed to be responsible for high δ^7Li values up to +1226 ‰ obtained in meteoric waters (Millot et al., 2010a; Négrel et al., 2010; Wang et al., 2015). For this reason, investigation of Li isotope variations during weathering and erosion in a specific area requires the consideration of anthropogenic and hydrothermal provided Li.

Lithium is the lightest lithophile element and has two stable isotopes that exist in nature, Lithium-6 (^{6}Li) and Lithium-7 (^{7}Li), with approximate abundances of 7.5 % and 92.5 %, respectively, and a relative mass difference of ~16 %. The single valence state, the low ionic charge, the relatively small ionic radius, the degree of covalency, and the high affinity of Li with fluids make it a unique tracer for fluid-rock interactions such as chemical weathering. The average δ^7Li composition of mid-ocean ridge basalts and the upper mantle is assumed homogenous around +3.5 ‰ (Jeffcoate et al., 2007; Marschall et al., 2017) while the upper continental crust averages around +1 ‰ (Teng et al., 2004; Sauzéat et al., 2015). In contrast, δ^7Li values in rivers, soil solutions, and soils or river sediments range between +1 and +44 ‰, -14 ‰ and + 27 ‰, and -20 and +9 ‰, respectively (Rudnick et al., 2004; Pogge von Strandmann et al., 2006; Lemarchand et al., 2010; Pogge von Strandmann et al., 2010; Pogge von Strandmann et al., 2012; Dellinger et al., 2015; Wang et al., 2015).

Experiments and field investigations on Li isotope variations during high temperature reactions yielded small (below 2 ‰ at 250 °C for precipitated smectite; Vigier et al., 2008) or no (Schuessler et al., 2009) Li isotope fractionation. Therefore, dissolution of magmatic (primary) minerals generates if any only small differences in δ^7Li between the mineral (bedrock) and solvent (e.g. Pistiner and Henderson, 2003). Silicate weathering is typically incongruent (France-Lanord and Derry, 1997) yielding both a solute and a secondary phase (see equation 1-I and 1-II). ^{6}Li is preferentially incorporated into the secondary weathering product whereas ^{7}Li becomes enriched in solution (e.g. Huh et al., 2001; Millot and Girard, 2007; Vigier et al., 2008). The preference of ^{7}Li to distribute into solution possibly strengthens fractionation (Burton and Vigier, 2012; Liu et al., 2013). For this reason, δ^7Li in soil solutions and streams are always higher and new-formed secondary minerals, suspended and riverbed sediments lower in δ^7Li compared to the drained bedrock (e.g. Huh et al., 2001). Partitioning of Li into secondary minerals removes initially solubilized Li from solution and increases its δ^7Li value,

which is determined by the fraction of removed Li and the involved isotope fractionation factor (e.g. Pogge von Strandmann et al., 2014). The involved isotope fractionation between solution and related secondary mineral ($\Delta^7Li_{sol-sec}$) at low temperature is proposed to be between +8 ‰ and +20 ‰ (Chan et al., 1992; Rudnick et al., 2004; Williams and Hervig, 2005; Vigier et al., 2008; Dellinger et al., 2015; Wimpenny et al., 2015).

Long sediment residence times due to low erosion rates may result in re-solubilization of Li from secondary phases providing Li with lower δ^7Li values than the related bedrock to soil solutions or streams (Henchiri et al., 2016). For this reason, the erosion rate of Li in isotopically fractionated material relative to its chemical weathering rate is also crucial in determining the Li isotope composition of solutions and sediments (Bouchez et al., 2013).
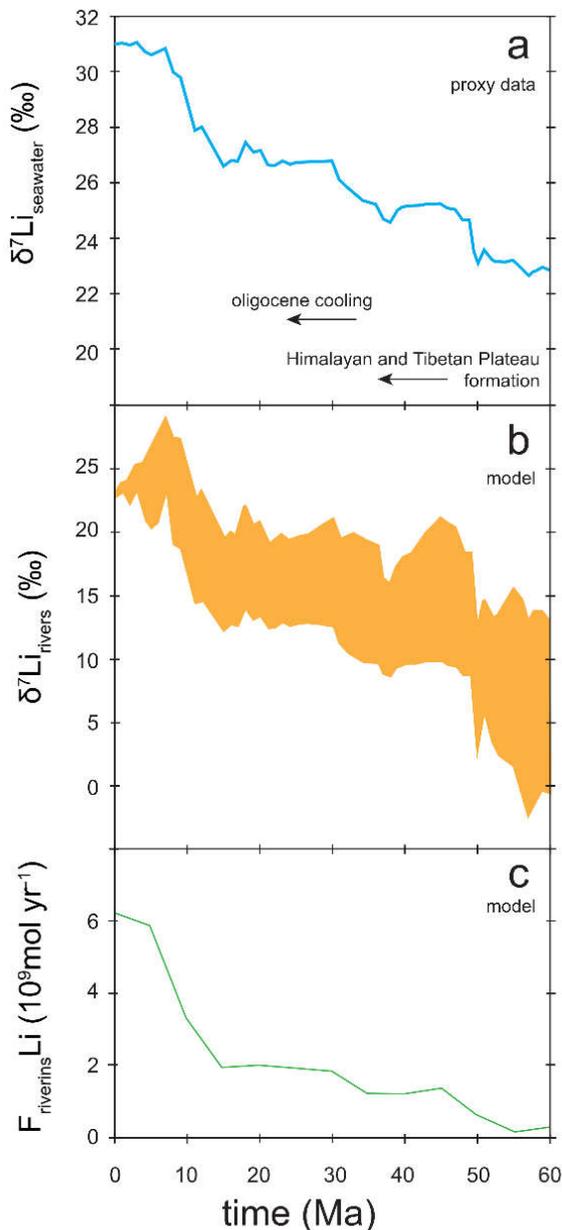
Figure 1-4

(a) Lithium isotope history of Cenozoic seawater, obtained from marine foraminifera and carbonates (Misra & Froelich, 2012). **(b)** The Li isotope composition of the global riverine Li flux able to create the oceanic δ^7Li increase (model calculations). Models assume about constant riverine and hydrothermal Li fluxes (Li and West, 2014; Vigier and Godderis, 2015). **(c)** Global riverine Li flux to the ocean. The seawater δ^7Li can be modelled with constant riverine Li isotope compositions but an increase of the riverine Li flux throughout the Cenozoic (Vigier and Godderis, 2015).

Silicate minerals considerably dominate the Li mass balance in rocks and Li isotopes fractionate during silicate weathering reactions. This combination makes lithium to a powerful tracer for silicate weathering processes and, therefore, possibly a proxy for the dominant atmospheric CO_2 sink. So far, the ultimate controls on observed Li isotope variations in and between sediments and related solutions (streams) are explained by variations in weathering rates (Vigier et al., 2009; Dosseto et al., 2015), fluid residence time in the critical zone (Wanner et al., 2014; Liu et al., 2015), the geomorphic regime and corresponding weathering intensity (Huh et al., 1998; Huh et al., 2001; Kisakurek et al., 2005; Millot et al., 2010c; Dellinger et al., 2015), and/or the concentration of riverine suspended particles (Pogge von Strandmann et al., 2006; Wanner et al., 2014). However, beside this tremendous progress in understanding Li isotope ratio variations in Earth surface environments the connection between δ^7Li variations in the weathering zone, silicate weathering processes, and related CO_2 consumption is still debated.

1.4.3 Lithium in archives and Cenozoic seawater δ^7Li variations
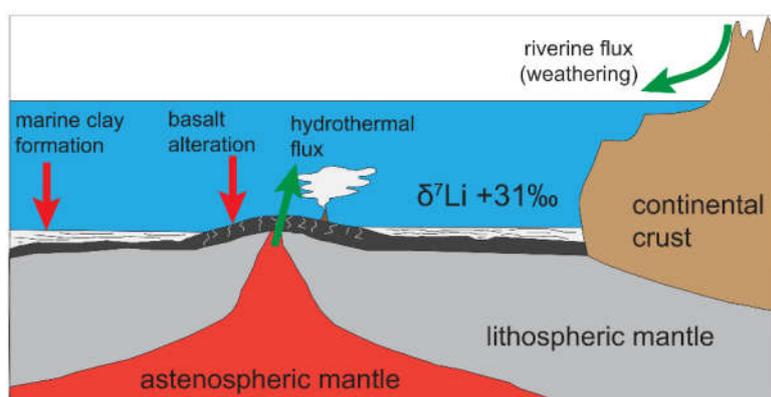
Figure 1-5

Oceanic lithium cycle with sources (green arrows) and sinks (red arrows)

Research on Li isotopes increasingly gains attention for the reconstruction of paleo-weathering and -climate conditions. Studies investigated lithium isotope variations in terrestrial or oceanic sedimentary archives (e.g. Hathorne and James, 2006; Misra and Froelich, 2012; Pogge von Strandmann et al., 2013; Dosseto et al., 2015; Pogge von Strandmann et al., 2017b; Pogge von Strandmann et al., 2017c). The investigation of lake archives may allows to constrain on the conditions of weathering and may climate in small-scale regions, e.g. lake catchments and nearby mountain belts, whereas the investigation on oceanic archives facilitates considerations on global weathering.

Research on Li in speleothems identified a coupling of temperature and Li isotopes (Pogge von Strandmann et al., 2017c) and research on sedimentary archives in the Nile fan a coupling of annual rainfall and Li isotopes (Bastian et al., 2017). Both couplings reflect climate induced variations of the weathering congruency, the ratio of Li solubilized from primary minerals to

13

Li partitioned into secondary minerals. In contrast, research on Li isotopes in fluvial sediments in the Himalayas detected no coupling of temperature and Li isotope variations (Dosseto et al., 2015). Here, the strong erosion dominated weathering regime inhibits a temperature control on chemical weathering reactions. Further research is required to understand the influence of climate on Li isotopes in weathering archives.

Despite the vagueness surrounding the major control on Li isotopes, studies applied the existing knowledge on Li isotope variations in marine carbonates and clays to constrain relative variations of paleo silicate weathering rates (e.g. Pogge von Strandmann et al., 2017b; Sun et al., 2018). Studies on marine foraminifera revealed a seawater increase in δ^7Li during the Cenozoic from +22 ‰ in the Paleocene to the modern value of +31 ‰ (Fig. 1-4a; Hathorne and James, 2006; Misra and Froelich, 2012). This trend is opposite to the development of the pCO$_2$ and the ocean temperature throughout the Cenozoic (Fig. 1-3). Understanding the connection of the δ^7Li seawater trend and silicate weathering possibly reveals the impact of silicate weathering rates on Cenozoic pCO$_2$ variations and the related climate change. The oceanic Li budget is balanced by Li supply from hydrothermal fluids and rivers, which drain the continents, and Li removal during oceanic crust (basalt) alteration and marine authigenic alumino-silicate clay formation (Fig. 1-5; Chan et al., 1992; Elderfield and Schultz, 1996; Misra and Froelich, 2012).

Misra and Froelich (2012), Froelich and Misra (2014), Li and West (2014), Dellinger et al. (2015), and Vigier and Goddéris (2015) proposed that an increase of the average global riverine δ^7Li raised the oceanic δ^7Li (Fig. 1-4b). Torres et al. (2014) and Caves et al. (2016) interpreted the raising marine lithium isotope ratios as an result of increasing continental silicate weathering rates during the Cenozoic, which is similar to the interpretation of the strontium and osmium seawater curves and agrees with proposed increasing riverine Li fluxes during the Cenozoic (Fig. 1-4c; Vigier and Goddéris, 2015). In contrast, Vigier et al. (2009), Dosseto et al. (2015), and Pogge von Strandmann et al. (2017b) claim that increasing silicate weathering rates create decreasing riverine δ^7Li, thus, weathering rates had to be high in the Early Cenozoic and low since the Oligocene.

A rise of the global riverine δ^7Li values requires an increasing fraction of initially solubilized Li that is incorporated into clays relative to the fraction that remains in solution. It is proposed that in the Paleocene (66 to 56 Ma) most Li that was solubilized during weathering processes remained as dissolved species whereas today most solubilized Li is incorporated into clays (Misra and Froelich, 2012; Froelich and Misra, 2014; Vigier and Goddéris, 2015). This changed the ratio of Li transported in eroded sediments to the export of Li as dissolved species

from 1:2 in the Early Cenozoic to the modern value of 4:1and is proposed to mirror the shift to more erosion dominated weathering (Froelich and Misra, 2014; Vigier and Goddéris, 2015). The reason for increased global Li incorporation into secondary minerals and related enhanced global riverine δ^7Li is still debated, if any, this represents the main reason for the oceanic δ^7Li rise at all.

Misra and Froelich (2012) and Wanner et al. (2014) call a change from congruent weathering (δ^7Li in solution close to bedrock δ^7Li) in the Paleocene and Early Eocene (from 56 Ma on) to incongruent weathering in the modern world as reason for enhanced Li incorporation into secondary minerals. This assumption is at odds with the occurrence of large laterite deposits in the Eocene (Nahon, 2003; Vigier and Goddéris, 2015), which indicate substantial secondary mineral formation, i.e. incongruent weathering.

Nowadays, the largest difference between dissolved δ^7Li in rivers and suspended sediments, i.e. secondary minerals, is observed in parts of catchments with the highest relief as shown for the Himalayas, Iceland, the Mackenzie, and the Orinoco basin (see Froelich and Misra, 2014, and references therein). For this reason, Froelich and Misra (2014) and Dellinger et al. (2015) propose that the increase in Cenozoic seawater δ^7Li reflects a change from a flat topography in the Early Cenozoic to a higher average global relief nowadays and propose a change from a supply- to kinetically-limited weathering regime. In agreement with this explanation, Li and West (2014) support an increase of the riverine δ^7Li but additionally claim a shift of the oceanic Li sinks from basalt alteration to incorporation in marine clays. The latter process is proposed to result from enhanced clay transport to the oceans driven by increased erosion rates due to mountain building. Both assumptions are consistent with a stepwise increase of the Cenozoic δ^7Li values in seawater following major orogenesis, in particular Himalayan and Tibetan Plateau formation (Fig. 1-4; Misra and Froelich, 2012). On the other hand, Henchiri et al. (2016) showed that riverine δ^7Li values in low-relief areas do not have distinct low values but display low or high δ^7Li values depending on the prevailing weathering regime.

In sum, uplift and formation of the Himalayas and the Tibetan Plateau are suggested as main reason for the Cenozoic rise in riverine and oceanic Li isotope ratios, which may is connected to declining Cenozoic pCO$_2$. For this reason, a comprehensive investigation of riverine Li isotope composition under different climates and geomorphic conditions across the Tibetan Plateau helps to identify the influence of plateau formation and the effect of climate on local and global riverine δ^7Li.
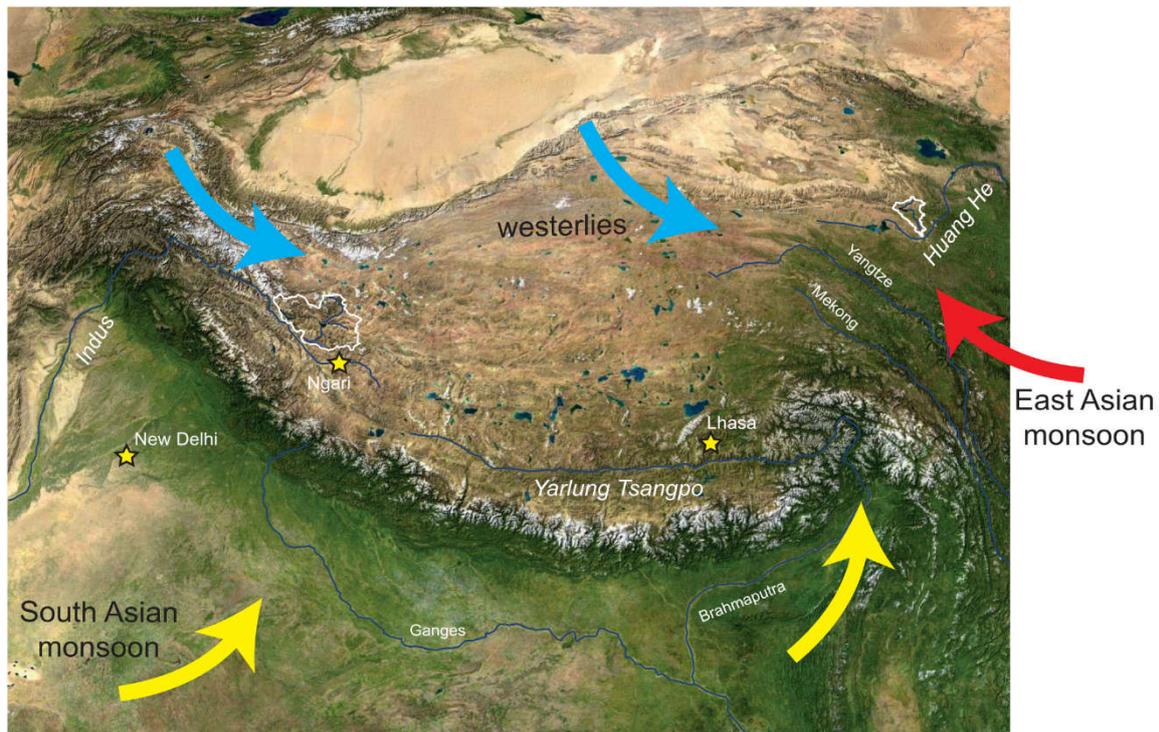
Figure 1-6

Overview map of the Tibetan Plateau including major rivers (investigated rivers are highlighted in large, italic letters). The catchments of Lake Donggi Cona on the northeastern and Lake Bangong on the western Tibetan Plateau are highlighted in white contours. Colored arrows indicate the prevailing atmospheric circulation systems. Satellite image from NASA.

1.5 THE TIBETAN PLATEAU

Some studies investigated Li isotopes in Ganges and Yangtze headwaters as well as some Himalayan streams (Kisakurek et al., 2005; Wang et al., 2015; Pogge von Strandmann et al., 2017). So far, no research was performed on Li isotopes in rivers and sediments on the Tibetan Plateau itself.

The Tibetan Plateau stretches around 2500 km east to west and around 1000 km north to south (Fig. 1-6) with an average altitude above 3500 m above sea level (asl; Molnar et al., 2010). Its glaciers, lakes, and streams are a huge freshwater reservoir and more than two billion people depend on the freshwater supplied by the large streams that origin on the plateau. Half of the area of the Tibetan Plateau is covered by endorheic catchments while the other half is drained to the Indian or North Pacific oceans (Phan et al., 2013). Large streams that contain a high proportion of the global dissolved and solid load carried to the oceans originate on the eastern (Huang He, Yangtze, Mekong, Salween), the southern (Yarlung Tsangpo-Brahmaputra, Ganges), and western (Indus) plateau (Fig. 1-7).
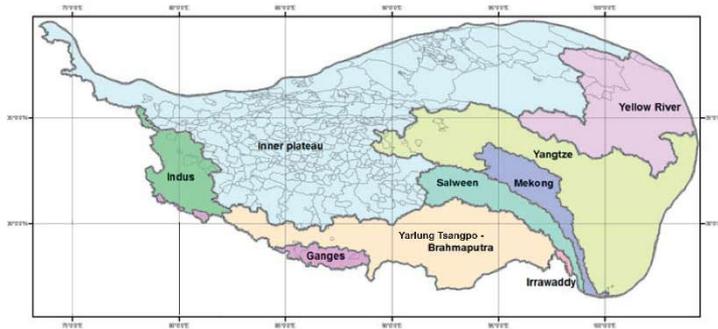
Figure 1-7

River catchments on the Tibetan Plateau from Phan et al. (2013). Water on the northern and inner plateau remains on the plateau whereas large rivers drain the south, east, and partly western plateau to the Indian and Pacific Ocean

Remarkable temperature fluctuations between day and night and summer and winter characterize the climate on the Tibetan Plateau leading to continuous and discontinuous permafrost in most areas across the plateau. Annual precipitation on the plateau varies from above 1000 mm in the southeast to less than 50 mm in the northwest (Fig. 1-8; Maussion et al., 2014). Formation und uplift of the Tibetan Plateau had profound impacts on the regional and global climate and weathering patterns since the onset of the Indian-Asian collision around 55 Ma ago (Yin and Harrison, 2000; An et al., 2001; Tapponnier et al., 2001; Garzione, 2008). Its high elevation changed atmospheric circulation patterns in Asia and the northern hemisphere (Kutzbach et al., 1993; Zhang et al., 2015a) by acting as an obstacle for cold northern air masses and the sub-tropical jet stream. The former substantially affected the formation and strength of the South Asian (Indian) monsoon and the latter the East Asian monsoon (Molnar et al., 2010). During the latest substantial uplift phase around 9 Ma ago the South Asian (also termed as Indian monsoon) and East Asian monsoon reached their modern intensity (An et al., 2001; Liu and Yin, 2002). Nowadays, moisture onto the Tibetan Plateau is mainly delivered by the monsoon systems and westerlies (Fig. 1-6). This results in strong intra-plateau and intra-annual fluctuations between the wet summer and dry winter season on the eastern and southern plateau (Araguas-Araguas et al., 1998; Bershaw et al., 2012; Caves et al., 2015). An intensification of the South Asian monsoon is proposed to increased regional silicate weathering rates that resulted in the final decrease of atmospheric CO_2 to pre-industrial values around 280 ppm after the Miocene climate optimum (Lefebvre et al., 2013).

Weathering, erosion, and vegetation are interacting with tectonic uplift and climate variations (Gaillardet et al., 1999b; Riebe et al., 2004; West et al., 2005; Jonell et al., 2017). Uplift resulted in considerably enhanced regional erosion rates at the plateau margins (Raymo and Ruddiman, 1992; Einsele et al., 1996; Jonell et al., 2017) with a regional or even global impact due to enhanced organic carbon burial and/or silicate chemical weathering rates promoting CO_2 removal (Raymo and Ruddiman, 1992; France-Lanord and Derry, 1997).

Erosion and weathering rates on the plateau, where the large rivers origin, are proposed to be low (Lal et al., 2003; Wu et al., 2005; Wu et al., 2008a; Wu et al., 2008b; Zhang et al., 2009).

Himalayan and Tibetan Plateau formation result in substantial hydrothermal activity along the major suture zones and lead to various geothermal fields and emerging of thermal waters across the plateau (Grimaud et al., 1985; Hochstein and Regenauer-Lieb, 1998; Zhao et al., 1998; Hoke et al., 2000; Guo et al., 2007; Craig et al., 2013; Zhang et al., 2015b). In most cases these thermal waters contain high amounts of Li (Grimaud et al., 1985; Guo et al., 2007; Tan et al., 2012; Yu et al., 2013; Zhang et al., 2015b).
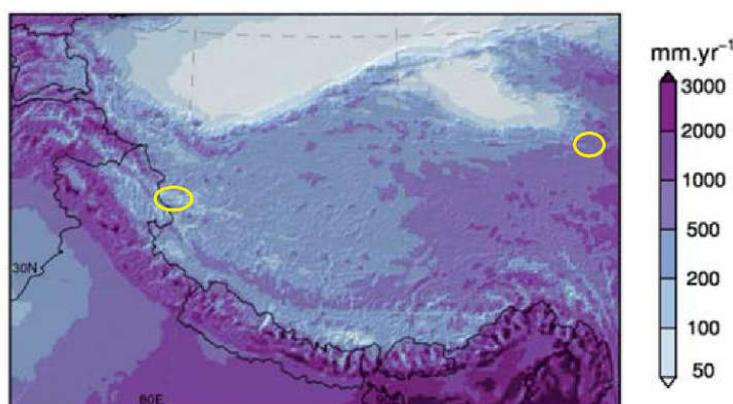
Figure 1-8

Decadal means of annual precipitation based on field data and HAR 10 model from Mausion et al. (2014). Yellow circles highlight the location of Lake Donggi Cona (~320 mm/a) and Lake Bangong (~80 mm/a).

1.6 SCOPE OF THE DISSERTATION

This dissertation is included into DFG priority program SPP 1372: "*Tibetan Plateau: Formation – Climate – Ecosystems (TiP)*". The TiP priority program investigated processes, interactions, and feedbacks of the driving forces of the plateau formation, climate and human impact, and their effect on ecosystems on three timescales: the period of plateau formation (from 70 Ma on), Cenozoic climate evolution (from 66 Ma on), and human impact and global change on ecosystems during the late Pleistocene and Holocene (from 20 ka on). Terrestrial and limnic archives in different climatic regions of the Tibetan Plateau were investigated by the different sub-projects.

The major objective of this dissertation is to understand the controls on lithium isotope variations in surface waters and sediments from two lake systems on the Tibetan Plateau and to use Li isotopes as a proxy of weathering intensity across a climate gradient from the northeastern to the western and southern Tibetan Plateau:

What controls lithium isotope variations in the two lake catchments? What are the implications for lithium in the large rivers as well as erosion and weathering across the Tibetan Plateau and the interpretation of Li archives?

In order to answer this questions, this thesis aims to understand geochemical variations, particularly Li isotope variations, in surface waters and sediments from the two lake catchments of Lake Donggi Cona and Lake Bangong and look for their connections to weathering, erosion, and climate. The results from the two lake systems are applied to hydrochemical variations in large rivers that integrate over large areas of the plateau with different climates and geomorphic regimes. Understanding the controls on Li isotope variations across the plateau enables to look for implications on the interpretation of Li archives, e.g. the Cenozoic Li isotope seawater curve. The potential connection of the Li seawater curve to continental silicate weathering may allow to hypothesize on reasons for Cenozoic climate change.

The Tibetan Plateau is ideal to study Li isotope variations in catchments and large streams under various climates and topographies as well as their response on uplift and weathering processes without notable anthropogenic impact. Furthermore, the widespread occurrence of hydrothermal activities across the plateau makes it well suited to investigate their impact on Li budgets and isotope variations in the weathering zone. The two investigated lake systems, the catchments of Lake Donggi Cona and Lake Bangong, are located on the northeastern and western Tibetan Plateau (Fig. 1-6). Lake Donggi Cona is a key locality of the SPP 1372 TiP project as well as for paleoclimatic research on the northeastern Tibetan Plateau (e.g. Dietze et al., 2010; Mischke et al., 2010a; Mischke et al., 2010b; Aichner et al., 2012; Dietze et al., 2012; Ijmker et al., 2012; Opitz et al., 2012; Stauch et al., 2012). Lake Bangong and its catchment are among the largest plateau-wide and the largest on the arid western plateau. For this reason, it became the key locality for lake basin research on the western plateau (Fontes et a., 1996; Gasse et al., 1996; Wen et al., 2016; Guo et al., 2017b). The climate on the northeastern plateau is characterized as semi-humid during the season, when soils, sediments, and surface waters are not frozen (Dietze et al., 2010), whereas the western plateau is a cold and dry desert with hyper-arid climate (Fontes et al., 1996). Denudation in the catchment of Lake Donggi Cona is proposed to be superficial and erosion dominated (Opitz et al., 2012; Opitz et al., 2016). The inner plateau and the arid western part are characterized by extreme low denudation rates and long lasting, stable topographic surfaces (Lal et al., 2003; Munack et al., 2014; Gourbet et al., 2017; Jonell et al., 2017). The upper Huang He, upper Indus, and the Yarlung Tsangpo were

also sampled (Fig. 1-6). The large rivers drain the northeastern, western, and southern plateau and the Himalayas (Fig. 1-7).

For this study, lake, stream, and thermal waters as well as river, limnic, and terrestrial sediments and bedrock samples were collected in both lake catchments to draw a detailed picture of geochemical and, in particular, Li isotope variations. Additionally, water samples and suspended particles were obtained from the three large rivers.

The water, sediment, and rock samples were analyzed for their Li isotope as well as major and trace element composition. Further, oxygen, hydrogen, and carbon isotope ratios were determined in water samples.

Lithium isotope are used as tracer for weathering and erosion processes. The chemical compositions of liquid and solid samples allows to identify sources of solutes (e.g. lithology, thermal waters) and processes in the sediments or water bodies (e.g. chemical weathering, sorting, evaporation). Oxygen and hydrogen isotopes were applied to identify sources of lake and stream waters, highlight alteration (e.g. evaporation), and establish a lake water balance for the lakes. Carbon isotopes of the dissolved inorganic carbon (DIC) were used to constrain carbon sources and identify organic processes, which may contribute to weathering.

This dissertation aims to answer the following questions:

I. **What are the influences of the lithology, climate, and thermal waters on the hydrochemistry of surface waters in the catchments of Lake Donggi Cona and Lake Bangong?**

This thesis aims to understand Li isotope variations in the two lake systems. This requires a detailed characterization of water and solute sources of surface waters as well as processes that occur within the water bodies itself.

So far, studies in the catchment of Lake Donggi Cona focused on tectonics, sources and transport of sediments, and climate reconstructions but provided only preliminary insights to the modern hydrochemistry as well as recent weathering and erosion.

Due to remoteness and the harsh climate, only a few studies were performed on lakes on the western Tibetan Plateau. Modern hydrochemistry, oxygen, hydrogen, and carbon isotopes and their connection to limnologic archives have been investigated in Lake Bangong catchment (Fontes et al., 1996; Gasse et al., 1996; VanCampo et al., 1996; Wen et al., 2016; Guo et al., 2017b). However, detailed characterizations for these parameters are not existent for both catchments but mandatory for the interpretation of the Li isotope variations.

Hydrochemistry in both catchments identifies solute and, in particular, Li sources. Oxygen, hydrogen, and carbon isotopes as well as chemical variations in surface waters are used to constrain moisture sources, evaporation, and organic activity. Comparing with paleo limnologic records links recent processes to Holocene variations in the catchment of Lake Donggi Cona and the northeastern Tibetan Plateau.

II.   **What is the influence of continental thermal waters on riverine Li isotope systematics on the Tibetan Plateau?**

The catchment of Lake Donggi Cona and Lake Bangong are located at large active faults, the Kunlun fault in the north and the Bangong Co fault in and the Bangong-Nujiang suture zone in the west. Hot springs are common in Lake Donggi Cona catchment and its surroundings. Emerging thermal waters are not reported for the catchment of Lake Bangong. However, its location close to large geothermal fields and near the Himalayan geothermal belt makes hydrothermal activity likely. Continental thermal waters have a massive impact on the Li mass balance in hydrothermally active regions as they have several orders higher Li concentrations compared to soil and river waters. Tomascak et al. (2003), Pogge von Strandmann et al. (2006), Vigier et al. (2009), Millot et al. (2011), Rad et al. (2013), Henchiri et al. (2014), and Pogge von Strandmann et al. (2016) identified a dominance of thermal waters on riverine Li budgets and isotope compositions as vast amounts of dissolved Lithium with δ^7Li between +1 and +10 ‰ were admixed. Hence, hydrothermally provided Li possibly overprints Li isotope variations derived from weathering reactions. Under those conditions, Li isotopes track Li sources, i.e. thermal waters, but not silicate weathering processes. For this reason, the influence of emerging thermal waters on the chemical composition of streams and the lake in the catchment of Lake Donggi Cona are investigated. The outcome is applied to a possible impact of hydrothermal activity in the Lake Bangong catchment.

In order to identify the impact of thermal waters on Li isotope variations in the surface waters in Lake Donggi Cona catchment, stream and thermal waters were analyzed on their hydrochemical and Li isotope composition. The contribution of thermal waters on hydrochemical budgets of stream and lake water is calculated. The Li isotope composition of a hydrothermally contaminated stream is modeled to identify admixing and/or elemental and isotope fractionation processes. Comparing hydrothermally contaminated and un-contaminated streams reveals the impact of thermal waters on Li isotope variations and their capacity to overprint the contribution of silicate weathering processes.

III. What controls Li isotope variations in the two lake systems? What are the implications on riverine δ⁷Li differences across the Tibetan Plateau?

After Li isotope variations in various reservoirs of the weathering zone and the influence of thermal waters are exposed, the inter-connection of Li isotope variations and weathering and erosion in the two lake catchments are investigated.

So far, Li isotope data on the Tibetan Plateau exist for the headwaters of the Yangtze River (Wang et al., 2015) and some Himalayan streams (Kisakurek et al., 2005; Pogge von Strandmann et al., 2017). This dissertation provides a comprehensive dataset of Li isotopes ratios in rivers of most of the non-endorheic catchments across the plateau.

A simple steady-state mass balance model for Li isotopes in the weathering zone of both lake catchments is established in order to understand the connection of Li isotope variations to relative differences in weathering, erosion, and climate. The catchments of the large rivers connect the two lake catchments and climatic zones of the north-eastern and western Tibetan Plateau. Hence, the conclusions from the two lake system are used to infer on riverine Li isotope variations and their implications on weathering and erosion across the plateau.

IV. Are Li isotope variations related to silicate weathering rates?

Variations of silicate weathering rates are proposed to influence pCO₂ (e.g. Raymo and Ruddiman, 1992). Vigier et al. (2009) and Dosseto et al. (2015) propose a control by silicate weathering rates on riverine δ⁷Li values thus, riverine Li isotopes trace silicate weathering rates. High rates create riverine δ⁷Li values close to the bedrock composition and vice versa, hence, the assumed Cenozoic riverine decline of δ⁷Li would reflect decreasing rates. In contrast, Torres et al. (2014) and Caves et al. (2016) attributed the rise in marine sedimentary δ⁷Li, [87/86]Sr, and [187/186]Os records to increasing silicate weathering rates provoked by Cenozoic orogenesis (mainly Himalayan and Tibetan Plateau formation). However, Dellinger et al. (2015) and Pogge von Strandmann et al. (2017) did not observe a relation between silicate weathering rates and Li isotope ratios in the Amazon and Ganges basins. This study investigates possible connections of δ⁷Li values and silicate weathering rates in rivers across the Tibetan Plateau. Riverine δ⁷Li variations across the plateau are compared with silicate weathering and denudation rates from the respective areas.

V. What are the consequences for the interpretation of limnologic or oceanic Li isotope archives? Is the uplift of the Himalayas and/or Tibetan Plateau capable to increase the average global riverine δ⁷Li value?

Li isotope variations in terrestrial archives gain increasing attention (e.g. Dosseto et al. 2015; Pogge von Strandmann et al., 2017b) as this allows to reconstruct the weathering or climate history of small areas, e.g. lake catchments or nearby mountain belts. Investigations on Li

22

isotopes in lake catchments on the Tibetan Plateau in specific, may allow to conclude on the interpretation of archives in arid regions or endorheic basins, as the Altiplano for instance.

The reasons for the increase of the seawater δ^7Li value by 9 ‰ throughout the Cenozoic (Misra and Froelich, 2012) is still debated (see 1.4.3). Misra and Froelich (2012), Bouchez et al. (2013), Li and West (2014), Wanner et al. (2014), and Vigier and Goddéris (2015) proposed a global riverine δ^7Li increase as main reason. Cenozoic orogenesis, mainly Himalaya and Tibetan Plateau formation, in turn, are suggested as main trigger for the global riverine δ^7Li increase.

The investigation of Li isotope variations in the two lake catchments that are located in different climates facilitate the interpretation of archives in arid regions or endorheic basins. Further, conclusions from the two lake catchments may identify the controls on Li isotope variations in the major rivers across the plateau. The identified controls on plateau wide Li isotope variations are discussed in the context of their possible impact on global riverine and oceanic Li isotope variations during the Cenozoic.

1.7 MAIN CHAPTERS OF THE DISSERTATION

The dissertation is a cumulative dissertation and consists of three scientific manuscripts (chapter 2 – 4). Chapter 2 and 3 are published in peer-reviewed journals and chapter 4 is in the final preparation stage for submission. Chapter 5 summarizes the overall conclusions and gives a brief outlook on possible future research.

The main goals and findings of each manuscript are listed below and indicate the contributions from co-authors and technical personal to the individual manuscripts.

1.7.1 Chapter 2 (published in Chemical Geology 2016. 435, 92-107)

The focus of the second chapter is a detailed characterization of the hydrochemical processes in the catchment of Lake Donggi Cona. Major and trace element composition of stream, lake, and thermal waters in the catchment of Lake Donggi Cona are used to identify the influence of rock weathering, thermal waters, as well as wet and dry deposition on solutes. Further, they reveal the hydrochemical evolution in soil and surface waters. Oxygen and hydrogen isotopes of surface waters are applied to identify sources and transport pathways of incoming precipitation, to highlight processes within the surface waters, and to establish a lake water balance. Carbon isotopes of the dissolved inorganic carbon (DIC) were used to constrain carbon sources and identify organic processes, which may contribute to weathering processes.

Comparison of modern hydrochemistry with chemical variations in the lake sediment are investigated for implications on climatic evolution of the catchment.

Sampling was performed by Marc Weynell in 2008 and by Marc Weynell and Uwe Wiechert in 2011. Elke Heyde performed major element analysis and Marc Weynell and Elke Heyde performed trace element analysis on water samples. Matthias Friebel helped during carbon isotope analysis and Marie Küssner during oxygen and hydrogen isotope analysis. Marc Weynell performed data reduction and interpretation and wrote the manuscript. Uwe Wiechert and Steffen Mischke revised the manuscript and helped throughout discussion. Frank Riedel, Uwe Wiechert, Steffen Mischke, and Tom Wilke obtained funding.

1.7.2 Chapter 3 (published in Geochimica et Cosmochimica acta 2017. 213, 155-177)

The focus of the third chapter is to highlight and understand the controls on Li isotope variations in the catchment of Lake Donggi Cona. The outcome of the second chapter is fundamental for this considerations. The average δ^7Li values for different sediment and surface waters were obtained to evaluate Li isotope variations between soil solutions, secondary minerals, and bedrock. Particular attention is given on the impact of thermal waters on riverine Li isotope compositions. For this purpose, major and trace element and Li isotope compositions of sediment and rock samples were determined as well as the Li isotope composition of stream, lake, and thermal waters in the catchment of Lake Donggi Cona as well as the Huang He.

Marc Weynell performed sampling in 2008 and Marc Weynell and Uwe Wiechert in 2011. Major and trace element concentrations of solid samples were obtained by XRF by Rudolf Naumann and Andrea Gottschee at GFZ Potsdam and partly by Marc Weynell at FU Berlin. Marc Weynell carried out Li sample preparation, measurements, data reduction, modelling, and wrote the manuscript. Jan Schüssler helped with Li isotope measurements, revised the manuscript, and helped throughout discussion. Frank Riedel, Uwe Wiechert, Steffen Mischke, and Tom Wilke obtained funding. Uwe Wiechert and Konrad Hammerschmidt revised the manuscript and helped throughout discussion.

1.7.3 Chapter 4 (in final stage of preparation for submission)

The focus of the fourth chapter is to examine chemical and Li isotope variations in stream and lake waters as well as sediments in the catchment of Lake Bangong, western Tibetan Plateau to disclose the controls on Li isotope variations under a cold and dry climate. Additionally, samples from the upper reaches of the Indus and the Yarlung Tsangpo are investigated to understand riverine Li isotope variations on the western and southern plateau. The results are compared with the outcome of chapter 3 to reveal the controls behind Li isotope

variations in rivers across the Tibetan Plateau and discuss implications on Cenozoic riverine and seawater Li isotope compositions and their possible connection to the Cenozoic climate change. For this purpose, major and trace element composition of stream and lake waters as well as river bed sediments, suspended particles, and lake sediments were determined. Oxygen and hydrogen isotopes in stream and lake waters were determined to characterize the influence of the local climate on surface waters. Additionally, Li concentrations and Li isotope composition for all samples were obtained.

Marc Weynell performed sampling in the catchment of Lake Bangong in 2012 and Sascha Barvencik sampling of the upper Indus and Yarlung Tsangpo in 2010. Major and trace element concentrations of solid samples were performed by Anja Schleicher, Rudolf Naumann, Andrea Gottsche, and Marc Weynell at GFZ Potsdam. Philip Hoelzmann performed XRD analysis on sediments, Marc Weynell performed the data reduction. Elke Heyde performed major element analysis and Marc Weynell and Elke Heyde performed trace element analysis on water samples. Matthias Friebel helped during carbon isotope analysis and Marie Küssner during oxygen and hydrogen isotope analysis. Marc Weynell carried out Li sample preparation and measurements for the 2012 samples and Sascha Barvencik and Jan Schüssler for the 2010 samples. Marc Weynell performed data reduction, interpretation and wrote the manuscript. Jan Schüssler helped with Li isotope measurements, revised the manuscript, and helped throughout discussion. Frank Riedel, Uwe Wiechert, Steffen Mischke, and Tom Wilke obtained funding. Uwe Wiechert revised the manuscript and helped throughout discussion.

CHAPTER 2

CHEMICAL AND ISOTOPIC (O, H, C) COMPOSITION OF SURFACE WATERS IN THE CATCHMENT OF LAKE DONGGI CONA (NW CHINA) AND IMPLICATIONS FOR PALEOENVIRONMENTAL RECONSTRUCTIONS

2.1 ABSTRACT

The oxygen, hydrogen, and carbon isotope ratios and major and trace element concentrations of surface waters are reported for the catchment of Lake Donggi Cona, Qinghai Province, China. The chemistry of the surface waters in the southeastern catchment is reflecting the dissolution of carbonate rocks, whereas thermal waters add sodium and chlorine to the waters in the northern catchment. The Dongqu River, draining the southeast catchment, contributes 87 to 94 % to the water budget of the lake. Thermal waters and waters from the northern catchment add 6 to 13 %. The combination of hydrogen and oxygen isotopes provides evidence that only small amounts of recycled lake water contribute to the precipitation in the catchment. Most of the moisture may be transported by the East Asian summer monsoon or an eastern branch of the South Asian monsoon into the Donggi Cona region. From oxygen isotope ratios it is calculated that about 45 % of the lake water input is evaporated and 55 % leaves the lake through a channeled outflow. The carbon isotope ratio identifies microbial respiration of organic matter, probably in soils and sediments of the catchment, as the major source of dissolved inorganic carbon in most surface waters and the lake. An isotope effect, from biological processes, in the lake is minor, and can be neglected in order to explain isotope ratios of inorganic carbon in lake water. The results imply that oxygen isotope ratios in the lake sediment archives mainly mirror the relation between precipitation and evaporation (P/E), which may be controlled by changes in the global water cycle like monsoon intensity or by tectonically driven local changes affecting the outflow flux. A comparison between lake archives based on ostracod shells and the modern system indicates similar $\delta^{18}O$ values for the lake water since 4.3 ka but different $\delta^{13}C_{DIC}$ values. This discrepancy between carbon isotope ratios in ostracod shells and modern lake water samples may be due to thermal waters with high $\delta^{13}C_{DIC}$ emerging near the coring site. It is suggested that carbon isotopes of ostracods from a sediment drill core reflect the activity of a local thermal spring at the lake bottom, whereas oxygen isotopes provide evidence for an open lake system since about 11 ka and that the climate and environment of the Donggi Cona region changed very little over the last 4300 years.

CHAPTER 3

LITHIUM ISOTOPES AND IMPLICATIONS ON CHEMICAL WEATHERING IN THE CATCHMENT OF LAKE DONGGI CONA, NORTHEASTERN TIBETAN PLATEAU

3.1 ABSTRACT

This study presents lithium (Li) isotope ratios (δ^7Li) for rocks, sediments, suspended particulate material, and dissolved Li from the Lake Donggi Cona catchment, located on the northeastern Tibetan Plateau, China. The average δ^7Li = +1.9 ‰ of the bedrocks is estimated from local loess. δ^7Li values decrease progressively within the sediment cascade from loess, to river and lake floor sediments. The lake floor sediments average at -0.7 ‰. The difference between bedrock and lake sediments reflects the preferential fractionation of dissolved 6Li into clay minerals (mostly illite) in the weathering zone and grain-size sorting during fluvial sediment transport. The δ^7Li values of stream and lake water samples range from +13.6 to +20.8 ‰, whereas thermal waters fall between +5.9 and +11.6 ‰. The δ^7Li values of lake water samples are close to +17 ‰ and reflect mixing of waters from two perennial inflows and thermal waters. Dissolved Li in streams represents an integrated isotopic signal derived from soil solutions in the weathering zone. An apparent isotopic fractionation of -17.8 ± 1.6 ‰ ($\alpha_{sed-DL} \sim 0.982$) between secondary minerals and solution was determined. An inflow that drains a sub-catchment in the north carries a high proportion of thermal waters. Despite of the high proportion of admixed thermal waters with high Li concentrations and low δ^7Li, this stream has the highest δ^7Li values of about +21 ‰. This is consistent with admixing of thermal waters to solutions in the weathering zone and subsequent fractionation by preferential uptake of isotopically light dissolved Li into secondary phases. Based on Li isotope ratios of the dissolved and solid export flux from the weathering zone we calculated that at least five times more Li is exported in particles than dissolved in streams. An average δ^7Li value of about +17 ‰ of most streams and the lake are reflecting low chemical weathering rates of about 4 t/km^2/a. Low weathering rates and an erosion dominated weathering system are consistent with moderate precipitations, the cold climate, and the high relief of the study area.

CHAPTER 4

A LOW δ^7LI WEATHERING REGIME ON THE WESTERN TIBETAN PLATEAU - SOURCE EFFECT OR SUPPLY LIMITED WEATHERING UNDER A HYPER-ARID CLIMATE?

Chapter 4: A low δ⁷Li weathering regime on the western Tibetan Plateau – source effect or supply limited weathering under a hyper-arid climate?

4.1 ABSTRACT

This first study of Li isotopes in surface waters and sediments on the western Tibetan Plateau aims to identify processes that control Li isotope variations during weathering under cold and hyper-arid conditions. In combination with data from the northeastern Tibetan Plateau and the Indus and Yarlung Tsangpo Rivers that drain the Himalayas and the southern plateau we explore a climatic and geomorphic gradient to identify the effect of Himalayan and Tibetan Plateau formation on Li isotope variations and the implications for Li paleo-weathering records. The lake and river sediments display δ^7Li values between -4.7 ‰ and -0.6 ‰. Li isotopes in river bed sediments correlate with weathering intensity tracers such as the chemical index of alteration (CIA), K/(Na+K), or Na/Ti and δ^7Li values decrease systematically within the sediment cascade. A control by modern weathering is indicated. Lake Bangong basins display δ^7Li values between +8.1 ‰ and +11.1 ‰. Strong evaporation of the lake water results in alteration of Li isotopes within the water body. The non-evaporated major inflows of Lake Bangong have dissolved δ^7Li values of +6.1 ‰ and +8.9 ‰. High Li/Na ratios in the stream waters indicate a hydrothermal impact on Li. Considerable differing hydrochemistry of nearby geothermal fields and stream waters contradict admixing but processing of thermal waters in the weathering zone. The δ^7Li of the large inflows reflect little (26 % and 42 %) net-incorporation of Li in secondary minerals during silicate weathering reactions. Similar low δ^7Li values in the dissolved and suspended load from the Indus headwaters and Yarlung Tsangpo provide evidence for a weathering regime characterized by low dissolved and sedimentary δ7Li all over the western and southern Tibetan Plateau. Here, mass balance calculations exhibit roughly balanced export fluxes of dissolved Li and Li eroded in clay minerals or rock detritus, which characterizes supply limited weathering. Higher dissolved δ^7Li values around +17 ‰ on the semi-humid, northeastern Tibetan Plateau are consistent with an at least five times higher particulate Li export flux compared to the dissolved Li flux. The δ^7Li gradient across the Tibetan Plateau mirrors the change from supply-limited to kinetically-limited weathering but silicate weathering rates are low and about constant. Hence, a change of the weathering regime has not necessarily come along with a change in silicate weathering rates.

4.2 INTRODUCTION

Chemical weathering of silicate rocks is a major sink for atmospheric CO_2 over geological time scales (Walker et al., 1981; Berner et al., 1983; Royer et al., 2004). A substantial decline of atmospheric CO_2 concentrations caused the transition from the Eocene hothouse to modern

icehouse climate (Beerling and Royer, 2011). The uplift of mountain ranges, e.g. the Himalayas and Tibetan Plateau, was proposed to force the CO_2 decline by enhancing physical erosion rates and related organic carbon burial (France-Lanord and Derry, 1997) and/or silicate weathering rates (e.g. Raymo and Ruddiman, 1992). To reconstruct past climate and weathering conditions over geological time scales from sedimentary archives, the use of different geochemical proxies and their correct interpretation is essential. The Li isotope (δ^7Li) system is such a proxy used to investigate changes in weathering conditions (e.g. Misra and Froelich, 2012).

Lithium is almost exclusively hosted in silicate rocks (e.g. Kisakurek et al., 2005; Millot et al., 2010c; Dellinger et al., 2015), which makes it unique to trace silicate weathering (e.g. Huh et al., 1998; Pistiner and Henderson, 2003; Vigier et al., 2009; Dellinger et al., 2014; Dellinger et al., 2015). Field studies identified a large range of δ^7Li values between +1 ‰ and +44 ‰ in streams (e.g. Pogge von Strandmann et al., 2006; Dellinger et al., 2015), whereas river bed and suspended sediments have lower δ^7Li values compared to the bedrock of a catchment (e.g. Huh et al., 2001; Dellinger et al., 2014). This is the result of preferential incorporation of ^6Li into secondary minerals, which leaves the corresponding aqueous solutions enriched in ^7Li (e.g. Vigier et al., 2008). The extent of Li isotope fractionation between the bedrock and Li in solution reflects the ratio of Li solubilized from bedrock (having low δ^7Li) to Li incorporated into secondary minerals (driving the solution to high δ^7Li). This ratio is proposed to be controlled by climate (Pogge von Strandmann et al., 2017c), weathering regime and the corresponding weathering intensity (e.g. Huh et al., 2001; Kisakurek et al., 2005, Millot et al., 2010c; Dellinger et al., 2015), and/or silicate weathering rates (e.g. Vigier et al., 2009).

Several studies investigated terrestrial (e.g. Dosseto et al., 2015; Pogge von Strandmann et al., 2017c) or oceanic (Hathorne and James, 2006; Misra and Froelich, 2012; Pogge von Strandmann et al., 2013; Bastian et al., 2017; Pogge von Strandmann et al., 2017b) weathering archives or focused on their interpretation (Li and West, 2014; Wanner et al., 2014; Vigier and Goddéris, 2015; Vigier et al., 2015; Dellinger et al., 2018; Roberts et al., 2018) to use Li as proxy for paleo weathering conditions. The δ^7Li of seawater increased throughout the Cenozoic following major orogenesis, in particular Himalayan and Tibetan Plateau formation, either due to an increase of the global riverine δ^7Li value (Misra and Froelich, 2012; Froelich and Misra, 2014; Li and West, 2014; Dellinger et al., 2015), a change in silicate weathering rates or Li fluxes (Vigier and Goddéris, 2015), and/or an increase in erosion rates (Li and West, 2014). The lithium isotope seawater curve may contribute to an improved understanding of the controls on atmospheric CO2 concentrations and Cenozoic cooling (Misra and Froelich, 2012).

The objective of this study is to identify processes that control Li isotope variations under hyper-arid conditions and use Li isotopes as a proxy of weathering intensity on the western Tibetan Plateau. This also facilitates the interpretation of lacustrine sedimentary archives from high-standing endorheic basins, e.g. the Tibetan Plateau or Altiplano, that would record something about the climate or weathering history. The comparison with data from the semi-humid northeastern Tibetan Plateau (Weynell et al., 2017) makes our approach well suited to identify the controls on Li isotope variations across the Tibetan Plateau. Further, this allows to investigate the possible effect of Himalayan and Tibetan Plateau formation on the global riverine Li isotope composition. To the best of our knowledge it is the first study of Li isotopes in surface waters and sediments on the western plateau.

Here, we study Li isotope variations in streams and sediments in the catchment of Lake Bangong located in the western part of the Tibetan Plateau, as well as the headwaters of Indus River and Yarlung Tsangpo. The climate on the western and southwestern plateau is cold and dry, providing an ideal setting to identify processes that control Li isotope variations under hyper-arid conditions. The sampled headwaters of the Indus and Yarlung Tsangpo drain the Himalayas and the western and southern Tibetan Plateau. Thus, detailed findings from the Lake Bangong catchment can be applied to a large area. Further, considering previously published Li isotope data from catchments in the erosion dominated geomorphic regime of the northeastern Tibetan Plateau (Weynell et al., 2017) with relative high annual precipitation of ~320 mm/a, allows us to systematically study the Li isotope behavior across both a climate and a geomorphic gradient and derive implications for weathering and erosion on the Tibetan plateau.

4.3 STUDY AREA

Lake Bangong (also referred to as Bangong Co or Pangong Co) is located on the western Tibetan Plateau (33°30' N; 79°50' E; Fig. 4-1a) at an altitude of 4253 m above sea level. With 31348 km^2 the catchment area is the second largest on the Tibetan Plateau (Gasse et al., 1996). Today, Lake Bangong is a closed lake and consists of five basins, separated by shallow sills. The Nyak Co represents the largest basin of the lake chain.

Three streams dewater into the eastern basin (Fig. 4-1b). The two largest, Chiao Ho (also referred to as Wujiang River) and Makha River (also referred to as Magazangbu River), drain the northern and southern catchment, respectively. The Chiao Ho has a high relief streambed with an altitude difference around 800 m whereas the Makha River has a flat relief streambed

with an altitude difference around 150 m. Both streams are dammed near the lake for the generation of hydroelectric power. The considerably smaller Nama Chu drains a karst lithology, swampy areas, and several salt water ponds in the eastern part of the catchment (Fontes et al., 1996). Road constructions result in damming of the inflow close to the lake. Lake Bangong and streams are frozen from November to April. Permafrost is discontinuous throughout the year, due to water limitation.

Sedimentary rocks (flysch facies with shale, sandstone, clastic sediments, calcschists), limestones, and large granitoitic plutons, mainly located in the south, dominate the lithology of the catchment. The basins of Lake Bangong are embedded in limestones, sandstones, and rarely ophiolites (Fontes et al., 1996; Shi et al., 2008; Liu et al., 2014; Gourbet et al., 2017; for geological map see supplement S4-1).

The average annual precipitation is 82 mm/a (2010 to 2016; Guo et al., 2017b) but substantial inter-annual variations between 46 mm (2010) and 134 mm (2011) exist (Wen et al., 2016). The amount of precipitation in the catchment decreases from south to north (Mukhopadhyay and Dutta, 2010). 80 % of the annual precipitation occurs during the monsoon season (Guo et al., 2017). The mean annual air temperature is about +8 °C during summer (May-October) and about -6 °C during winter with an annual mean of +2 °C. The estimated mean annual evaporation is ca. 2449 mm (Fontes et al., 1996) making the western Tibetan Plateau the most severe alpine desert on Earth (Fort and van Vliet-Lanoe, 2007). In summary, the climate on the western Tibetan Plateau is hyper-arid with low temperatures, low humidity, and strong winds resulting in a thin vegetation cover with bare rock / sediments and thin, barely developed soils. Vegetation in the form of patchy grasslands is limited close to the major streams and the lake (Guo et al., 2017).

The catchment of the Indus headwaters, located around 50 to 150 km southeast of Lake Bangong, is characterized by similar geology, climate, topography, and vegetation as the Lake Bangong catchment (Ahmad et al., 1998). The Yarlung Tsangpo, designated as Brahmaputra after crossing the Himalayas, was sampled on a 700 km long transect (Fig. 4-1a). The Yarlung Tsangpo drains mainly shales and plutonic rocks. Climate and vegetation at the most western sample location resemble the conditions in the catchment of Lake Bangong with annual precipitations of around 50 mm. Annual precipitation increases towards the east and reaches around 200 mm at the location where the most eastern sample (Bra 7) from the Yarlung Tsangpo has been taken (Hren et al., 2007; Maussion et al., 2014).
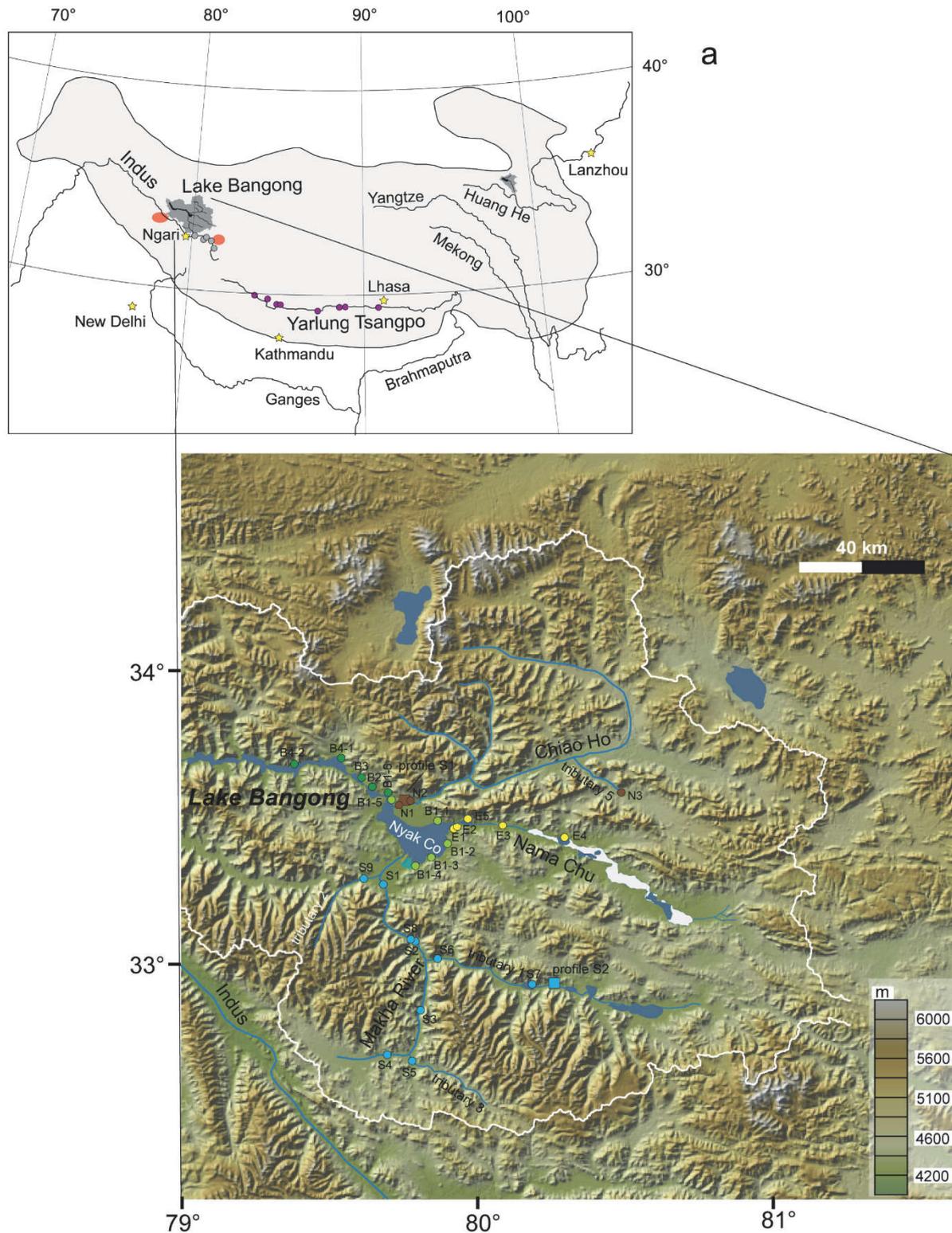
Figure 4-1

(a) Map of the study area: Major rivers draining the plateau and catchments of Lake Bangong, located on the western plateau and Lake Donggi Cona, located on the northeastern plateau, are shown (the two lake catchment are shown as dark grey areas). Sample locations of Indus headwaters are shown in grey and of Yarlung Tsangpo in purple. Two light red areas close to Lake Bangong indicate geothermal fields (also shown in Fig. 4-2). Grey area shows Tibetan Plateau defined by 3500 m contour line. **(b)** Morphological map (created with geomapapp: http://www.geomapapp.org; Ryan et al., 2009) of the catchment of Lake Bangong (red line) with sample locations (colors represent: lake (green), southern catchment (blue), northern catchment (brown), and eastern catchment yellow).

4.4 SAMPLING AND ANALYTICAL METHODS

4.4.1 Sampling

Samples from the catchment of Lake Bangong were collected in September 2012, sample locations are shown in Fig. 4-1b. The rivers Yarlung Tsangpo and Indus were sampled in October 2010 (for details on sample locations see supplementary Table S4-1 and supplementary satellite data). River bed sediments (RBS) and lake sediments (LS) were collected in the catchment of Lake Bangong by a shovel at 20 to 40 cm water depth. Particles >1 mm were removed, and the remaining material was homogenized. Suspended particles (SP) are filtered from about 1 L water samples from rivers in the Lake Bangong catchment as well as from the Yarlung Tsangpo and Indus headwaters.

Two sediment profiles were sampled in alluvial fans in the upper (S2) and lower (S1) reaches of the catchment (Fig. 4-1b). The Chiao Ho formed a large alluvial fan north of Nyak Co and cut a 2 m deep channel into the floodplain sediments. The upper 40 cm of these sediments are shown in profile S1. At this location, the alluvial plain is covered with grasses. Roots are common in the upper 5 to 10 cm, with some of them reaching depths of 30 cm. Sediments in profile S1 show a bright color and rhizo-concretions around roots and carbonate coatings (caliche) are common. Profile S2 is located in the upper reaches of the catchment near a small tributary of the Makha River. The profile consists of brownish and clayey floodplain sediments of an alluvial fan which were collected from a hand-dug pit.

Surface waters in the catchment of Lake Bangong, Indus headwaters (spring area), and Yarlung Tsangpo were sampled. pH, specific conductivity (SC in µS cm⁻¹) and water temperature (T in °C) were measured using a Hach® HQ 40d portable meter. Water samples for cation analysis were filtered through a 0.45 µm cellulose acetate filter, acidified with ultrapure nitric acid (HNO_3), and stored in 60 ml polyethylene (PE) bottles. Water samples for anion and isotope analysis were filtered and stored in PE-bottles sealed with rubber septum caps. Suspended particles were recovered from the cellulose-acetate filters.

4.4.2 Analytical procedures

Major and trace element composition of sediment samples were determined by XRF analysis (PANalytical® AXIOS Advanced) at GFZ Potsdam (for details on method see Fischer-Godde et al., 2011). Li concentration data for sediments were obtained by ICP-MS at Freie Universität Berlin after acid digestion (for details on methods see Weynell et al., 2017). Major and trace element composition of surface waters are determined by ICP-OES, ICP-MS, and ion chromatography. Alkalinity concentration for surface waters from Lake Bangong catchment

were achieved with a Thermo Fisher Scientific® MAT 253 isotope-ratio mass-spectrometer (IRMS) at the Institute of Geological Sciences of the Freie Universität Berlin. Alkalinity concentrations for water samples from the Indus and Yarlung Tsangpo were determined with Merck® alkalinity tests in the field. $\delta^{18}O$ and δD data from surface waters as well as $\delta^{13}C$ data of dissolved organic carbon (DIC) was obtained by Thermo Fisher Scientific® MAT-253 gas-mass-spectrometry (for details on methods and analytical uncertainty see Weynell et al., 2016).

For Li isotope analysis powdered sediment samples were digested with a $HF+HNO_3$ mixture. Water aliquots containing ~200 ng Li were dried at 85 °C. Lithium was separated using 2.4 mL-columns containing Bio-Rad™ AG 50W-X12 (200-400 mesh) resin (Magna et al., 2004). Isotope ratio measurements were performed on a Neptune MC-ICP-MS (Thermo Fisher Scientific™) at the Helmholtz Laboratory for the Geochemistry of the Earth Surface (HELGES) at the German Research Center for Geosciences GFZ, Potsdam. Details on chemical procedures and measurements are described in Weynell et al. (2017). The uncertainty of the method was evaluated by repeated analysis of CPRG UB N; USGS MAG 1, NIST SRM2709a "San Joaquin Soil", CCRMP Till 1, and OSIL Atlantic seawater reference materials. These results indicate an uncertainty in $\delta^{7}Li$ of ±0.5 ‰ (2σ; see Table S4-2).
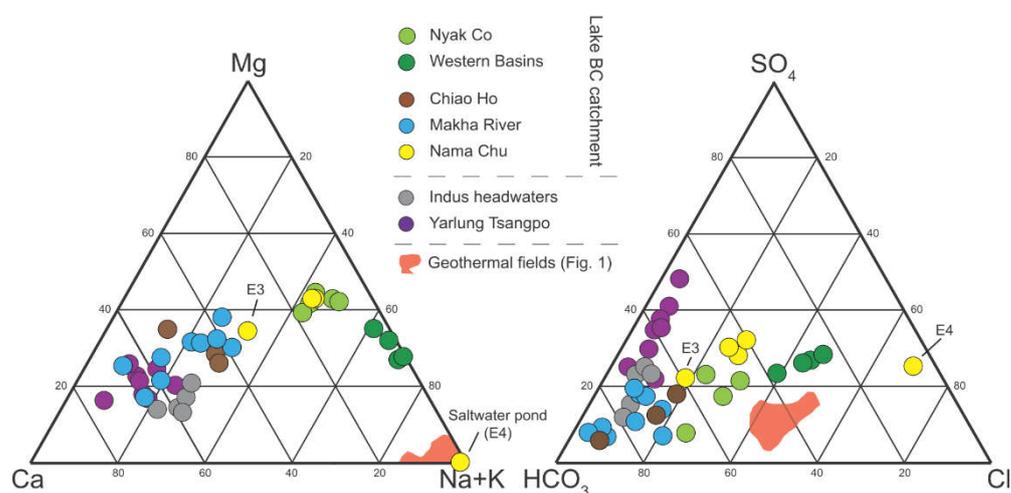
Figure 4-2

Ternary diagram – Piper plot of sampled waters from this study. The chemical composition of thermal waters from two geothermal fields are shown, located close to Lake Bangong catchment (see Fig. 4-1). Waters from the lake basins and Nama Chu are strongly enriched in Na and Cl due to strong evaporation. Sample E3 is not affected by evaporation and resemble the ion composition of samples from the catchments of Chiao Ho and Makha River. Chemistry of thermal waters from nearby geothermal fields and sampled surface waters that are not affected by evaporation differ considerably.

Table 4-1

δ⁷Li values and major and trace element data of sampled river bed sediments (RBS) and sediment profiles

sample	depth (cm)	δ^7Li_{RBS} (‰)	Li_{RBS} (µg/g)	SiO_2 (%)	TiO_2 (%)	Al_2O_3 (%)	Fe_2O_3 (%)	MnO (%)	MgO (%)	CaO (%)	Na_2O (%)	K_2O (%)	P_2O_5 (%)	LOI (%)	TOC (%)	TIC (%)	Ba (µg/g)	Cr (µg/g)	Ga (µg/g)	Nb (µg/g)	Ni (µg/g)	Rb (µg/g)	Cs (µg/g)	Sr (µg/g)	V (µg/g)	Y (µg/g)	Zn (µg/g)	Zr (µg/g)
Lake Bangong																												
Nyak Co																												
B1-4		-2.2	41.6	n.a.	n.a.	7.9	2.7	0.04	1.7	22.0	1.0	1.6	n.a.	--			255	n.a.	n.a.	n.a.	n.a.	72	11	900	n.a.	n.a.	n.a.	n.a.
western basins																												
B2		-3.3	34.1	59	0.5	10.7	3.2	0.05	2.2	9.9	2.0	2.0	0.1	9.9	0.1	1.9	372	69	10	11	25	71	7	679	71	17	49	136
B4-1		-4.1	20.7	10	0.2	2.9	0.9	0.01	1.0	42.2	0.2	0.6	0.0	41.4	1.2	9.9	309	20	<10	<10	14	12	10	3284	37	<10	21	82
Catchment																												
northern catchment (Chiao Ho)																												
N1*		-4.3	44.7	41	0.5	10.1	3.8	0.07	1.9	18.8	0.8	2.1	0.1	20.1	0.5	4.3	452	53	12	12	28	87	26	1311	72	22	60	176
N3		-3.8	19.6	36	0.3	7.0	3.0	0.07	3.2	37.2	0.8	1.5	0.2	10.7	4.1	6.3	354	113	10	<10	23	70	14	650	49	16	42	92
southern catchment (Makha River)																												
S1*		-4.1	47.3																									
S3		-3.5	56.6	55	0.5	11.9	3.6	0.07	2.5	10.1	1.4	2.6	0.1	11.6	0.1	2.5	326	75	14	12	48	117	13	304	76	21	60	161
S4		-2.5	31.1	63	0.5	12.0	3.1	0.07	1.6	7.0	1.7	2.6	0.1	7.8	0.0	1.4	321	96	13	12	49	122		217	57	20	50	170
S5		-1.6	34.1	68	0.5	13.5	3.2	0.05	1.2	3.8	2.1	3.2	0.1	3.9	0.0	0.5	343	78	14	11	35	141		165	66	20	47	220
S6				58	0.5	13.2	4.1	0.12	2.1	7.2	1.6	2.7	0.1	9.7	0.5	1.5	318	72	14	11	41	116		266	68	22	59	145
S7		-0.6	24.2	69	0.2	12.8	1.7	0.02	0.7	3.6	2.4	2.5	0.1	7.0	1.7	0.5	321	40	13	<10	20	93		270	40	14	31	104
eastern catchment (Nama Chu)																												
E2		-1.5	31.3			7.5	2.7	0.04	1.5	20.8	1.0	1.4					208					62	8	1679				
E3		-2.4	26.3			5.7	2.1	0.03	3.6	29.5	0.5	1.2					199					57	16	832				
E4		6.3	48.4	47	0.3	9.3	2.0	0.04	4.5	15.7	1.7	2.2	0.1	17.0	0.0	4.0	316	41	<10	<10	26	86	8	988	36	15	32	107
Sediment profiles																												
profile 1 (N)																												
S1-1	0-5	0.5	48.0	14	0.1	2.8	1.0	0.02	2.0	39.3	1.0	0.8	0.1	34.0	0.7	8.5	334	19	<10	<10	10	15		4163	25	<10	20	101
S1-2	5-10	4.3	39.2	10	0.1	2.2	0.7	0.01	1.0	43.0	1.3	0.7	0.0	38.9	0.0	10.2	351	16	<10	<10	<10	<10		4498	15	<10	16	94
S1-3	10-15	2.9	30.9	8	0.1	2.0	0.7	0.01	0.7	45.5	0.9	0.6	0.0	39.4	0.3	10.0	370	<10	<10	<10	<10	<10		4897	20	<10	14	96
S1-4	15-20	0.3	21.2	7	0.1	1.7	0.6	0.01	0.7	46.6	0.4	0.4	0.0	40.7	0.2	11.0	380	10	<10	<10	<10	<10		5311	17	<10	11	93
S1-5	20-25	-3.3	16.1	8	0.1	2.0	0.6	0.01	0.7	49.0	0.3	0.4	0.0	37.8	1.3	9.7	403	15	<10	<10	<10	<10		5330	13	<10	16	107
S1-6	25-30	-4.2	19.8	11	0.1	3.1	0.9	0.02	0.9	43.0	0.3	0.7	0.0	38.8	0.0	10.1	379	22	<10	<10	<10	<10		4482	27	<10	22	92
S1-7	30-35	-4.6	19.2	10	0.1	2.8	0.9	0.02	0.8	45.3	0.2	0.6	0.0	38.2	0.5	9.9	395	18	<10	<10	10	<10		4838	17	<10	22	99
S1-8	35-40	-4.0	14.3	9	0.1	1.9	0.5	0.01	0.6	49.8	0.3	0.4	0.0	36.3	1.6	9.1	403	15	<10	<10	<10	<10		5243	<10	<10	16	110
profile 2 (S)																												
S2-1	0-3.5	1.2	39.6	61	0.6	12.9	4.5	0.07	3.6	4.3	1.3	2.4	0.1	8.6	0.8	0.7	333	99	16	12	50	108		209	87	25	69	172
S2-2	3.5-5	0.7	40.8	59	0.7	13.5	5.1	0.08	3.7	5.1	1.2	2.5	0.1	8.8	0.9	1.0	358	105	18	14	57	114		222	110	24	80	212
S2-3	5-8	-0.2	50.8	52	0.8	15.9	6.4	0.11	4.0	5.3	0.9	3.0	0.1	11.1	0.9	1.1	399	123	18	15	68	137		231	135	26	98	153
S2-4	8-11	-0.9	51.2	51	0.8	16.9	6.7	0.11	3.3	5.2	0.7	3.0	0.1	11.4	1.0	1.1	434	122	20	16	72	144		231	132	28	101	135
S2-5	11-15	-1.1	52.4	54	0.8	16.4	6.8	0.10	3.0	4.4	0.9	3.0	0.1	9.9	0.6	1.0	422	120	20	14	67	141		174	145	29	102	147
S2-6	15-20	-0.7	48.2	57	0.8	15.6	6.1	0.10	2.7	4.9	1.0	2.8	0.1	8.4	0.5	0.8	424	115	19	13	65	133		208	122	29	94	159
S2-7	20-21	-0.9	48.8																									
S2-8	21-27	-1.1	59.9																									

*: mouth of stream to lake; empty space: not analyzed; LOI includes TOC

4.5   RESULTS

4.5.1   Chemical composition of sediments and surface waters

Major and trace element data of sediments and surface waters are given in Table 4-1 and Table 4-2, respectively. Major elements in sediments from Lake Bangong catchment reflect the differences in the lithology with high CaO and low SiO_2 (7 to 41 %) mass fractions in lake and river bed sediments from the north and east but low CaO and high SiO_2 (55 to 61 %) and Al_2O_3 (11.9 to 16.9 %) mass fractions in the southern catchment.

Total dissolved solids (TDS) in the streams range between 146 and 643 mg L^{-1} and are substantially higher than the global average of 65 mg L^{-1} and higher than in mountainous streams, as well (Stallard and Edmond, 1983; Gaillardet et al., 1999b; Kisakurek et al., 2005; Dellinger et al., 2015). The ion compositions of all three inflows to Lake Bangong are characterized as Ca-Mg-Na-HCO$_3$-waters. The headwaters of the Indus resemble the chemical composition of the northern and southern inflow but Yarlung Tsangpo headwaters have considerably higher sulfate concentrations at the expense of alkalinity (Fig. 4-2).

4.5.2   Lithium isotopes and concentrations

Li mass fractions in the river bed and lake sediments from the lake catchment range from 19.6 to 56.6 µg/g (average: 35.4 µg/g; n=13), which resembles the average composition of the upper continental crust (e.g. Teng et al., 2004; Table 4-1). Suspended particles show higher Li mass fractions between 31.9 and 87.4 µg/g (average: 63.1 µg/g; n=5) consistent with a higher proportion of fine clay particles (Table 4-2). δ⁷Li values of river bed and lake sediments (Fig. 4-3) range from -4.3 ‰ to -0.6 ‰ (average: -2.8 ‰; n=12) and decrease towards the lake. Suspended particles from the northern and southern catchment range lower between -4.7 ‰ and -2.5 ‰ (average: -3.3 ‰; n=7) but have higher values from +1.7 ‰ to +10.6 ‰ (average: +6.5 ‰; n=5) in the eastern catchment and the lake basins.

Lithium in the streams range from 0.3 to 49.2 µmol L^{-1} and from 64.7 to 391.3 µmol L^{-1} in the basins of the Lake (Table 4-2). To the best of our knowledge, these are among the highest concentrations reported for streams (see supplement S4-2). δ⁷Li$_{DL}$ values of surface waters in the catchment (Fig. 4-3) range between +5.1 ‰ and +29 ‰, but the main channels display low values between +5.1 ‰ and +10.5 ‰. The highest and most variable δ⁷Li$_{DL}$ values in the streams are obtained from the southern catchment and the lowest from the northern catchment. δ⁷Li values in the Indus and the Yarlung Tsangpo range low between -4.1 ‰ and -1.9 ‰ in

132

suspended particles and +4.1 ‰ and +8.9 ‰ in the dissolved load resembling samples from the

Lake Bangong catchment (Table 4-2).

Table 4-2

Specific conductivity, pH, Li, O, H, and C isotope data, and element concentration data for dissolved load (DL) and Li isotope and concentration data for suspended particles (SP)

sample		SC	pH	δ^7Li_{DL}	Li_{DL}	δ^7Li_{SP}	Li_{SP}	$\delta^{18}O_W$	δD_W	$\delta^{13}C_{DIC}$	K	Na	Mg	Ca	Sr	B	Al	Mn	Fe	HCO_3	Cl	SO_4	NO_3	F	Si	TDS
		µS/cm		‰	µmol/L	‰	µg/g	‰	‰	‰	µmol/L	µmol/L	µmol/L	µmol/L	µmol/L	µmol/L	µmol/L	µmol/L	µmol/L	µmol/L	µmol/L	µmol/L	µmol/L	µmol/L	µmol/L	mg/L
Lake Bangong																										
Nyak Co																										
B1-1	lake	909	9.3	8.1	71.1			-3.9	-48.8	2.4	624	4741	2292	439	2.7	312	0.4	bdl	0.1	4338	2821	999	bdl	26	18	667
B1-2	lake	920	8.9	8.1	64.7			-3.5	-48.6	2.2	223	4654	2218	482	2.1	300	0.5	bdl	0.1	5390	2933	895	bdl	21	7	708
B1-4	near wetlands	1178	7.5	10.4	75.0			-6.7	-65.9	0.7	327	5394	2971	818	5.0	495	0.4	2.5	4.9	7925	3018	479	bdl	26	242	878
B1-5	near inflow Chiao Ho	1058	9.0	8.1	67.7	1.7	71.3	-11.0	-89.4	-1.6	547	4741	2427	1110	10.3	280	0.4	0.1	0.5	6931	2821	1488	bdl	53	445	900
B1-6	near inflow Chiao Ho	1032	8.4					-9.6	-79.4	-0.2										6682	2821	2446	11.3	42	160	
western basins																										
B2	lake	1757	9.0	10.0	138.8			-2.7	-43.1	2.6	483	11657	3501	357	1.4	680	0.4	bdl	0.1	6744	6826	2134	1.6	21	43	1245
B3	lake	2650	9.1	10.5	215.7			-1.9	-39.2	2.8	767	19182	4855	274	1.0	1069	0.4	bdl	0.1	8467	11875	3685	1.0	32	25	1891
B4-1	lake	3930	9.0	10.9	312.5	10.6		-3.4	-49.8	2.1	1177	32623	6501	574	2.7	bdl	0.4	0.1	0.4	12083	18898	5829	9.7	37	68	2944
B4-2	lake	4860	9.1	11.1	391.3			-0.7	-33.4	2.9	1501	39148	8105	192	0.6	bdl	0.3	bdl	bdl	13106	24681	7671	1.6	32	4	3575
B1-3	pond	2370	10.4	8.8	176.7			4.3	-13.1	-10.1	529	14746	5184	1003	13.1	796	0.5	bdl	0.1	1593	8011	7494	bdl	21	7	1627
Lake catchment																										
northern catchment																										
N1*	Chiao Ho	555	8.8	6.1	25.2	-3.2		-13.9	-100.2	-1.0	74	1662	876	1332	6.7	76	0.6	0.1	0.2	3686	1015	531	43.5	11	185	428
N2	tributary 4 (springwater)	645	7.6	5.8	32.1			-13.8	-99.0	-0.7	47	1805	979	1647	11.0	90	0.3	bdl	0.2	5012	1100	448	43.5	21	228	537
N3	tributary 5 (springwater)	286	8.8	5.1	4.1			-14.2	-98.7	-3.8	23	435	576	841	2.7	14	0.4	bdl	0.4	2666	189	93	17.7	11	167	237
southern catchment																										
S1*	Makha river	239	8.5	8.9	12.7	-4.7		-13.3	-99.3	-6.5	49	557	407	586	1.8	120	0.5	0.1	0.7	1875	296	135	11.3	2	68	186
S8°	Makha river	423	7.5	8.1	33.0			-12.5	-99.0	-5.2	69	1174	605	773	2.6	302	0.5	0.2	1.4	2885	810	146	0.8	16	78	231
S2	Makha river (after trib 1)	307	8.9	10.5	18.7	-4.3		-13.6	-102.9	-7.0	69	857	568	716	2.1	193	1.0	0.1	1.1	2095	496	216	1.3	21	93	294
S3	Makha river	221	8.9	9.0	12.4	-3.4		-13.6	-107.8	-6.5	51	565	473	459	1.6	118	0.6	bdl	0.3	1545	254	193	bdl	3	36	167
S4	Makha river	225	8.3	14.2	0.3	-2.5	60.7	-14.7	-109.3	-5.8	41	183	333	866	1.7	bdl	0.4	0.1	0.8	2149	59	99	24.2	2	150	191
S5	Tributary 3	179	8.0	10.0	1.8	-3.1	87.4	-17.3	-129.0	-6.9	43	265	157	691	1.0	31	1.1	0.1	0.5	1389	164	177	29.0	2	85	144
S6	ributary 1	263	8.4	9.0	11.4			-12.4	-97.8	-8.2	56	587	485	724	2.0	121	0.7	0.1	0.9	2469	237	102	bdl	2	132	225
S7	tributary 1 (pond)	141	9.6	18.2	0.9	-2.9	31.9	-12.4	-89.3	-9.0	33	222	218	444	1.2	19	0.5	0.1	0.7	818	87	111	3.2	2	139	93
S9	tributary 2	172	8.2	12.0	8.7	-2.5	64.0	-14.6	-105.2	-6.2	41	326	207	569	1.5	bdl	bdl	0.1	bdl	1612	93	91	17.7	2	139	147
eastern catchment																										
E1*	Nama Chu	814	9.1	7.4	44.6	7.7		-8.6	-77.4	0.0	151	3741	1909	674	9.1	136	0.5	0.2	0.3	3633	2200	1166	1.6	37	256	577
E2	Nama Chu	786	9.3	7.5	42.6	7.7		-8.4	-75.7	0.1	143	3741	1917	599	8.6	125	0.5	0.1	0.7	3327	2200	1343	bdl	37	274	572
E5	Nama Chu	855	8.8	7.7	49.2			-7.9	-75.0	-7.1	141	4045	2057	636	12.1	138	0.7	0.2	1.0	4155	2257	1322	bdl	42	303	634
E3	Nama Chu	731	8.4	6.8	28.9	4.9		-13.0	-91.5	0.7	113	2540	1399	1347	17.8	88	0.4	bdl	0.3	4827	1439	916	14.5	37	281	584
E4	salt water pond	41600	8.8	29.0	234.6					6.2	4692	165652	32709	1397	12.0	bdl	bdl	1.8	0.2	22786	299834	541	bdl	bdl	310	bdl
Western and southern Tibetan Plateau																										
Indus River																										
Ind1	main channel	234	8.5	6.3		-2.1		-15.3	-121.7	-4.6	50	620	190	750	140.0			bdl	0.5	1800	140	300	11.3		140	194
Ind2	main channel	248	8.4	6.5	4.4	-2.0		-15.0	-122.5	-4.3	50	680	230	750	140.0			bdl	0.4	1700	170	330	11.3		140	195
Ind3	main channel	318	8.1	8.9	3.9			-14.1	-113.2	-6.1	60	880	220	970	210.0			0.7	0.5	2600	280	280	21.0		210	262
Ind4	tributary	328	8.2	16.3	2.8	-3.1		-13.7	-113.6	-6.2	70	680	240	1100	230.0			0.7	0.7	2800	310	230	1.6		230	272
Ind5	main channel	297	8.7	7.2	9.6	-1.9		-15.2	-119.8	-5.6	60	800	350	860	170.0			bdl	bdl	2100	280	370	11.3		170	237
Yarlung Tsangpo																										
Bra 1	main channel	214	9.0	5.6	7.6	-4.1		-15.6	-122.9	-4.4	59	548	271	749	2.2			bdl	0.7	1468	226	239	3.2			172
Men 1	Men Chu (tributary)	294	8.5	6.3	4.2			-19.3	-149.0	-3.1	38	261	296	1347	2.9			bdl	0.5	2246	85	406	19.4			248
Bra 2	main channel	354	8.2	4.1	14.9	-3.9		-19.2	-149.7	-3.3	51	800	391	1497	4.8			0.9	0.7	2100	169	833	19.4			304
Bra 3	main channel	303	8.5	4.9	9.2	-3.8		-17.7	-143.1	-3.2	43	613	362	1297	2.3			bdl	1.3	2100	169	500	16.1			259
Bra 4	main channel	343	8.3	4.5	8.8	-3.2		-17.9	-142.4	-2.3	38	374	370	1038	2.9			bdl	bdl	2009	141	677	16.1			253
Bra 5	main channel	431	8.5	6.1	7.2	-2.9		-17.3	-135.9	-6.4	38	383	588	1447	3.4			bdl	bdl	2106	113	1083	46.8			319
Bra 6	main channel	290	8.4	5.4	7.3	-3.2		-18.7	-147.1	-4.4	38	409	346	1023	2.3			bdl	0.5	2018	113	593	37.1			244
Bra 7	main channel	289	8.5	6.7	8.0	-2.8		-18.4	-144.2	-4.7	43	522	428	1010	2.3			bdl	bdl	1885	141	583	45.2			241

*: mouth of stream to lake; °: dead arm, with link to Makha river; inflows to lake are partly dammed by hydroelectric power plant are road construction before samles N1, S1, and E2, respectively; bdl: below detection limit; empty space: not analyzed
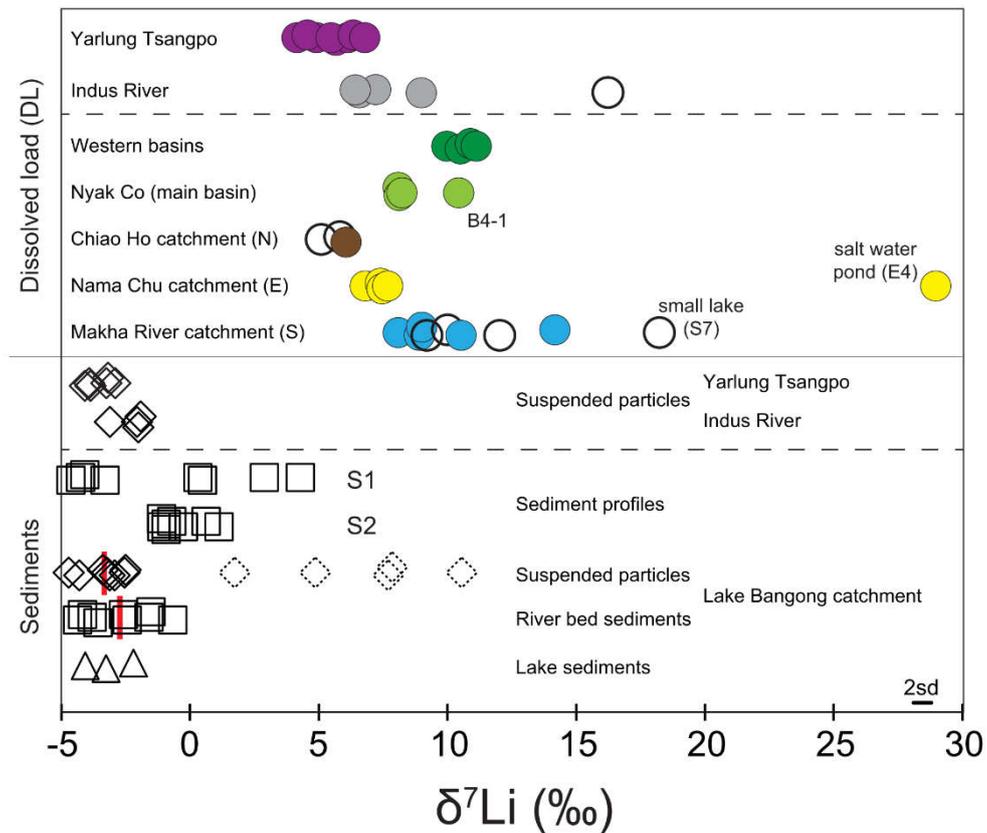
Figure 4-3

δ⁷Li values (in permill relative to L-SVEC) of analyzed surface waters and sediments. Filled circles of stream samples indicate samples from main channel and open circles tributaries. Red bar represent average of river bed and suspended sediments. Dotted diamonds indicate suspended sediments from the Nama Chu and lake basin (samples are excluded from average).

4.5.3 Oxygen, hydrogen, and carbon isotopes

δ¹⁸O and δD values of stream waters from the southern and northern catchment, sample E3 from the Nama Chu in the east and the upper reaches of the Indus and the Yarlung Tsangpo River range from -19.3 ‰ to -12.4 ‰ and -149.7 ‰ to -89.3 ‰ (Table 4-2), respectively, and fall closely around the Local Meteoric Water Line (LMWL; Guo et al., 2017). In contrast, samples from Nama Chu and samples from the basins of Lake Bangong range higher from -8.6 to -0.7 ‰ in δ¹⁸O and from -77.4 ‰ to -33.4 ‰ in δD and are shifted form the LMWL (Fig. 4-4).

135

Streams in the southern catchment display the lowest $\delta^{13}C_{DIC}$ values from -9.0 to -5.2 ‰ (Table 4-2). The northern catchment exhibits higher values between -3.8 and -0.7 ‰. Samples from the Nama Chu and basins of Lake Bangong show the highest values around 0 ‰ and +2.5 ‰, respectively.
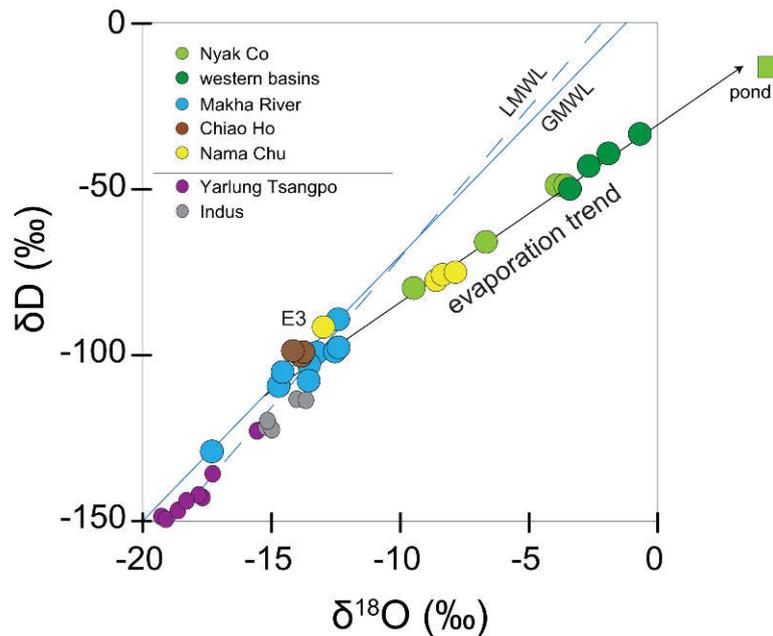

Figure 4-4

$\delta^{18}O$ vs δD diagram of surface waters: surface waters from the Indus, Yarlung Tsangpo, Makha River and Chiao Ho catchments as well as sample E3 plot on the Local (LMWL) and Global (GMWL) Meteoric Water lines. Nama Chu and lake water samples plot on the calculated evaporation trend based on local climatic humidity and temperature.

4.6 DISCUSSION

4.6.1 Lithium in fluvial sediments
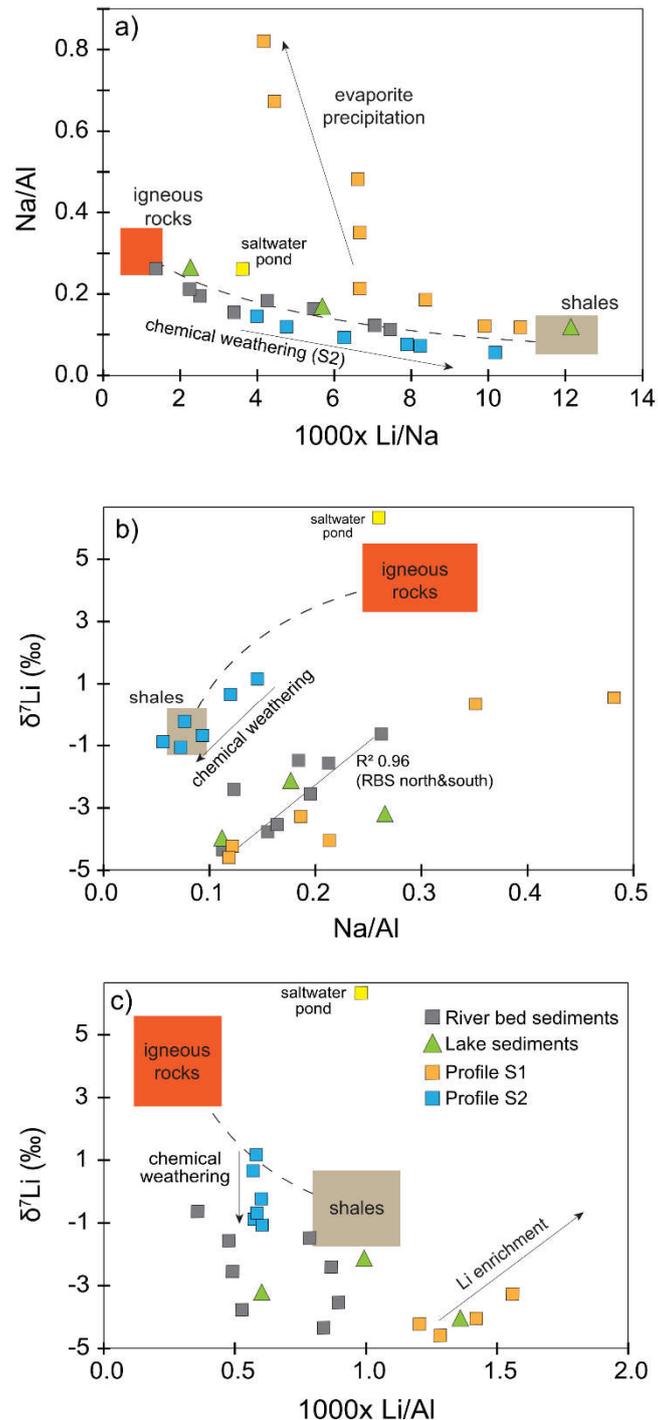
Figure 4-5

(a) Variations of Na/Al vs. 1000•Li/Na mass fractions; **(b)** δ⁷Li values vs. Na/Al, **(c)** δ⁷Li values vs. 1000•Li/Al. Mass fractions are not corrected for carbonated content. Grey dotted lines are mixing hyperbola between an igneous and sedimentary (shale) endmember (endmember values for granitoids from the catchment from Liu et al. (2014) and global endmember values are compiled in Dellinger et al., 2014).

In the following, we discuss δ^7Li variations among river sediments in the catchment of Lake Bangong and among river sediments of the upper Indus and Yarlung Tsangpo rivers to infer processes controlling chemical weathering and physical erosion in the area.

4.6.1.1 River beds

River bed sediments in the Lake Bangong catchment display δ^7Li values between -4.3 ‰ and -0.6 ‰ (Table 4-1). These values are among the lowest reported so far for river bed sediments (see S4-3). Lithium isotope ratio variations are either induced by mixing of distinct proportion of bedrock fragments with varying δ^7Li (e.g. Millot et al., 2010c; Dellinger et al., 2014; Wang et al., 2015), grain size sorting (e.g. Dellinger et al., 2014; Dellinger et al., 2017), or recent chemical weathering and preferential fractionation of ^{6}Li into secondary minerals, e.g. clays (e.g. Vigier et al., 2008). A control by the source would imply that the low δ^7Li values are inherited from old, recycled sediments, thus, old weathering processes. Often, coarse river bed sands are collected as a proxy for the average bed rock composition (e.g. Dellinger et al., 2014). In this study, river bed sediments substantially contain fine materials. In connection with the low δ^7Li values the river bed sediments perhaps represent weathered material but not the average bedrock composition. Mass fraction ratios of Na/Al versus Li/Na in river bed, lake, and profile S2 sediments exhibit a negative correlation, which may reflect mixing of igneous and shale rock fragments (Fig. 4-5a). Lithium isotopes co–vary with the chemical index of alteration (CIA = [Al$_2$O$_3$/(Al$_2$O$_3$+Na$_2$O+CaO$_{silicate}$+K$_2$O)]•100), K/(Na+K), Fe/(Na+Fe), and Na/Ti ratios (Fig. 4-6), which likewise could be explained by mixing of shale and magmatic rock fragments. However, explaining the δ^7Li variations as simple mixtures requires unusually low δ^7Li values of about 0 ‰ for the felsic igneous and about -5 ‰ for the sedimentary rock endmember. This is considerably lower than the reported global average of δ^7Li values for felsic igneous rocks (+4 ± 2 ‰) and sedimentary rocks (0 ± 2 ‰) (Magna et al., 2006; Tomascak et al., 2008; Schuessler et al., 2009; Teng et al., 2009; Qiu et al., 2011; Dellinger et al., 2014; Tomascak et al., 2016). Such low values have been reported for some small areas (Teng et al., 2004; Qiu et al., 2009) and the Indian lower crust beneath the Himalaya (Tian et al., 2017), hence, cannot be completely excluded. However, beside samples that are proposed to reflect the Indian lower crust (Tian et al., 2017), investigated lithologies on the Tibetan Plateau resemble common upper crust compositions in δ^7Li (Tian et al., 2017; Weynell et al., 2017; Tian et al., 2018). Relatively constant Li/Al (Fig. 4-5c) and Al/Si (see S4-4) ratios are inconsistent with grain size induced δ^7Li variations or mixing of different lithologies having distinct δ^7Li values (e.g. Pogge von Strandmann et al., 2017b). Furthermore, large granitoid bodies prevail in the lower reaches and

sedimentary rocks (flysch sediments) in the upper reaches of the southern sub-catchment (Gourbet et al., 2017). A lithological control on Li in river bed sediments would result in low δ^7Li values in the upper and high values in the lower reaches, opposite to the observed decrease from +1.2 ‰ (uppermost layer of profile S2) or -1.6 ‰ (upper reaches of Makha River) to -4.0 ‰ close to the lake (Table 4-2). For this reasons, we consider a lithological control on Li isotope variations unlikely.
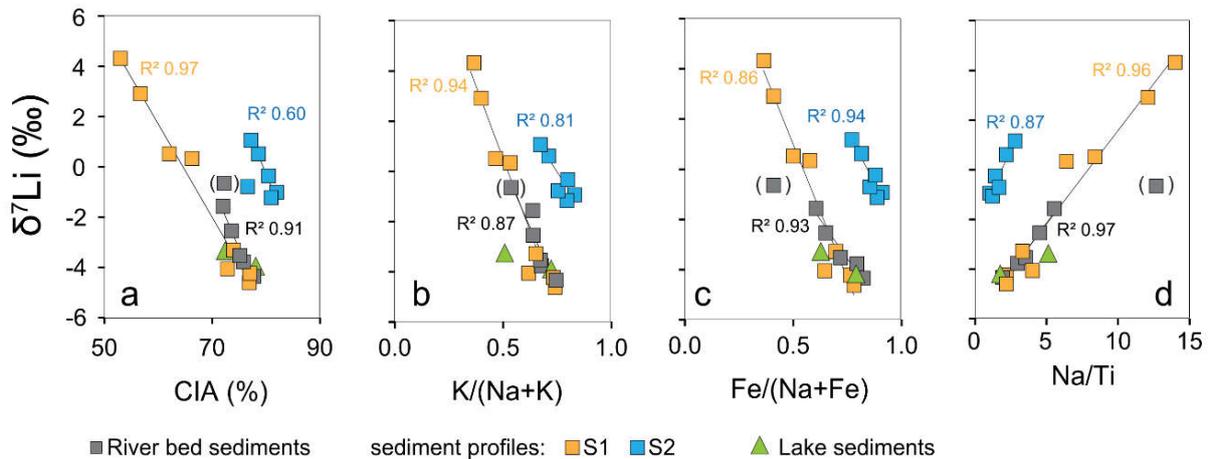

Figure 4-6

δ^7Li values of river bed sediments, sediments from the two profiles (ancient fluvial sediments), and lake sediments against weathering intensity proxies: higher values indicate a higher intensity for the **(a)** CIA, **(b)** K/(Na+K), and **(c)** Fe/(Na+Fe) ratio and a lower intensity for the **(d)** Na/Ti ratio. River bed samples from the eastern sub-catchment are excluded due to intense mineral precipitation in the Nama Chu catchment.

The above mentioned elemental ratios are common proxies for the weathering intensity (e.g. Stallard and Edmond, 1983; Edmond et al., 1995; Wei et al., 2006). CIA values up to 78 % in the river bed sediments indicate intense weathering ($CIA_{granite}$ ~55 %; CIA_{shale} ~70 %). As a lithological control on Li isotope variations is considered unlikely, the co-variation of Li isotopes with weathering intensity indicators (Fig. 4-6) provides evidence for a control of Li isotope variations by the weathering intensity. This is in agreement with several studies that named Li isotopes in the weathering environment as a proxy for the weathering intensity (e.g. Huh et al., 2001, Kisakurek et al., 2005; Millot et al., 2010c; Dellinger et al., 2015). Thus, significant weathering and an increasing weathering intensity towards the center of Lake Bangong catchment is indicated. We have to concede that some of the Li isotope variations in the river bed sediments are provenance induced but the low δ^7Li values, the relative constant Li/Al and Al/Si ratios, the systematic decrease of δ^7Li values and increase of the weathering

intensity proxies towards the lake in the southern catchment is best explained by continuous chemical weathering.

4.6.1.2 Alluvial fans

The sediment profiles from alluvial fans in the upper and lower reaches of the catchment provide further information on Li isotope variations and weathering. Sediment profile S2 is located in the upper reaches of the southern sub-catchment (Fig. 1-1b). The profile consists of muddy, clayey intensely weathered sediments (CIA: 73 to 82). δ^7Li values decrease in the upper 20 cm and remain constant in the lower part. Some of the δ^7Li variation in profile S2 might be due to grain size sorting during transport as indicated by a weak correlation with Al/Si (Fig. 4-7a; see S4-4; Lupker et al., 2011). However, a sodium mass fraction decrease in the upper 10 cm and accumulation of Al, Ti, Fe, Rb, and Li below 10 cm is consistent with leaching of alkali elements in the uppermost section and clay mineral formation in the lower sections. Together with upward increasing TOC abundances (Fig. 4-7a) in-situ weathering and soil formation is indicated. δ^7Li values of sediments from profile S2 correlate with weathering intensity indicators (Fig. 4-6). Obviously, significant weathering of sediments takes place in alluvial plains, contributing to the Li isotope variation among sediments. However, δ^7Li values in the lower section are constant at around -1 ‰ and are not as low as δ^7Li values of river bed sediments near the lake. This implicates continuous weathering of sediments in floodplains that formed along major streams and rivers. Chemical weathering of profile S2 sediments creates trends that resemble those of the river bed sediments in Fig. 4-4a, b, and c, giving further indication that Li isotope variations in the river bed sediments are induced by modern chemical weathering.

Sediment profile S1 close to Lake Bangong highlights additional processes (Fig. 4-1b). High CaO contents around 40 % are related to carbonates within the sediments (Table 4-1). Carbonate precipitation around roots and concretions in the profile identify their diagenetic origin. Subtracting the $CaCO_3$ content from the bulk sediments leads to Si, Al, Fe, Mn, and Ti contents that resemble sediments from the river beds and profile S2. After correction for carbonates Na contents increase upwards from around 1.3 to 6.7 % and lithium contents increase upwards from around 90 to 210 µg/g (for details on carbonate correction see supplement S4-5), which are by far the highest mass fractions determined for sodium and lithium in sediments from the catchment. The Li/Al (Fig. 4-7b), Li/Si, Na/Al (Fig. 4-5a), and Na/Si ratios strongly increase towards the top layer. Hence, enrichment of Li and Na in the uppermost section is explained, like the high carbonate content, by precipitation from soil

140

waters. The diagenetic addition of sodium corrupts the CIA index and other sodium-based proxies (Fig. 4-6). Towards the top increasing δ^7Li values likely reflect precipitation of Li from aqueous solutions with δ^7Li values around +5 ‰. Similar δ^7Li values have been detected for stream waters close to profile S1. If local surface waters are the source of the precipitated Li in profile S1 some element fractionation is required because the Li/Na ratios of surface waters are considerably higher. Alternatively, thermal waters might have leached Li from granitoids at depth with low Li/Na ratios and δ^7Li values of about +4 ‰ and transported Li and Na to the surface. So far, emerging thermal waters were not reported for the catchment but the active Bangong Co fault extents north of the lake basins, close to profile S1 (Gourbet et al., 2017). Thus, hydrothermal activity is conceivable in this area. Li isotope and element ratios of sediments below 20 cm resemble river bed sediments from the north and south (Fig. 4-5 and 4-6). Hence, Li isotope and elemental variations in profile S1 have been altered by precipitation of carbonates and/or chlorides from ascending and near surface evaporated aqueous solutions.

4.6.1.3 Suspended particles
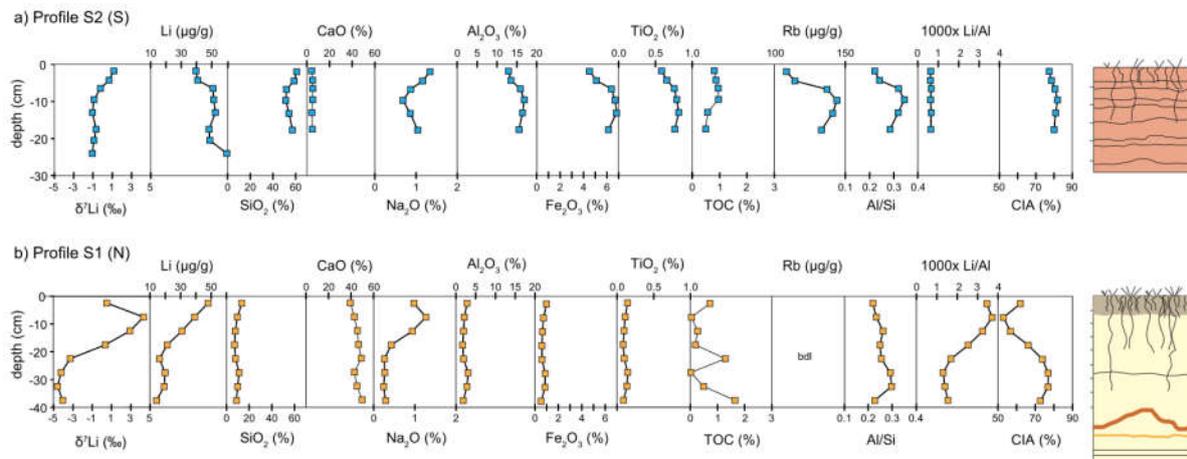
Figure 4-7

δ^7Li values, element, and TOC mass fractions, Al/Si ratio (proxy for grain size), Li/Al, and CIA value variations with depth in the two alluvial fans. The Al/Si ratio is used as a grain size proxy and the Li/Al ratio shows relative Li enrichment (trend is similar for Na/Al). Ca$_{silicate}$ was calculated from total inorganic carbon and total CaO content. Profile sketches illustrate **(a)** bright, carbonate rich sediments with brownish (fossil soil?) horizons and **(b)** continuous clayey sediments with layers slightly differing in brownish-red color.

The suspended load of small streams is usually not well homogenized with regards to grain size or spatial variability and still mirrors the heterogeneity of the lithology (Gaillardet et al., 1999a; Weynell et al., 2017). For example, suspended particles collected in the eastern catchment and lake basins exhibit extremely high δ^7Li values from +1.7 ‰ to +10.7 ‰

(Table 4-2). Such high δ^7Li values were reported for some granites and ophiolites (Tomascak, 2004). Similar lithologies are located close to these sample locations (Liu et al., 2014). Suspended particles in the upper reaches of the southern catchment display lower δ^7Li values from -4.7 ‰ to -2.5 ‰ compared to river bed sediments. This is explained by a higher content of clay particles with low δ^7Li in the suspended load. The offset diminishes towards the lake, Li isotope compositions of river bed sediments and suspended particles resemble each other at the mouth of the Chiao Ho and Makha River. This implies that either suspended particles are just suspended river bed sediments at locations close to the lake or river bed sediments at the mouth contain a large fraction of fine material. δ^7Li values of lake sediments display similar low values (Table 4-1), thus, suspended particles and river bed sediments close to the lake closely average the eroded material that is deposited in the lake basin.

δ^7Li values of suspended particles from the inflows of Lake Bangong, the Indus headwaters, and Yarlung Tsangpo resemble each other (Table 4-2). These samples are likewise considered representative for the eroded material and provide evidence for a similar weathering intensity on the western and southern Tibetan Plateau despite eastwards increasing annual precipitation amounts.

In summary, the low δ^7Li values in solid samples indicate significant weathering of fluvial sediments in the Lake Bangong catchment despite the cold and dry climate, very little vegetation, and weak soil formation. This is explained by low erosion rates and multiple processing of sediments. In such a geomorphic regime sediment transport is limited to high elevations, major streams and rivers. Along the major rivers sediments are multiple weathered in floodplains before deposition in the Lake Bangong basin.

4.6.2 Lithium in surface waters

4.6.2.1 Lithium sources

The Riverine Li concentrations in the Lake Bangong catchment, the upper Indus, and the Yarlung Tsangpo are among the highest reported for rivers worldwide (see S4-2). In order to assess Li behavior during silicate weathering the contribution of other Li sources has to be estimated. Samples from the Nama Chu and the lake basins display the highest Li concentrations in combination with the highest δ^{18}O and δD values (Table 4-2). δ^{18}O and δD values of Nyak Co samples indicate an evaporative lake water loss of 69 %, which increases to around 86 % at the westernmost sample location (see S4-6 and Wen et al., 2016). Lake and Nama Chu samples fall on an evaporation trend based on the climatic parameters of the catchment in the δ^{18}O-δD-diagram (Fig. 4-4; for details on calculation of the evaporation trend

see chapter 2.6.2). Hence, the considerably higher Li concentrations in the Nama Chu and the lake basins compared to the other surface waters result from strong evaporation.

The samples from the Makha River and Chiao Ho as well as the upper Indus and the Yarlung Tsangpo fall closely around the Local Meteoric Water Line (Fig. 4-4), thus, these river waters are not substantially affected by evaporation. However, Li concentrations in these rivers are still remarkable high (see S4-2). The sources of dissolved Li in these samples are closer explored in the following. The contribution of lithium from precipitation and anthropogenic activities are assumed negligible as the study area is nearly unpopulated and far away from industrial areas and annual precipitation is low. Dissolution of calcite and dolomite contributes around 80 % to the dissolved ion load and chlorine around 10 to 20 % to the anion budget of the rivers (Fig. 4-2 and S4-7). Marine sedimentary rocks cover a large part of the study area, which may host evaporite sequences. Continental evaporites can form in discontinuous permafrost or hyper-arid climates (Wang et al., 2015). Thus, dissolution of carbonates or evaporite minerals may contribute Li.

The fraction of Li derived from carbonates or evaporites ($Li_{calculated}$) is calculated with the calcium or chlorine concentration of each sample ($[X]_{sample}$) and the respective $(Li/Ca)_{carb}$ and $(Li/Cl)_{eva}$ ratio (Li/X) of carbonates or evaporites.

$$Li_{calculated} = [X]_{sample} \cdot (Li/X) \; (\mu mol/L) \qquad\qquad (4\text{-}I)$$

Less than 1 % of Li is derived from carbonates. The calculated contribution from marine evaporites is negligible (< 0.2 %), and continental evaporites may contribute up to 10 % Li to the ion budget of the Makha River, Chiao Ho, upper Indus, and the Yarlung Tsangpo (for calculation details see S4-8). This implies that most of dissolved Li in these rivers has to be solubilized from silicates.

The 1000•Li/Na ratio between 5 and 30 in the Chiao Ho and Makha River are higher than reported for granitoids in the Lake Bangong catchment (around 2 to 3), common sedimentary rocks (around 10 to 20), and the river bed sediments (between 1 and 8; see S4-9). Congruent weathering generates Li/Na ratios in the range of weathered rocks or sediments. Incongruent weathering would produce even lower Li/Na ratios as Li is significantly incorporated into secondary minerals unlike Na. Thus, weathering of rocks or sediments cannot explain the high Li/Na ratios. Such high Li/Na values have been reported solely for thermal waters (e.g. Tomascak et al., 2003; Millot and Négrel, 2007; Millot et al., 2011) including Himalayan and Tibetan Plateau hot springs (Kisakurek et al., 2005; Weynell et al., 2016; see S4-9). Some

water/rock interactions at elevated temperatures, e.g. albitization, removes Na but little Li from aqueous solutions. By far the highest Li/Na ratios were detected in samples in the middle and lower reaches of the Makha River and the lower reaches of the Chiao Ho. A hydrothermal contribution is indicated and may explain high Li concentrations (Table 4-2). This implies that riverine Li is either solubilized in the weathering zone by chemical weathering or in the basement by hydrothermal dissolution. A correction for the contribution of Li provided by thermal waters is not possible as endmember values are not available for this area. An emergence of thermal waters to the surface was not observed or reported for the catchment of Lake Bangong. Major element compositions of nearby geothermal fields (Fig. 4-1a), which are assumed to resemble thermal waters from Lake Bangong area, considerably differ from non-evaporated streams in the catchment (Fig. 4-2; Ahmad et al., 1998; Shen et al., 2011). This contradicts admixing of hydrothermally derived ions to the streams but reveals alteration of their ion composition. Alteration of large quantities of hydrothermally provided Li in the weathering zone was shown for the catchment of Lake Donggi Cona on the northeastern Tibetan Plateau (Weynell et al., 2017). Here, thermal waters supply large amounts of Li, which mix with solubilized Li from the weathering zone. Subsequently, the Li mix is processed similar to hydrothermally-unaffected solutions in the weathering zone (regarding fraction of Li removed from solutions and isotopic fractionation). Similar to the catchment of Lake Bangong, soils in the catchment on the northeastern plateau are also thin, poorly developed, and under the influence of discontinuous permafrost. For this reason, we propose that riverine Li in Lake Bangong catchment was also processed in the weathering zone and reflects silicate weathering processes and not hydrothermal admixing.

Ahmad et al. (1998), Karim and Veizer (2000), and Hren et al. (2007) showed that the chemical composition of Indus headwaters and Yarlung Tsangpo samples is dominantly derived from weathering of carbonate and silicate rocks, and any hydrothermal contribution is barely visible. Thus, weathering of silicate rocks is the source of most Li in the upper Indus and Yarlung Tsangpo because the contribution from carbonates to the dissolved Li flux is minor (see above and e.g. Kisakurek et al., 2005).
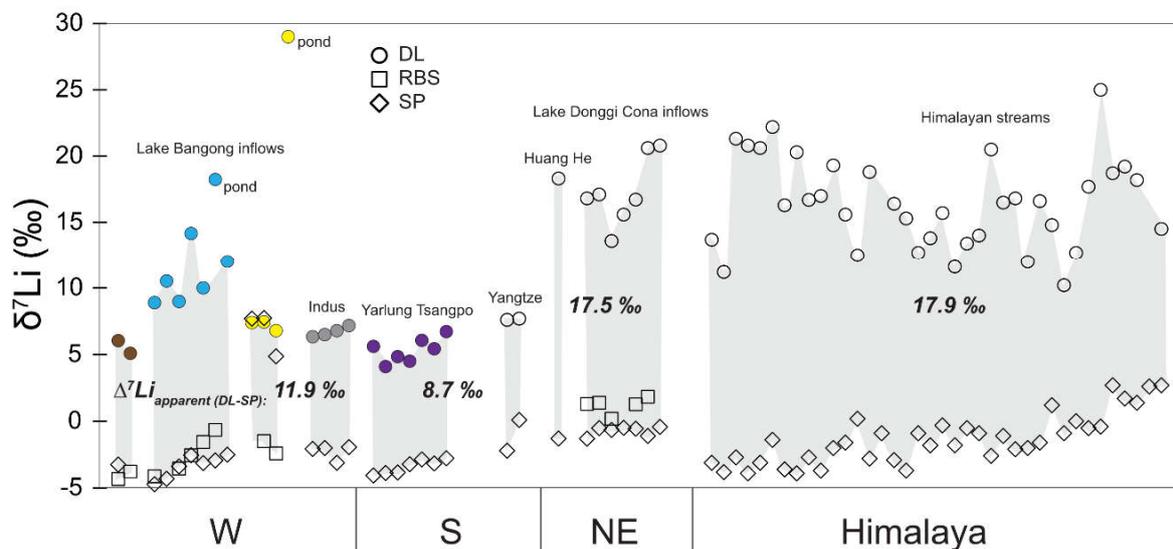
Figure 4-8

δ^7Li values of rivers and suspended particles of investigated samples, Yangtze (Wang et al., 2015), Huang He, Lake Donggi Cona catchment (Weynell et al., 2017), and Himalayas (Kisakurek et al., 2005) are shown. Large numbers reflect average apparent isotope offset for each region (see Table S4-4).

4.6.2.2 Lithium isotopes

The average δ^7Li values of the major inflows of Lake Bangong are +6.1 ‰ and +8.9 ‰. Similar low δ^7Li values have been detected for the Indus headwaters and Yarlung Tsangpo (Fig. 4-8). The controlling processes are explored next.

Congruent solubilization (S_{BR}) of lithium from bedrock causes little or no isotope fractionation (Pistiner and Henderson, 2003) whereas preferential uptake of ^{6}Li during partitioning (P) of lithium into secondary minerals is accompanied by a strong isotope effect (Vigier et al., 2008). Hence, the ratio of Li solubilized from primary minerals relative to the fraction of Li partitioned into secondary minerals, the P/S_{BR} ratio, defines δ^7Li. It is required to consider the net incorporation of Li (P_{net}), thus, the difference between Li incorporated and Li re-solubilzed from secondary minerals ($P_{net} = P - S_{sec}$; see Fig. 4-9a). Further, the involved fractionation factor determines δ^7Li$_{DL}$. An isotopic fractionation Δ^7Li$_{DL-sec}$ of about +17.5 ± 1.0 ‰ between solution and secondary minerals at low temperatures is reported from experiments (Vigier et al., 2008; Millot et al., 2010b; Wimpenny et al., 2015) and modeling using field data (Chan et al., 1992; Dellinger et al., 2015; Weynell et al., 2017). The estimated isotope fractionation is larger than the apparent isotope fractionation ($\Delta_{DL-SP} = \delta^7Li_{DL} - \delta^7Li_{SP}$)

145

of +14.2 ‰ and +9.3 ‰, which reflect the observed difference between dissolved Li and Li in suspended sediments in the southern and northern catchment of Lake Bangong, respectively (see Table S4-4). Dellinger et al. (2014 and 2017) have shown that Li in suspended sediments is a mixture of secondary minerals and bedrock fragments, hence, the offset does not represent the "true" isotope fractionation between solution and related secondary minerals (Fig. 4-9a and b).

The P_{net}/S_{BR} ratio, the fraction of lithium incorporated in secondary minerals or rather remaining in solution f_{DL} (F_W/S_{BR}; Fig. 4-9a) in the catchment of Lake Bangong can be calculated with a simple mass balance equation. In and out going lithium fluxes to/from the involved solution (P_{net}; S_{BR}; F_W: flux of dissolved Li out of the weathering reactor) and the pool of secondary minerals (P; S_{sec}) are assumed at steady state (see S4-10).

$$S_{BR} \cdot \delta^7 Li_{BR} = P_{net} \cdot \delta^7 Li_{sec} + F_W \cdot \delta^7 Li_{DL} \qquad (4\text{-}II)$$

Rearranging equation 4-II yields the fraction of lithium remaining in solution (see S4-10)

$$f_{DL} = 1 - \left(\frac{\delta^7 Li_{DL} - \delta^7 Li_{BR}}{\Delta^7 Li_{DL\text{-}sec}} \right)$$

δ^7Li data for the bedrock is not existent for the catchment and river bed sediments in the catchment are not usable as bedrock proxy (see 4.6.1.1). For the bedrock a $\delta^7 Li_{BR} > +1.2$ ‰ is constrained by the uppermost sediments of profile S2. High δ^7Li values of suspended sediments in the Nama Chu and lake basins identify lithologies with δ^7Li up to +10.7 ‰, however, we consider them as not representative as they likely represent small rock-bodies of ophiolites and sandstone (see S4-1). Most river bed sediments consist of quartz, feldspar, biotite, amphibole, illite/muscovite, chlorite, and carbonate minerals (Table S4-3), beside carbonates similar to potential granitoid source rocks of the catchment (Liu et al., 2014). This indicates weathering of granitoids, which have on global average somewhat higher δ^7Li values around +3 ‰ (Magna et al., 2006; Schuessler et al., 2009; Teng et al., 2009). A δ^7Li value between 0 ‰ and +3.0 ‰ is assumed as sedimentary rocks and granitoids are the main Li bearing lithologies. The Makha River and Chiao Ho with dissolved δ^7Li values of +8.9 ‰ and +6.1 ‰ close to Lake Bangong integrate over the two sub-catchments. For the incorporation of Li in clay minerals an isotope fractionation of $\Delta^7 Li_{DL\text{-}sec} = +17.5$ ‰ is used (see above) as we assume batch fractionation. With these values we have calculated that around 58 ± 20 % and 74 ± 15 % of initially

solubilized Li remains in solution in the southern and the northern sub-catchment, respectively (see Table S4-5). The large uncertainty reflects the large assumed range for the bedrock δ^7Li. However, a large fraction of initially solubilized Li is not incorporated into secondary minerals, keeping the δ^7Li of streams low.

A lower f_{DL} indicates more incorporation into secondary minerals in the southern compared to the northern catchment. $\delta^{13}C_{DIC}$ values in the southern catchment are substantial lower compared to the northern sub-catchment (Table 4-2). Low $\delta^{13}C_{DIC}$ values between -9.0 ‰ and -5.2 ‰ reveal CO_2 from plant respiration or soil air as major constituent of dissolved inorganic carbon in the streams (Clark and Fritz, 1997). Acidity derived from soil air or organic acids drives weathering reactions (West et al., 2005). Most precipitation events are localized in the high-relief upper reaches of the south (Guo et al., 2017b), which results in a precipitation gradient from south to north (Mukhopadhyay and Dutta, 2010). Thus, the lower f_{DL} and higher dissolved δ^7Li values in the south may result from more precipitation resulting in stronger vegetation cover, clay formation, and, finally, Li exchange.

Beside the fraction of lithium incorporated into clay minerals, the composition of the weathering substrate is also affecting Li isotope ratios of dissolved Li. The sediments from the upper reaches are reworked and deposited multiple times in floodplains before reaching Lake Bangong. These "cannibalised" sediments provide an increasingly low δ^7Li substrate for weathering at lower reaches of Lake Bangong catchment for example. In summary, the low δ^7Li values of dissolved lithium in streams at Lake Bangong, Indus headwaters, and Yarlung Tsangpo are caused by (1) incorporation of a relatively small fraction of solubilized Li into clay minerals and (2) weathering of low-δ^7Li sediments.

δ^7Li values and Li concentrations increase simultaneously in the lake basins and in the Nama Chu between sample sites E3 and E5 (Table 4-2). This trend is not observed within the Makha River and Chiao Ho. The progressively increasing Li concentrations in the lake basins and at location E5 in the Nama Chu are caused by evaporation (Fontes et al., 1996; see section 4.6.2.1). The reason for increasing δ^7Li values during evaporation is not evident. δ^7Li values and Li/Cl ratios in the lake basins are negatively correlated (R^2 0.912; see S4-11), indicating Li isotope fractionation during relative Li removal. Mineral saturation indices progressively increase in Nama Chu and the lake basins, likely induced by the evaporative increase of the ionic strength (Table S4-6). For this reason, the increasing δ^7Li values and the relative Li removal in Nama Chu and the lake basins maybe represent Li incorporation into or adsorption onto transformed secondary minerals. Further research is required to understand the Li isotope

fractionation within the strongly evaporated surface waters, which alters the Li isotope composition coming from weathering processes.
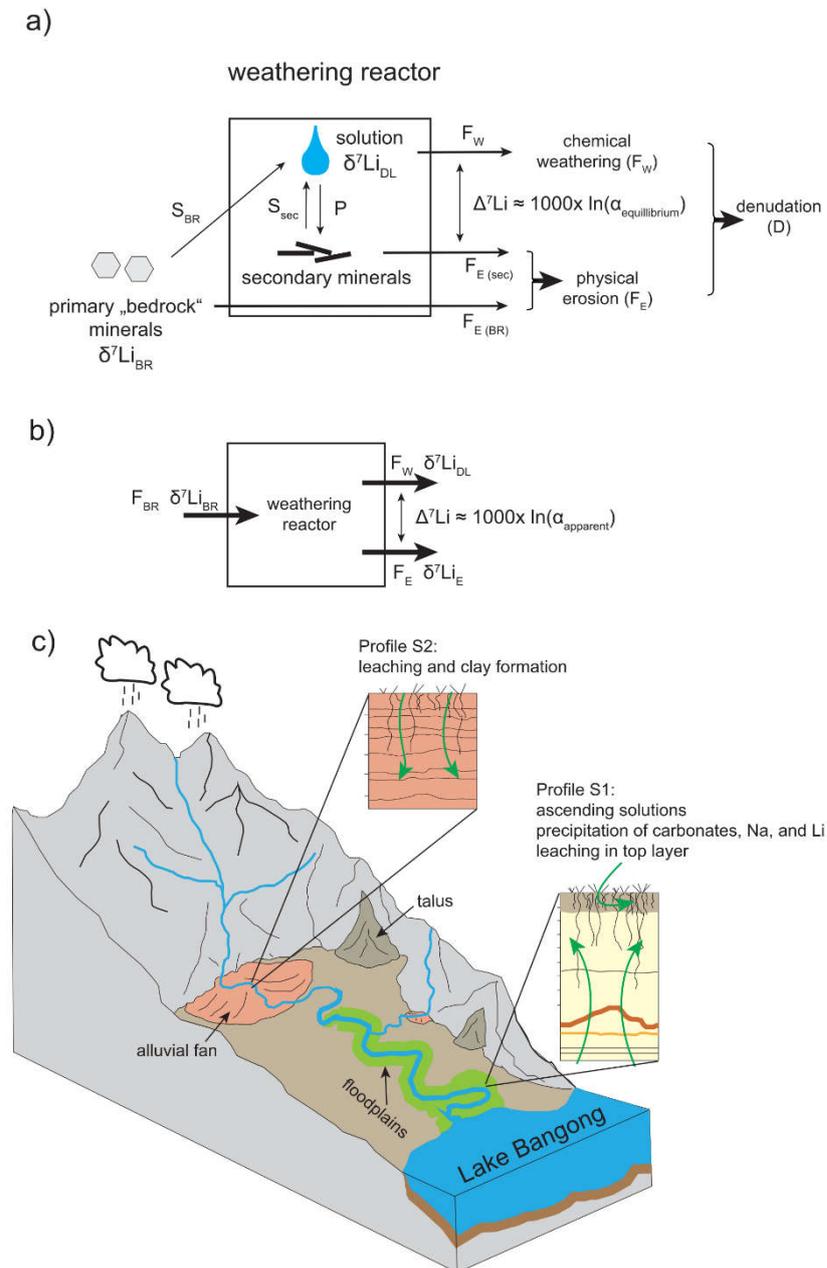
Figure 4-9

Geomorphic processes in Lake Bangong catchment **(a)** weathering fluxes and Li isotope exchange processes. Lithium is solubilized from bedrock, i.e. primary minerals, without substantially fractionating isotopes whereas a strong isotope effect is observed when lithium partitions into secondary minerals. **(b)** box model of the weathering zone with in and out going fluxes. The in going flux equal primary mineral solubilization, and the two export fluxes 1) the chemical weathering flux F_W (dissolved Li), and 2) erosional flux of Li in secondary minerals ($F_{E\,(sec)}$) and unweathered minerals/ rock fragments ($F_{E\,(BR)}$). Both sum up in the erosion flux F_E. The apparent isotope fractionation is calculated from the δ⁷Li values of the two export fluxes F_W and F_E. **(c)** schematic drawing showing weathering sites and processes affecting lithium isotopes in the catchment of Lake Bangong.

4.6.3 Implications for weathering and erosion

We propose a small offset between δ^{7}Li of the bedrock and dissolved lithium for the Lake Bangong catchment consistent with low Li net-incorporation into secondary minerals. This is characteristic either for extreme kinetically limited weathering, thus, low formation of secondary minerals causing low Li incorporation, or supply limited weathering, thus, low supply of "fresh" minerals from the weathering front and multiple processing of secondary minerals causing re-solubilization of Li. Under kinetically limited weathering the physical erosion flux of Li considerably exceeds the chemical weathering flux whereas supply limited weathering creates a substantial export of dissolved Li via chemical weathering (e.g. Dellinger et al., 2015). The major lithium fluxes and reservoirs in the Lake Bangong catchment are shown in Fig. 4-9b. Here, we use a box model focusing on the processes in the weathering zone. The Li flux from the bedrock (F_{BR}^{Li}) is balanced by the sum of dissolved Li in streams (F_W^{Li}) and Litransported in eroded sediments (F_E^{Li}). The Li flux ratio (F_E/F_W)^{Li} can be calculated from the isotopic composition of the bedrock (δ^{7}Li$_{BR}$), the bulk eroded sediments (δ^{7}Li$_E$), and the involved solutions (δ^{7}Li$_W$). For details on the model see Bouchez et al. (2013) and Weynell et al. (2017).

$$F_{BR}^{Li} \cdot \delta^7Li_{BR} = F_E^{Li} \cdot \delta^7Li_E + F_W^{Li} \cdot \delta^7Li_{DL} \qquad (4\text{-III})$$

Thus,

$$\left(F_E / F_W\right)^{Li} = \frac{\delta^7Li_W - \delta^7Li_{BR}}{\delta^7Li_{BR} - \delta^7Li_E}$$

It is assumed that the material flux through the weathering zone is at or close to steady state. Eventually, Li in solution and sediments are exported to the lake (Fig. 4-9c). δ^{7}Li$_W$ and δ^{7}Li$_{BR}$ values have been introduced in section 4.6.2.2. Major element composition of lake sediments and river bed sediments close to the lake as well as the Li isotope composition of lake, river bed, and suspended sediments (close to the lake) are similar (Fig. 4-6). Therefore, suspended and river bed sediments at the mouth of the Makha River and Chiao Ho with δ^{7}Li between -4.7 and -3.2 ‰ integrate the eroded sediments. We calculated a (F_E/F_W)^{Li} of 0.9 ± 0.4 and 1.4 ± 0.5 for the northern and southern sub-catchment, respectively (see Table S4-7). Roughly balanced Li fluxes for F_E and F_W are indicated. With these values a Li specific (F_W/D)^{Li} ratio (denudation D = F_E+F_W) of 0.54 ± 0.37 and 0.42 ± 0.32 has been calculated for the

northern and southern sub-catchment, respectively. We are aware that the calculation is very sensitive to the input values of the bedrock composition, which is expressed in the large uncertainties. However, the ratios are considerable higher than reported for catchments where weathering is kinetically limited (Dellinger et al., 2015; Dellinger et al., 2017). This statement is still valid when a lower δ^7Li of 0 ± 1.5 ‰ is assumed for the bedrock (then $(F_W/D)^{Li}_{north}$=0.39 ± 0.30 and $(F_W/D)^{Li}_{south}$=0.30 ± 0.25). The results indicate that about half of Li is transported as dissolved species in Lake Bangong catchment. The high $(F_W/D)^{Li}$ ratios and intensely weathered sediments in Lake Bangong catchment characterize a "supply-limited" (to a certain extent equivalent to "transport limited") weathering regime (Bouchez et al., 2013; Dellinger et al., 2017). The prevalence of supply limited weathering in the hyper-arid basin of Lake Bangong surprises as water in the catchment is clearly limiting for weathering to proceed. This means that the transfer of sediments from bedrock to the lake basin is so slow that it allows to overcome the water limitation over long time scales. Thus, physical erosion has to be nearly absent and residence times in the alluvial plains where moisture concentrates considerably long. The negative δ^7Li of river sediments is largely related to low erosion rates and processing of sediments in floodplains.

For the catchment of the Yarlung Tsangpo chemical weathering rates around 6.6 t/km²/a (Hren et al., 2007; Jiang et al., 2015) and cosmogenic nuclide derived denudation rates around 16 t/km²/a are reported (Lal et al., 2003). Here, the average F_W/D ratio is 0.4 (range between 0.3 and 0.6; see Table S4-7), likewise characteristic for supply limited weathering. The F_W/D ratio for the total weathering zone in the Yarlung Tsangpo catchment resembles the calculated lithium weathering flux for Lake Bangong catchment. We want to emphasize the fact that the Li specific and total weathering zone ratios for F_W/D resemble each other, although the former is based on the behavior of a trace element and the latter on major elements. Similar low δ^7Li values are detected for the headwaters of the Yangtze draining the southeastern Tibetan Plateau (Wang et al., 2015). Silicate weathering and physical erosion rates in the Yangtze headwaters are coupled (Wu et al., 2008), which is characteristic for supply-limited weathering (West et al., 2005). For this reason, we propose that the low δ^7Li values of rivers and river sediments on the western and southern Tibetan Plateau reflect supply-limited weathering.

4.6.4 Comparison with high-δ⁷Li weathering regimes

Lithium in streams and fine fluvial sediments on the northeastern Tibetan Plateau (Huang He and inflows to Lake Donggi Cona, Fig. 4-1a) and the southern Himalayas (Fig. 4-8) have higher δ^7Li values around +17 ‰ and -1 ‰ (Kisakurek et al., 2005; Weynell et al., 2017).

Around 85 % of initially solubilized Li is incorporated into clays and the lithium weathering flux $(F_W/D)^{Li}$ is maximum at 16 % of the total denudation rate of lithium but likely considerably lower (Weynell et al., 2017). These low $(F_W/D)^{Li}$, thus, high $(F_E/F_W)^{Li}$ ratios characterize kinetically-limited weathering (Bouchez et al., 2013; Dellinger et al., 2015). For this reason, we attribute the shift from low to high riverine δ⁷Li values across the Tibetan Plateau to a change from supply-limited weathering, on the western and southern plateau, to kinetically-limited weathering in the northeast.

Under kinetically-limited conditions fresh minerals, i.e. feldspar and mica, are dissolved and new secondary minerals, i.e. clay minerals, are formed. Most of the lithium in granitoid rocks is hosted in micas. Potassium feldspar and plagioclase provide aluminum and silica that is converted into clay minerals, whereas most Na^+, K^+, Mg^{2+}, Ca^{2+}, and Li^+ ions are in solution. Under extreme supply-limited conditions feldspar is completely consumed and solely secondary minerals (e.g., illite) can precipitate and re-dissolve (e.g. West et al., 2005). Therefore, the net-formation of clay minerals (the difference between new clay formation to re-dissolution of clays) is lower on the western and southern plateau and a larger fraction of lithium remains in solution during supply-limited weathering than during kinetically-limited weathering of fresh minerals.

There is no indication that silicate weathering rates directly control isotope ratios of riverine lithium because silicate weathering rates (ca. 1 t/km²/a), chemical weathering rates (ca. 7 t/km²/a), and overall denudation rates (15 to 25 t/km²/a) vary little across the Tibetan plateau (Lal et al., 2003; Hren et al., 2007; Wu et al., 2008; Zhang et al., 2009; Zhang et al., 2013; Munack et al., 2014; Jiang et al., 2015). Hence, the change from low to high dissolved δ⁷Li and a supply-limited to a kinetically-limited geomorphic regime is not related to weathering rates. Although the altitude varies more in the western catchment, both lake catchments have steep slopes and there is no significant difference. Therefore, relief is unlikely to control the weathering regime change on the Tibetan Plateau. The temperatures are not substantially different. The most significant difference is the annual precipitation rate. The majority of precipitation falls at high-altitude in the Lake Bangong catchment, feeding major streams and rivers that flood plains bordering inflows in the lower reaches (Fort and van Vliet-Lanoe, 2007). This impedes substantial sheet erosion and chemical weathering at mountain slopes at lower reaches. Sediment transport is occurring mainly along the major drainage system and chemical weathering is restricted along rivers (Fig. 4-9c).

4.6.5 Implications on the interpretation of Li weathering archives

The Li isotope composition of rivers and the lake on the northeastern Tibetan Plateau represent the weathering solutions integrated over a catchment (e.g. Weynell et al., 2017), thus, lake archives are well suited to investigate paleo weathering conditions in the catchment. In this study, we identified alteration of Li isotopes during strong evaporation of lake water. Thus, proxies that record the lake water composition, e.g. carbonates, possibly do not show the initial Li isotope composition of the weathering solution. This has to be in mind, if lake archives in hyper-arid regions are investigated.

Several studies focused on the interpretation of oceanic Li isotope archives to conclude on variations of local or global weathering (Hathorne and James, 2006; Misra and Froelich, 2012; Pogge von Strandmann et al., 2013; Pogge von Strandmann et al., 2017a). Here, the 9 ‰ increase of the δ^7Li of seawater during the Cenozoic (Misra and Froelich, 2012) is intensively discussed as this may allow to infer on the coeval decline of pCO$_2$. Several studies suggested an increase of the global riverine δ^7Li as causal for the seawater increase (e.g. Misra and Froelich, 2012; Bouchez et al., 2013; Li and West, 2014), which in turn was attributed to major orogenesis, mainly the uplift of the Tibetan Plateau and the Himalayas. An elevated topography is proposed to changed global weathering from supply limited to kinetically limited (e.g. Bouchez et al., 2013; Li and West, 2014; Dellinger et al., 2015) and the global $(F_E/F_W)^{Li}$ ratio from 1:2 to modern 4:1 (Froelich and Misra, 2014; Vigier and Godderis, 2015). The low $(F_E/F_W)^{Li}$ ratios and riverine δ^7Li values on the western and southern Tibetan Plateau do not support the assumption that uplift resulted in enhanced global riverine δ^7Li values. In contrast, the high $(F_E/F_W)^{Li}$ ratio and riverine δ^7Li values around +17 ‰ on the northeastern Tibetan Plateau are in agreement with this assumption. Hence, if the global increase of riverine δ^7Li reflects the formation of the Tibetan Plateau and the Himalayas than streams from regions with a kinetically limited weathering regime cause the global riverine increase in δ^7Li. These are the orogenic belts, which frame the relatively dry inner Tibetan Plateau.

It is still debated if the weathering regime change throughout the Cenozoic is connected to increasing silicate weathering rates, which may explain pCO$_2$ decline (e.g. Raymo and Ruddiman, 1992). Our findings support the assumption that a weathering regime change is able to occur under stable denudation fluxes, similar to what is proposed for the Late Cenozoic (Willenbring and von Blanckenburg, 2010) and quaternary glacial-interglacial cycles (von Blanckenburg et al., 2015).

4.7 CONCLUSIONS

This study shows that low δ^7Li values in streams and river sediments on the western Tibetan Plateau reflect little net-incorporation of solubilized Li into secondary minerals and intense weathering of river sediments. The hyper-arid climate impedes erosion leading to long sediment residence times and chemical weathering is restricted to small floodplains bordering the main channels. Here, the sparse precipitations accumulate. Mass balance modelling highlights that the flux of Li exported as dissolved species from the weathering zone is roughly balanced to the export in eroded secondary minerals or rock detritus. This is characteristic for supply-limited weathering.

Thermal waters have an impact on the Li budget of streams in the catchment of Lake Bangong. However, the low δ^7Li values in the major inflows to Lake Bangong catchment as well as the upper Indus and the Yarlung Tsangpo are caused by silicate weathering reactions.

A δ^7Li change from low values in rivers on the western and southern plateau to high values on the northeastern Tibetan Plateau reflects the change from supply-limited to kinetically-limited weathering conditions. This change is primarily related to increasing annual precipitations, i.e. climate. There is no evidence for a first order control of silicate weathering rates on riverine lithium isotopes on the plateau.

Strong evaporation under the hyper-arid climate results in alteration of Li isotopes within a minor inflow and Lake Bangong. Thus, Li isotopes in lake archives in hyper-arid basins possibly do not reflect the weathering induced Li isotope signal but also alteration within the lakes.

4.8 SUPPLEMENTARY INFORMATION CHAPTER 4

Table S4-1 Geographical coordinates and elevation for sample locations

sample ID	locations	date sampled	latitude	longitude	sample elevation	water temerature
			(°N)	(°E)	(m a.s.l.)	(°C)
Lake Bangong						
Nyak Co						
B1-1	Nyak Co	14.09.2012	33.5767	79.8695	4257	19
B1-2	Nyak Co	11.09.2012	33.5152	79.9043	4257	18
B1-4	Nyak Co	17.09.2012	33.4420	79.7829	4253	8
B1-5	Nyak Co	14.09.2012	33.6336	79.7137	4259	17
B1-6	Nyak Co	14.09.2012	33.6524	79.7018	4257	14
western basins						
B2	lake basin	14.09.2012	33.6678	79.6402	4257	14
B3	lake basin	14.09.2012	33.6933	79.6176	4249	13
B4-1	lake basin	12.09.2012	33.7533	79.5451	4259	19
B4-2	lake basin	12.09.2012	33.7254	79.3915	4258	14
pond						
B1-3	pond; 10m from E shore	11.09.2012	33.4725	79.8505	4246	19
Lake Bangong catchment						
northern catchment						
N1	Chiao Ho (mouth)	14.09.2012	33.6219	79.7633	4263	13
N2	tributary 3 (springwater)	15.09.2012	33.6272	79.7753	4264	15
N3	tributary 4 (springwater)	16.09.2012	33.6696	80.4657	4461	18
southern catchment						
S1	Makha river (mouth)	17.09.2012	33.3945	79.6880	4257	11
S2	Makha river	18.09.2012	33.2326	79.7870	4340	19
S8	Makha river (dead arm)	13.09.2012	33.2336	79.7832	4340	12
S3	Makha river	13.09.2012	33.0243	79.8079	4378	14
S4	Makha river	19.09.2012	32.9049	79.7324	4384	5
S5	tributary 3	13.09.2012	32.9082	79.7834	4394	10
S6	tributary 1	13.09.2012	33.1783	79.8630	4352	17
S7	tributary 1 (pond)	18.09.2012	33.1031	80.1980	4360	11
S9	tributary 2	17.09.2012	33.4148	79.6442	4262	10
eastern catchment						
E1	Nama Chu (mouth)	11.09.2012	33.5565	79.9309	4257	17
E2	Nama Chu (after damming)	11.09.2012	33.5573	79.9319	4260	14
E5	Nama Chu (dammed part)	11.09.2012	33.5681	79.9476		13
E3	Nama Chu	16.09.2012	33.5581	80.0558	4288	23
E4	salt water pond	16.09.2012	33.5326	80.2346	4295	20
profiles						
profile S1 (N)		15.09.2012	33.6271	79.7740	4265	--
profile S2 (S)		18.09.2012	33.1071	80.2581	4356	--
Indus River						
Ind1	Indus river	04.10.2010	32.1828	81.2771	4606	9
Ind2	Indus river	04.10.2010	32.3813	81.1287	4522	10
Ind3	Indus river	05.10.2010	32.4624	80.9007	4473	4
Ind4	tributary	05.10.2010	32.4005	80.8225	4479	5
Ind5	Indus river	05.10.2010	32.5183	80.1554	4304	12
Yarlung Tsangpo						
Bra 1	Brahmaputra	08.10.2010	29.7787	83.9062	4576	18
Men 1	Men Chu (tributary)	09.10.2010	29.5428	84.6187		3
Bra 2	Brahmaputra	09.10.2010	29.3456	85.1003	4498	9
Bra 3	Brahmaputra	09.10.2010	29.3212	85.2538	4475	12
Bra 4	Brahmaputra	10.10.2010	29.1212	87.5770	3995	10
Bra 5	Brahmaputra	11.10.2010	29.2548	88.9137	3891	9
Bra 6	Brahmaputra	11.10.2010	29.3168	89.1355	3810	11
Bra 7	Brahmaputra	11.10.2010	29.2790	90.8219	3566	14

Table S4-2 Standards: in-house solution were used to monitor instrumental; error of the method was calculated on international reference materials that were processed together with samples; error: ±0.5 ‰ (2sd)

reference standard	reference ID	δ^7Li (‰) measurement	δ^7Li (‰) average	2sd	N	comment
in-house solution	BM	43.0	42.6	0.4	7	not processed through columns, only used for precision of measurements
	BM	42.6				
	BM	42.6				
	BM	42.6				
	BM	42.3				
	BM	42.5				
	BM	42.3				
in-house solution	LiCO3	6.5	6.4	0.2	7	not processed through columns, only used for precision of measurements
	LiCO3	6.4				
	LiCO3	6.4				
	LiCO3	6.4				
	LiCO3	6.3				
	LiCO3	6.2				
	LiCO3	6.3				
in-house solution	LiNO3	0.7	0.5	0.2	7	not processed through columns, only used for precision of measurements
	LiNO3	0.5				
	LiNO3	0.6				
	LiNO3	0.5				
	LiNO3	0.4				
	LiNO3	0.5				
	LiNO3	0.4				
Osil seawater	Osil 14.6	30.6	30.9	0.4	10	
	Osil 20.4.	30.7				
	osil0.4m	30.9				
	Osil2 re	31.2				
	Osil2 se	31.2				
	Osil5.3.	31.1				
	Osila so	30.8				
	Osilb so	30.9				
	OsilSL11	31.1				
	OsilT12D	30.9				
Atlantik seawater	ASW 14.6	30.6	30.9	0.5	5	
	ASW1 ref	31.1				
	ASW2 ref	31.1				
	ASWasoil	30.7				
	ASWbsoil	30.9				
CCRMP Till-1	Tii1brep	6.7	6.4	0.3	5	
	Till1 14	6.3				
	Till1a13	6.4				
	Till1are	6.3				
	Till1b13	6.4				
USGS MAG-1	MAG1a13.	0.2	0.1	0.4	5	
	MAG-1b r	0.4				
	MAG1b13.	0.1				
	MAG1SED	0.2				
	MAG1SL	-0.1				
NIST 2709a	NISTa13.	-0.6	-0.5	0.2	2	
	NISTb13.	-0.5				

Table S4-3 XRD data of fluvial and lake sediments from Lake Bangong (data obtained with RIGAKU Miniflex600; data reduction with X'pert highscore software) o: <5 %; +: 5-10 %; ++: 10-20 %; +++: 20-30 %; ++++: >30 %

sample	calcite	aragonite	dolomite	quartz	K-fsp	plg	biotite	amphibole	chlorite	illite/ muscovite	gypsum
Lake Bangong											
Nyak Co											
B1-4	+	+	o	++	o	++++	o	o	o	++	o
western basins											
B2	o	o	o	++	+	++++	o	o	o	+++	o
B4-1	o	o	o	++	+	++	+	+	+	+++	o
Catchment											
northern catchment											
N1*	+	+	o	++	o	++	+	o	+	++	o
N3	++	o	+	++	o	+++	o	o	o	+++	o
southern catchment											
S1*	o	o	o	++	++	++++	o	o	o	+++	o
S3	o	o	o	++	+	+++	+	+	+	+++	o
S4	o	o	o	++	+	+++	o	o	+	+++	o
S5	o	o	o	++	+	+++	o	+	o	+++	o
S6	o	o	o	++	+	++++	+	o	o	+++	o
S7	o	o	o	++	+	++++			o	+++	o
S9	o	o	o	++	+	++++	o	o	o	+++	o
eastern catchment											
E3	+++	o	+	++	+	++	+	o	+	++	o
E4	o	o	o	++	+	++++	o	o	o	+++	o
Sediment profiles											
section 1 (N)											
S1-1	+	+++	o	++	o	++	o	o	+	++	+
S1-2	+	+++	o	+	+	+++	+	o	o	++	o
S1-3	+	++++	o	o	+	++	+	o	+	++	o
S1-4	++	++++	o	o	+	+++	+	o	+	++	o
S1-5	+	++++	o	+	+	++	+	o	+	++	o
S1-6	++	++++	o	+	+	++	+	o	+	++	o
S1-7	+	++++	o	+	o	++	+	o	+	++	o
S1-8	+	++++	o	+	+	++	+	o	+	++	o
section 2 (S)											
S2-1	o	o	o	++	+	++++	+	o	o	++++	o
S2-2	o	o	o	++	+	+++	+	+	o	++++	o
S2-3	o	o	o	+++	+	+++	+	o	o	++++	o
S2-4	o	o	o	+++	+	+++	+	o	o	++++	o
S2-5	o	o	o	+++	+	+++	+	o	o	++++	o
S2-6	o	o	o	++	+	+++	+	++	o	++++	o
S2-7	o	o	o	++	+	++	+	++	o	++++	o
S2-8	o	o	o	+++	+	+++	+	o	o	++++	o

Table S4-4 Calculation of average apparent isotope fractionation Δ^7Li_{DL-SP} ($= \delta^7Li_{DL} -\delta^7Li_{SP}$ (‰)) shown in Fig. 4-8a

Region	sample	δ^7Li_{DL}	δ^7Li_{SP}	δ^7Li_{RBS}	Δ DL-SP	ΔØLake BC catchment	ΔØregion	
West							11.9	
	Lake Bangong - north							
	N1	6.1	-3.2	-4.3	9.3	9.3		
	N3	5.1		-3.8				
	Lake Bangong - south							
	S1	8.9	-4.7	-4.1	13.6	14.2		
	S2	10.5	-4.3		14.8			
	S3	9.0	-3.4	-3.5	12.4			
	S4	14.2	-2.5	-2.5	16.7			
	S5	10.0	-3.1	-1.6	13.1			
	S7	18.2	-2.9	-0.6	21.2			*excluded, sample location is a pond*
	S9	12.0	-2.5		14.5			
	Lake Bangong - east							
	E1	7.4	7.7		-0.3			
	E2	7.5	7.7	-1.5	-0.3			
	E3	6.8	4.9	-2.4	1.9			
	E4	29.0		6.3				
	Indus headwaters							
	Ind1	6.3	-2.1		8.4			
	Ind2	6.5	-2.0		8.5			
	Ind4	6.8	-3.1		9.9			
	Ind5	7.2	-1.9		9.1			
South							8.7	
	Yarlung Tsangpo							
	Bra 1	5.6	-4.1		9.7			
	Bra 2	4.1	-3.9		8.0			
	Bra 3	4.9	-3.8		8.7			
	Bra 4	4.5	-3.2		7.7			
	Bra 5	6.1	-2.9		8.9			
	Bra 6	5.4	-3.2		8.6			
	Bra 7	6.7	-2.8		9.5			
	Yangtze headwaters (Wang et al., 2015)							
	CJ 1	7.6	-2.2		9.8			
	CJ 3	7.7	0.1		7.6			
Northeast							17.5	
	Lake Donggi Cona catchment (Weynell et al., 2017)							
			SP(avg)					*SP deduced from deposited clays in lake*
	E11-1	16.8	-0.8	1.3	17.6			
	E11-4	17.1	-0.8	1.4	1.0	17.9		
	E11-3*3	13.6	-0.8	0.2	14.4			
	E11-5	15.6	-0.8		16.4			
	E11-6	17.2	-0.8		18.0			
	S11-1	16.7	-0.8	1.3	17.5			
	S08-5	17.6	-0.8		18.4			
	N11-2t	20.6	-0.8	1.8	21.4			*excluded; influenced by thermal waters*
	N11-1t	20.8	-0.8		21.6			*excluded; influenced by thermal waters*
	N08-3	17.8	-0.8		18.6			
	Huang He	18.0	-0.9		18.9			
Himalayan streams (Kisakürek et al., 2005)							17.9	
		13.7	-3.1		16.8			
		11.2	-3.8		15.0			
		21.3	-2.7		24.0			
		20.8	-3.9		24.7			
		20.6	-3.1		23.7			
		22.2	-1.4		23.6			
		16.3	-3.6		19.9			
		20.3	-3.9		24.2			
		16.7	-2.7		19.4			
		17.0	-3.7		20.7			
		19.3	-2.0		21.3			
		15.6	-1.6		17.2			
		12.5	0.2		12.3			
		18.8	-2.8		21.6			
		29.9	-0.9		30.8			*excluded, influenced by fertilizer*
		16.4	-2.9		19.3			
		15.3	-3.7		19.0			
		12.7	-0.9		13.6			
		13.8	-1.8		15.6			
		15.7	-0.3		16.0			
		11.6	-1.8		13.4			
		13.4	-0.5		13.9			
		14.0	-0.9		14.9			
		20.5	-2.6		23.1			
		16.5	-1.1		17.6			
		16.8	-2.1		18.9			
		12.0	-2.0		14.0			
		16.6	-1.6		18.2			
		14.8	1.2		13.6			
		10.2	-0.9		11.1			
		12.7	0.0		12.7			
		17.7	-0.5		18.2			
		25.0	-0.4		25.4			
		18.7	2.7		16.0			
		19.2	1.7		17.5			
		18.2	1.4		16.8			
		25.9	2.6		23.3			*excluded, influenced by fertilizer*
		14.5	2.7		11.8			

157

Table S4-5 Calculation of f_{DL}

assumed Li equilibrium isotope fractionation (see text)

$\Delta^7\text{Li}_{equil}$	±
17.5	1.0

Lake Bangong catchment

			±		f_{DL}	±
BC(south)	$\delta^7\text{Li}_{initial}$	1.5	1.5			
	$\delta^7\text{Li}_{DL}$	8.9	0.5		**0.58**	**0.20**
			±			
BC(north)	$\delta^7\text{Li}_{initial}$	1.5	1.5			
	$\delta^7\text{Li}_{DL}$	6.1	0.5		**0.74**	**0.15**

The uncertainty for the dissolved load reflects the analytical uncertainty.
The uncertainty for the bedrock (initial) reflects the reasonable range for bedrock in the catchment.

For equation and calculation of f_{DL} see section 4.6.2.2 and equation 4-II.

Table S4-6 Saturation indices of water samples; calculated with USGS PHREEQ software (values > 0 means supersaturation and vice versa; T: temperature in °C; wateq4 database used for calculation)

sample		Calcite	Aragonite	Dolomite	Strontianite	Magnesite	Siderite	Quartz	Al(OH)3(a)	Gibbsite	Fe(OH)3(a)	Fe3(OH)8	Goethite	Illite	Montmorillonite-Ca	Chlorite-7A	Chlorite-14A
Lake																	
Nyak Co																	
B1-1	open lake	1.2	1.0	3.2	-0.1	1.4	-6.0	-0.8	-3.7	-0.9	0.6	-3.8	6.3	-4.6	-6.2	4.9	8.3
B1-2	open lake	1.0	0.8	2.7	-0.5	1.2	-4.7	-1.1	-3.1	-0.4	0.9	-2.6	6.5	-5.2	-6.2	0.7	4.2
B1-4	near wetlands	-0.1	-0.3	0.1	-1.5	-0.2	-0.2	0.6	-1.4	1.5	2.4	3.6	7.6	3.4	3.8	-7.2	-3.6
B1-5	near inflow Chiao Ho	1.5	1.3	3.4	0.3	1.3	-4.1	0.7	-3.3	-0.5	1.6	-0.5	7.2	1.1	0.1	6.5	9.9
western basins																	
B2	lake	0.9	0.8	2.8	-0.6	1.4	-4.6	-0.3	-3.2	-0.4	1.1	-1.9	6.6	-2.1	-3.3	3.6	7.1
B3	lake	0.9	0.7	3.0	-0.7	1.6	-4.7	-0.5	-3.2	-0.4	1.2	-1.8	6.6	-2.7	-4.2	3.8	7.3
B4-1	lake	1.2	1.1	3.6	-0.2	1.8	-4.2	-0.1	-3.4	-0.6	1.4	-1.2	7.1	-1.8	-3.3	5.6	9.0
B4-2	lake	0.8	0.6	3.2	-0.8	1.9	-5.2	-1.4	-3.4	-0.6	0.5	-4.0	5.9	-6.0	-7.8	1.7	5.2
pond near lake																	
B1-3	pond	1.5	1.3	3.7	0.4	1.7	-10.3	-1.7	-4.7	-1.9	-0.5	-8.4	5.1	-9.1	-11.6	11.9	15.3
Catchment																	
northern catchment																	
N1*	Chiao Ho	1.2	1.0	2.2	-0.2	0.4	-3.9	0.4	-2.7	0.1	1.6	-0.2	7.1	0.5	0.3	1.8	5.3
N2	tributary 3	0.2	0.1	0.2	-1.1	-0.5	-1.8	0.5	-1.9	0.9	1.2	-0.2	6.7	1.9	2.2	-7.5	-4.0
N3	tributary 4 (groundwater)	1.0	0.8	1.8	-0.7	0.3	-4.2	0.3	-3.1	-0.4	1.5	-0.6	7.2	-1.2	-1.1	1.4	4.9
southern catchment																	
S1*	Makha river	0.3	0.2	0.4	-0.3	-0.4	-3.2	0.0	-2.5	0.4	2.0	1.2	7.3	-0.8	-0.7	-3.8	-0.3
S2	Makha river	0.8	0.7	1.5	-0.9	0.1	-3.8	0.1	-2.8	0.0	2.1	1.3	7.6	-0.7	-1.0	0.7	4.2
S8°	Makha river	-0.3	-0.5	-0.7	-2.1	-0.9	-1.4	0.0	-1.6	1.1	1.7	1.3	7.4	0.1	0.9	-9.1	-5.7
S3	Makha river	0.5	0.4	1.1	-1.2	0.0	-4.2	-0.3	-2.6	0.2	1.9	0.5	7.4	-1.8	-2.2	0.2	3.6
S4	Makha river	0.2	0.1	-0.1	-1.7	-0.9	-2.0	0.5	-1.9	1.0	2.7	3.9	7.9	1.7	2.2	-5.7	-2.2
S5	tributary 3	-0.3	-0.5	-1.3	-2.2	-1.5	-2.1	0.1	-1.5	1.3	2.2	2.6	7.6	1.2	1.9	-8.9	-5.4
S6	tributary 1	0.5	0.4	0.9	-1.2	-0.2	-2.9	0.2	-2.4	0.3	2.0	1.4	7.6	-0.1	0.1	-1.9	1.5
S7	tributary 1 (pond)	0.9	0.7	1.3	-0.8	0.0	-5.9	0.2	-3.5	-0.6	1.9	0.0	7.3	-1.4	-2.0	4.4	7.9
S9	tributary 2	-0.1	-0.2	-0.7	-1.8	-1.1		0.4									
eastern catchment																	
E1*	Nama Chu (after damming)	1.1	1.0	2.8	0.1	1.1	-4.8	0.5	-3.3	-0.5	1.4	-1.3	7.0	0.0	-0.7	6.4	9.9
E2	Nama Chu (after damming)	1.2	1.0	2.8	0.2	1.1	-4.8	0.5	-3.3	-0.5	1.9	0.1	7.4	0.2	-0.7	7.4	10.9
E5	Nama Chu (dammed part)	0.9	0.7	2.2	0.0	0.8	-3.2	0.6	-2.6	0.2	2.3	1.9	7.7	1.7	1.2	4.0	7.5
E3	Nama Chu	1.0	0.9	2.2	0.0	0.6	-3.5	0.4	-2.9	-0.2	1.2	-1.4	7.0	0.0	-0.1	1.5	4.9
E4	salt water pond	1.3	1.2	4.2	0.0	2.3	-3.9	0.5			1.1	-2.0	6.8				

*: mouth of stream to lake; °: dead arm, with connection to Makha river; no value: SI = -1000

Table S4-7 Calculation of Li specific $(F_E/F_W)^{Li}$ ratio and related weathering intenisty, the $(F_W/D)^{Li}$ ratio (for formulas and description see text)

	δ^7Li_E	±	δ^7Li_{BR}	±	δ^7Li_W	±	F_E/F_W	±	F_E/F_W (max)	F_E/F_W (min)	F_W/D	±	F_W/D (min)	F_W/D (max)
southern catchment	-3.9	0.8	1.5	1.5	8.9	0.5	1.4	0.5	2.8	0.8	0.42	0.32	0.26	0.57
northern catchment	-3.9	0.8	1.5	1.5	6.1	0.5	0.9	0.4	1.9	0.4	0.54	0.37	0.34	0.71
Lake Donggi Cona catchment	-0.8	0.4	1.9	0.5	16.6	0.4	5.4	1.3			0.16	0.14		

δ^7Li_E from Lake Donggi Cona catchment defines minimum value. Larger values lead to higher F_E/F_W and lower F_W/D (data from Weynell et al., 2017)

Table S4-7 : b) Calculation of element unspecific F_E/F_W ratio and related weathering intensity, the F_W/D ratio (for formulas and description see text) using chemical weathering rates (CWR), physical erosion rates (PER), and overall denudation rates (D) (rates in t/km^2/a)

	CWR	CWR_{avg}	PER	PER_{avg}	D	D_{avg}	F_E/F_W (avg)	F_E/F_W (max)	F_E/F_W (min)	F_W/D	F_W/D (min)	F_W/D (max)
Yarlung Tsangpo (middle reaches)	5.3 7.9	6.6			14.0 18.0	16.0	1.4	2.4	0.8	0.41	0.29	0.56

CWR: means of several measurements from different periods of the year (data from Hren et al., 2007 and Jiang et al., 2015)
D: cosmogenic derived denudation rates from Lal et al., 2003 (a sediment densitiy of 2 g/cm^3 was used (Sharma, 1997) to convert mm/a to t/km^2/a)

	CWR	CWR_{avg}	PER	PER_{avg}	D	D_{avg}	F_E/F_W (avg)	F_E/F_W (max)	F_E/F_W (min)	F_W/D	F_W/D (min)	F_W/D (max)
Lake Qinghai catchment (northeastern plateau)	4.4		17.4 32.0	24.7			5.6	7.3	4.0	0.15	0.12	0.20

CWR_{avg}: discharge weighted average of several inflows (data from Zhang et al., 2009)
PER: derived from continuous sediment gauging throughout the year (data from Zhang et al., 2013)

160

S4-1 Geological map of Lake Bangong catchment
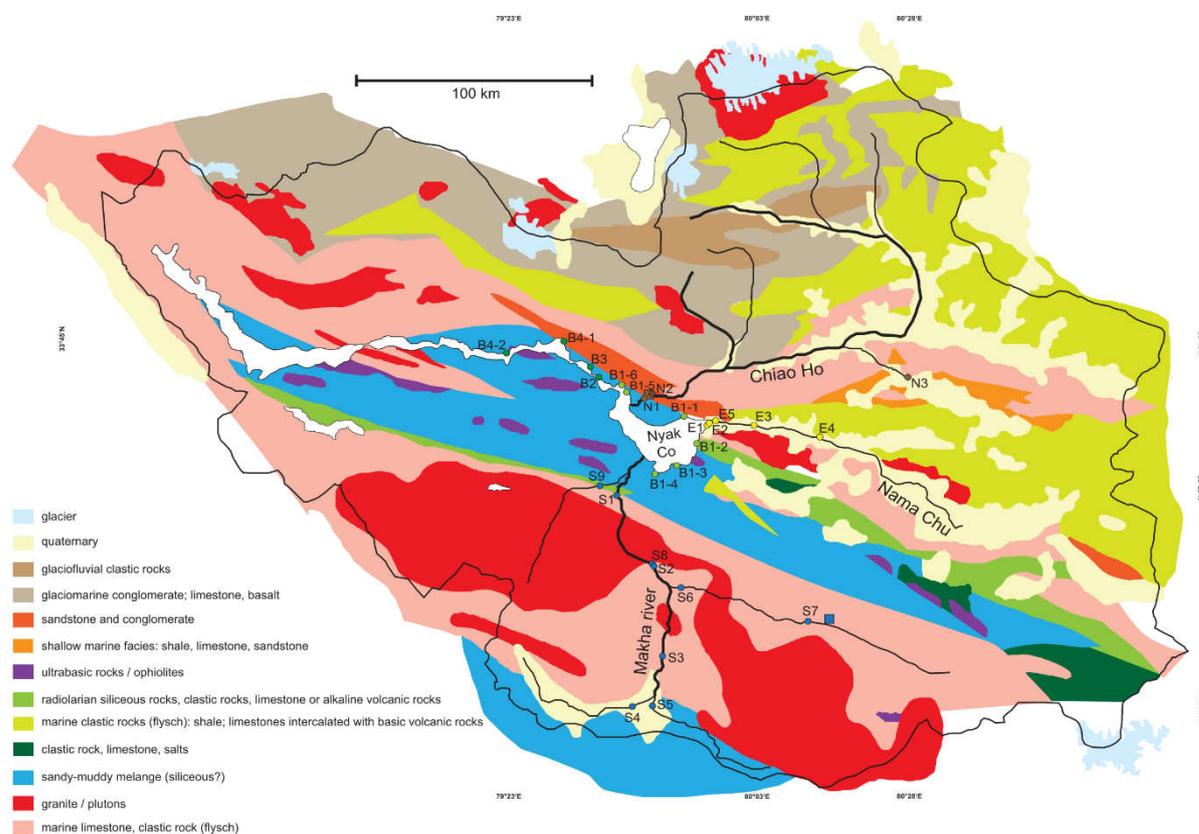
Map is based on Pan, G., Ding, J., Yao, D., Wang, L., 2004. Geological Map of the Qinghai-Xizang (Tibet) Plateau and Adjacent Areas. Chengdu Institute of Geology and Mineral Resources, China Geological Survey.

S4-2 Compilation: δ⁷Li values and Li concentrations in streams reported so far
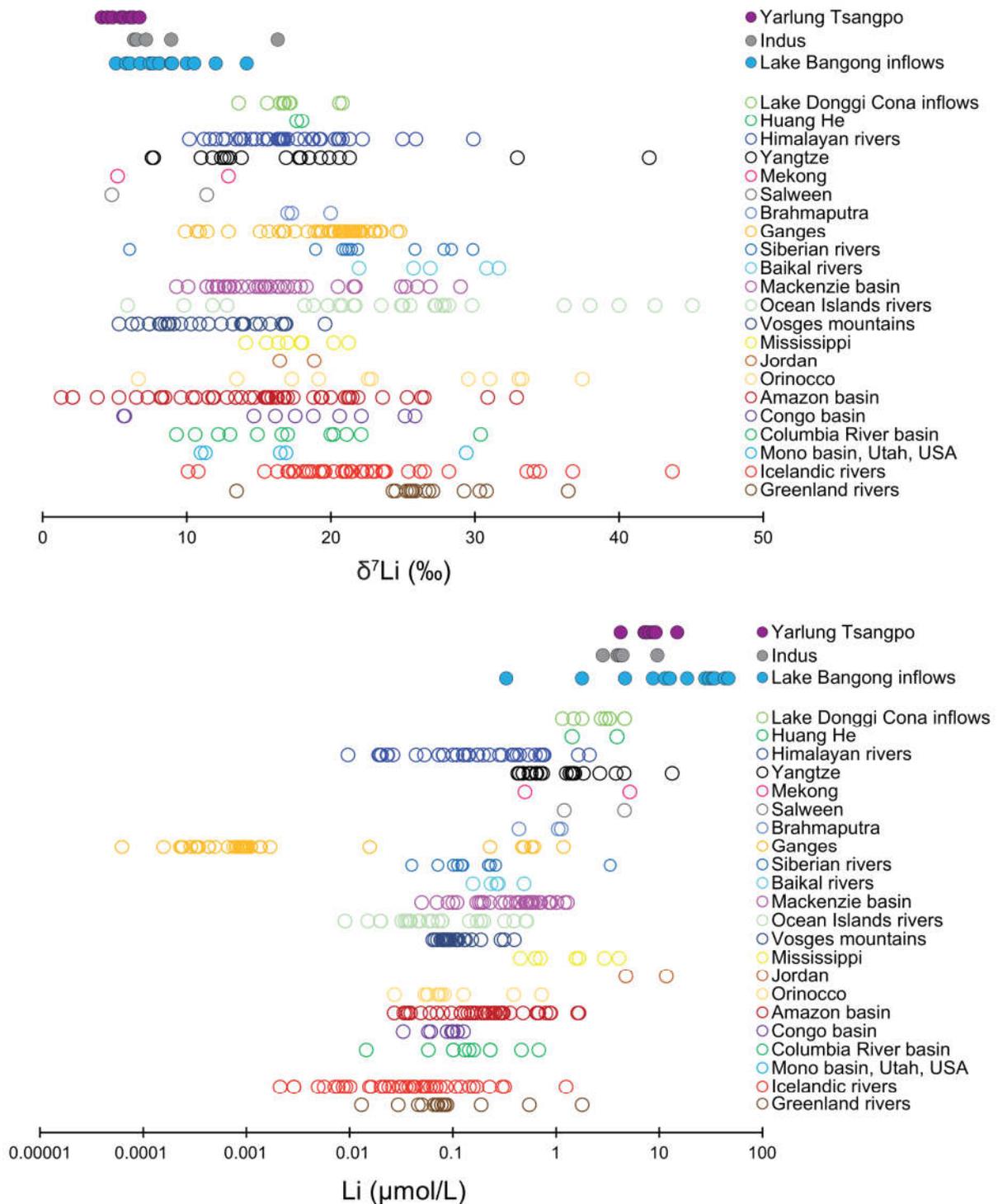
Lithium data from (Huh et al., 1998; Huh et al., 2001; Tomascak et al., 2003; Kisakurek et al., 2005; Pogge von Strandmann et al., 2006; Vigier et al., 2009; Lemarchand et al., 2010; Millot et al., 2010; Pogge von Strandmann et al., 2010; Wimpenny et al., 2010; Liu et al., 2011; Rad et al., 2013; Henchiri et al., 2014; Bagard et al., 2015; Clergue et al., 2015; Dellinger et al., 2015; Liu et al., 2015; Wang et

al., 2015; Henchiri et al., 2016; Pogge von Strandmann et al., 2016; Pogge von Strandmann et al., 2017; Weynell et al., 2017).

S4-3 Compilation of δ⁷Li values in river bed sediments
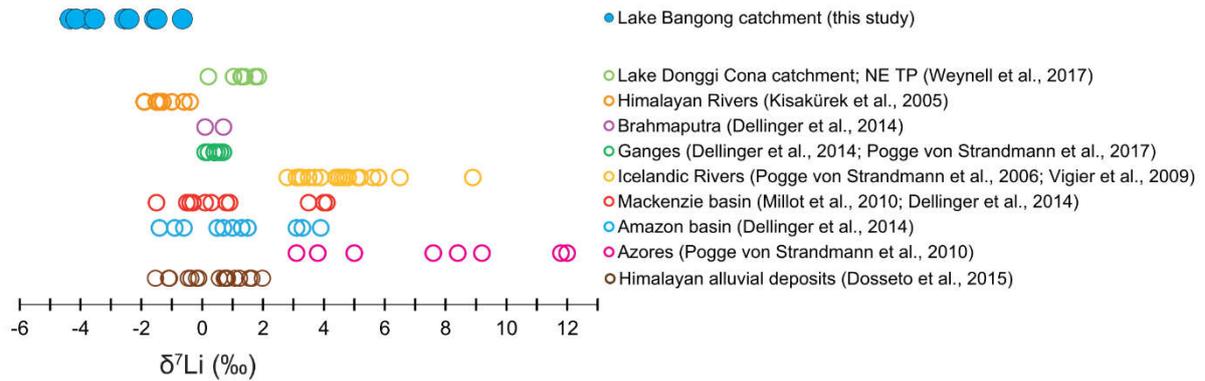
Compilation of δ⁷Li values of river bed sediments reported in the literature and in Lake Bangong catchment. All samples represent bulk river bed sediment, which are collected within the streambed of modern rivers. The samples are not corrected for grain size or provenance. Samples from fluvial terraces from the Himalayas and foreland (Dosseto et al., 2015) are old deposits (between 10 and 45 ka).

S4-4 δ⁷Li values of sediments vs. Al/Si
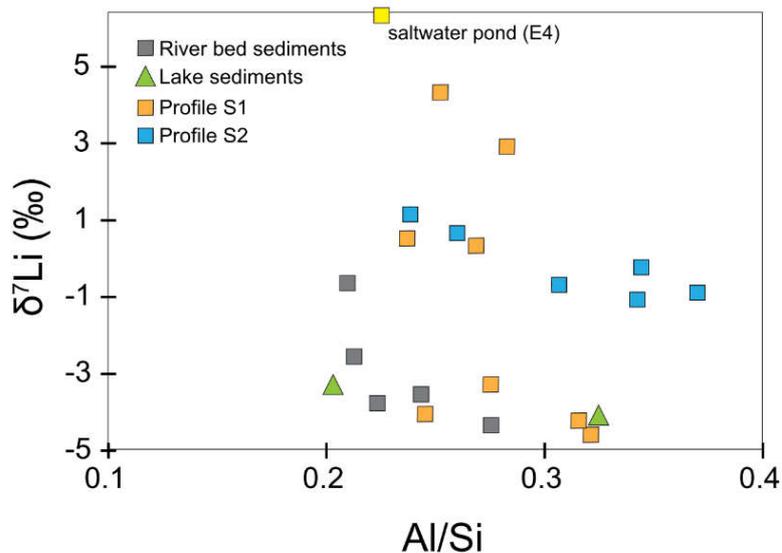
Using the Al/Si ratio as grain size proxy was introduced in Bouchez et al. (2011) and Lupker et al. (2011). High Al/Si reflect finer and low Al/Si coarser sediments. None of the different types of

sediments displays a clear reltionship of δ^7Li and Al/Si ratios. Only samples from profile S2 from the south show two clusters with the first one having δ^7Li values around 1 ‰ and Al/Si around 0.25 and the second δ^7Li around -1 ‰ and Al/Si ratios above 0.3.

S4-5 Correction for precipitated carbonates of sediments from profile S1

We assume that Mg, Mn, and most Ca are deduced from carbonate minerals and Si, Al, K, Ti, Na, 5 % Ca, and Li from silicate minerals. Each mass fraction of Si, Al, K, Ti, 5 % Ca, and Na was normalized to the sum of all mass fractions from Si, Al, K, Ti, 5 % Ca, and Na. This gives the mass fraction of each silicate derived element (X_{sil}) for the hypothetic silicate fraction.

X_{sil} (%) = (X_{sil} / $\sum$ (Si, Al, K, Ti, 5 % Ca, Na))•100

We want to emphasize that silicates contain also minor fractions of Mg and Mn, so the correction gives only a rough estimation of the mass fractions before carbonate precipitation within profile S2. However, the carbonate corrected values (highlighted in grey) yield considerable higher Na mass fractions compared to any other analyzed sediment in the catchment of Lake Bangong.

Lithium values were calculated with the equation:

Li (μg/g) = Li/SiO$_2$ • [SiO$_2$]$_{carb\ corrected}$

The Li/SiO$_2$ (μg/g / %) ratio represents the ratio before correction from each sample and the [SiO$_2$]$_{carb\ corrected}$ represent the carbonate corrected mass fraction of SiO$_2$.

sample	Li	SiO$_2$	TiO$_2$	Al$_2$O$_3$	MnO	MgO	CaO	CaO$_{carb}$	CaO$_{sil}$	Na$_2$O	K$_2$O	SiO$_2$	TiO$_2$	Al$_2$O$_3$	CaO$_{sil}$	Na$_2$O	K$_2$O	Li/SiO$_2$	Li
	μg/g	%	%	%	%	%	%	%	%	%	%	%	%	%	%	%	%		μg/g
profile S1																			
S1-1	48.0	14	0.1	2.8	0.0	2.0	39.3	34.3	5.0	1.0	0.8	58.2	0.6	12.2	0.2	4.2	3.3	3.5	206
S1-2	39.2	10	0.1	2.2	0.0	1.0	43.0	38.0	5.0	1.3	0.7	51.2	0.6	11.5	0.3	6.7	3.4	4.1	208
S1-3	30.9	8	0.1	2.0	0.0	0.7	45.5	40.5	5.0	0.9	0.6	47.7	0.6	12.0	0.3	5.8	3.4	4.0	190
S1-4	21.2	7	0.1	1.7	0.0	0.7	46.6	41.6	5.0	0.4	0.4	48.4	0.6	11.5	0.3	2.9	3.0	3.0	143
S1-5	16.1	8	0.1	2.0	0.0	0.7	49.0	44.0	5.0	0.3	0.4	50.8	0.6	12.4	0.3	1.7	2.7	2.0	102
S1-6	19.8	11	0.1	3.1	0.0	0.9	43.0	38.0	5.0	0.3	0.7	54.7	0.7	15.3	0.2	1.3	3.3	1.8	98
S1-7	19.2	10	0.1	2.8	0.0	0.8	45.3	40.3	5.0	0.2	0.6	53.0	0.7	15.1	0.3	1.3	3.3	1.9	103
S1-8	14.3	9	0.1	1.9	0.0	0.6	49.8	44.8	5.0	0.3	0.4	53.2	0.5	11.6	0.3	1.8	2.6	1.6	87

S4-6 Steady state model for δ^{18}O and δD

The model allows to calculate the proportion of incoming water that leaves the Nyak Co via the its outflow to the next western basin (proportion is named X) and via evaporative loss (evaporation from the lake surface, named with 1-X). The model is explained in detail in section 2.6.2.
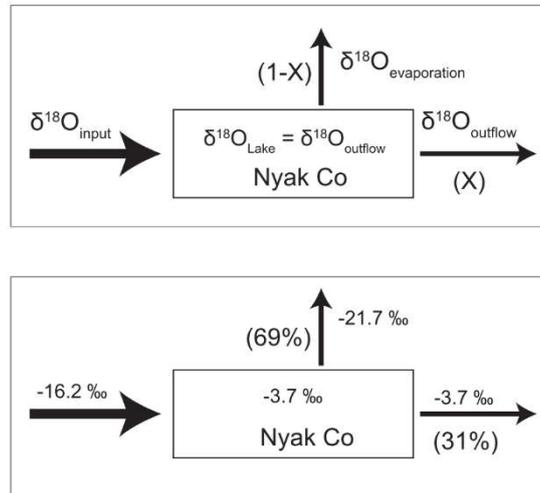
The steady state assumption requires:

$\delta^{18}O_{input} = \delta^{18}O_{output}$ = -16.2 ‰ (annual weighted average of δ^{18}O of precipitation at Lake Bangong from Guo et al., 2017)

The mass balance calculation is:

$$\delta^{18}O_{output} = (1-X) \cdot \delta^{18}O_{evaporation} + X \cdot \delta^{18}O_{outflow}$$

$\delta^{18}O_{outflow}$ is calculated with:

$$\delta^{18}O_{outflow} = \delta^{18}O_{Lake} = -3.7 ‰ \text{ (samples B1-1 and B1-2)}$$

$\delta^{18}O_{evaporation}$ is calculated with:

$$\delta^{18}O_{evaporation} = \delta^{18}O_{Lake} + \varepsilon^{18}O_{l-v(evaporation)}$$

$\varepsilon^{18}O_{l-v(evaporation)} = \varepsilon_{equillibrium} + \varepsilon_{kinetic}$ (with $\varepsilon = (\alpha-1) \times 1000$)

$\varepsilon_{equillibrium}$:   10.6 ‰ for δ^{18}O (calculated after Majoube (1971) with T: +10.0 °C)

$\varepsilon_{kinetic}$:   7.4 ‰ for δ^{18}O (calculated after Gonfiantini (1986) with h: 48 %)

165

(values for T and h are precipitation weighted; only the period of the year is considered when the lake surface is not frozen)

Included to mass balance equation: $-3.7 = (1-X) \cdot (-3.7-18.0) + X \cdot -12.5$

$$X = 0.31$$

Therefore, 31 % of the incoming water leaves the Nayk Co basin via the outflow to the next basin and 69 % due to evaporative loss. The evaporative water loss increase to 86 % at the most western sample location B4-2, which has a δ^{18}O of -0.7 ‰.

S4-7 Major element concentrations of investigated rivers
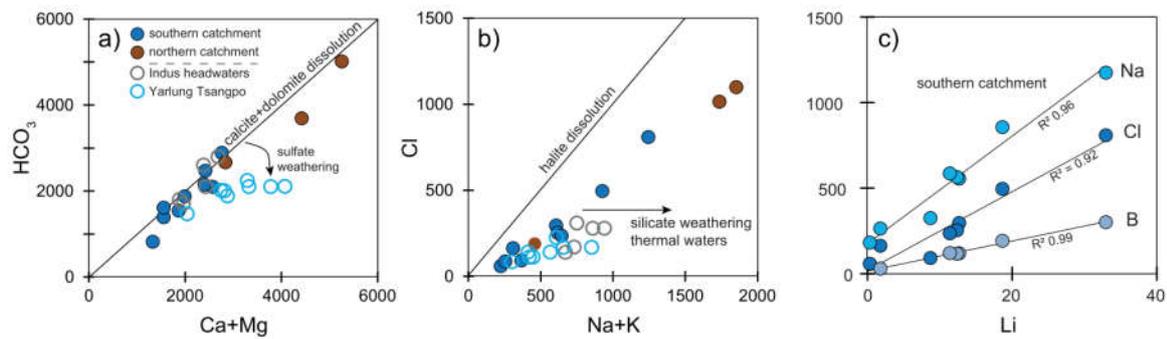
a) Alkalinity vs. Ca+Mg concentrations in µmeq/L, solid line indicates dissolution of carbonate minerals. Dissolution of carbonate minerals provides most of the ion load of streams in the Lake Bangong catchment and Indus headwaters. b) Cl vs. Na+K concentrations in µmeq/L, solid line indicates halite dissolution, c) Lithium concentration vs. Na, Cl, and B concentrations of streams from the southern sub-catchment of Lake Bangong (concentrations in µmol/L).

S4-8 Lithium contribution from carbonate or evaporite dissolution

The amount of lithium provided by carbonate dissolution was calculated with

Li_{carb} (calc) = Ca_{carb} (sample) $\cdot$ $(Li/Ca)_{carb}$ (µmol/L)

(Ca_{carb} was estimated by assuming that all Ca is derived from carbonates. This gives an absolute maximum estimation as weathering of silicates possibly contributes Ca, too. Values between $1 \cdot 10^{-6}$ and $20 \cdot 10^{-6}$ were used for $(Li/Ca)_{carb}$ given in (Hoefs and Sywall, 1997; Dellinger et al., 2015; Wang et al., 2015).

The amount of lithium provided by evaporite dissolution was calculated with

$$Li_{eva} \text{ (calc)} = Cl_{sample} \bullet (Li/Cl)_{eva} \text{ (}\mu mol/L)$$

(with Li_{eva}: amount of Li derived from evaporates in $\mu mol/L$; Cl_{sample}: amount of Cl in distinct sample and derived from evaporites, as anthropogenic input and precipitation is excluded all Cl is assumed to result from the dissolution of evaporites; $(Li/Cl)_{eva}$: Li/Cl ratio of evaporates. Assuming congruent dissolution of evaporites than $Cl_{eva} = Na_{eva}$.) Dissolution of evaporites on the Tibetan Plateau leads to considerably higher Li/Na ratios around $2.2\bullet10^{-3}$ (Wang et al., 2015; Weynell et al., 2016) compared to marine evaporites with ratios around $3\bullet10^{-5}$ (Dellinger et al., 2015) and references therein). A high Li/Cl of $2.2\bullet10^{-3}$ was used in the calculation.

sample	Li	Cl	Ca	Li from carb diss	carbonate contribution	Li from evaporite diss	evaporite contribution
	$\mu mol/l$	$\mu mol/l$	$\mu mol/l$	$\mu mol/l$	% max	$\mu mol/l$	%
N1	25.2	1015	1332	0.03	0.1	2.54	10.1
N2	32.0	1100	1647	0.03	0.1	2.75	8.6
N3	4.1	189	841	0.02	0.4	0.47	11.5
S1	12.7	296	586	0.01	0.1	0.74	5.8
S2	18.7	496	716	0.01	0.1	1.24	6.7
S8	32.9	810	773	0.02	0.0	2.02	6.1
S3	12.3	254	459	0.01	0.1	0.63	5.1
S4	0.3	59	866	0.02	5.3	0.15	44.9
S5	1.8	164	619	0.01	0.7	0.41	22.9
S6	11.4	237	724	0.01	0.1	0.59	5.2
S7	0.9	87	444	0.01	1.0	0.22	23.9
S9	8.7	93	569	0.01	0.1	0.23	2.7
E1	44.6	2200	674	0.01	0.0	5.50	12.3
E2	42.5	2200	599	0.01	0.0	5.50	12.9
E5	49.1	2257	636	0.01	0.0	5.64	11.5
E3	28.9	1439	1347	0.03	0.1	3.60	12.4
Ind1	4.2	140	750	0.02	0.4	0.35	8.4
Ind2	4.4	170	750	0.02	0.3	0.43	9.7
Ind3	3.9	280	970	0.02	0.5	0.70	17.8
Ind4	2.8	310	1100	0.02	0.8	0.78	27.3
Ind5	9.6	280	860	0.02	0.2	0.70	7.3
Bra 1	7.6	226	749	0.01	0.2	0.56	7.4
Men 1	4.2	85	1347	0.03	0.6	0.21	5.0
Bra 2	14.9	169	1497	0.03	0.2	0.42	2.8
Bra 3	9.2	169	1297	0.03	0.3	0.42	4.6
Bra 4	8.8	141	1038	0.02	0.2	0.35	4.0
Bra 5	7.2	113	1447	0.03	0.4	0.28	3.9
Bra 6	7.3	113	1023	0.02	0.3	0.28	3.8
Bra 7	8.0	141	1010	0.02	0.3	0.35	4.4

For samples S4, S5, and S7 from tributaries in the southern catchment of Lake Bangong a contributions from evaporite minerals between 20 and 40 % has been calculated. The fraction of Cl relative to the sum of anions (Cl/TZ^-) is similar or considerably lower compared to other samples in the northern and

southern catchment. Thus, the lithium content of evaporites in the study area is probably over estimated. The calculated contributions are the uppermost possible fraction of lithium from evaporites and likely much lower than estimated.

S4-9 Compilation of δ⁷Li values and Li/Na ratios of global rivers, continental thermal waters, and streams investigated during this study
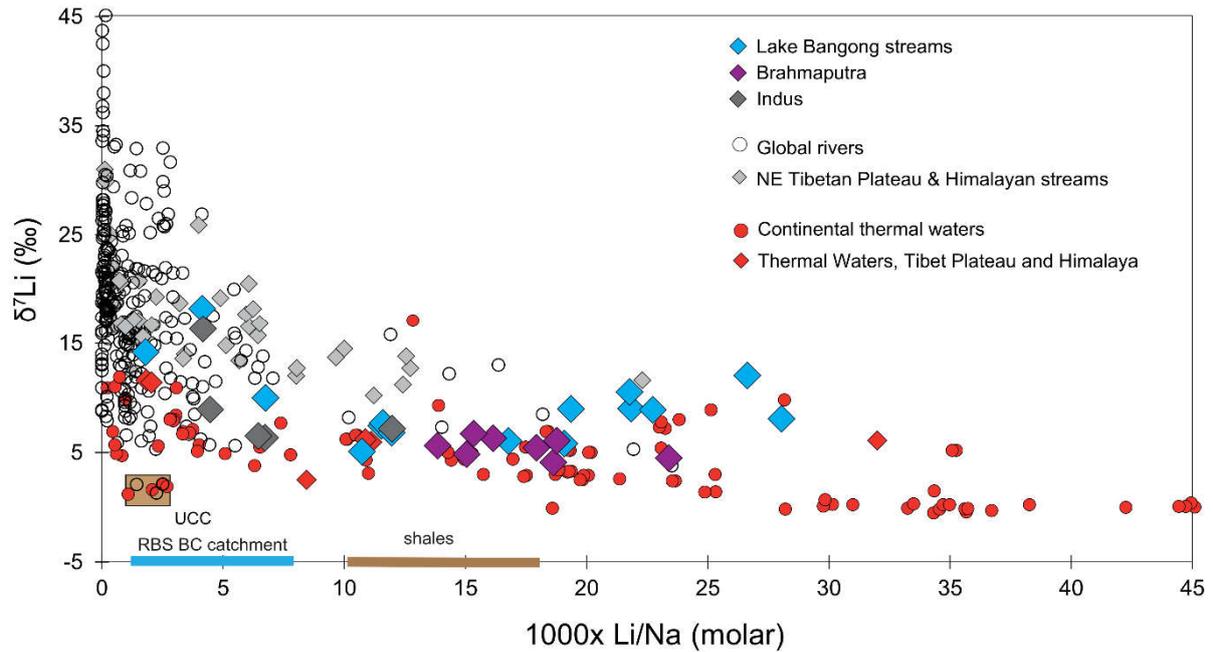
Compilation of δ⁷Li values vs. 1000•Li/Na values from streams and rivers from this study (Lake Bangong catchment, Indus and Yarlung Tsangpo), global rivers, streams from the northeastern Tibetan Plateau and the Himalayas, continental thermal waters and thermal waters from the northeastern Tibetan Plateau and the Himalayas are shown. The average composition of the upper continental crust (UCC), common shales, and river bed sediments from Lake Bangong catchment (RBS BC catchment) are shown for comparison. In general, Li/Na ratios of rivers are in the range of crustal rocks whereas thermal waters display high Li/Na ratios. References for rivers are given in S2; thermal waters are from (Tomascak et al., 2003; Kisakurek et al., 2005; Pogge von Strandmann et al., 2006; Millot and Négrel, 2007; Millot et al., 2007; Pogge von Strandmann et al., 2010; Millot et al., 2012; Rad et al., 2013; Henchiri et al., 2014; Pogge von Strandmann et al., 2016; Weynell et al., 2017).

S4-10 Calculation of the fraction of initially solubilized Li (f_{DL}) remaining in solution
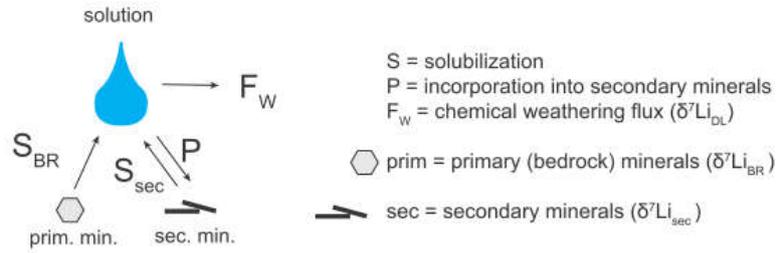
$(P-S_{sec})/S_{prim} = P_{net}/S_{BR} = f_{sec} = 1- f_{DL}$ (fraction of Li solubilized from primary minerals and partitioned into clays)

Assumption

We just consider the net incorporation flux into secondary minerals: $P_{net} = P-S_{sec}$.

In- and outgoing fluxes to the weathering solution (S_{BR}; P_{net}; F_{DL}) are in steady state $S_{BR} = P_{net} + F_{DL}$

$\delta^7Li_{sec} = \delta^7Li_{DL} - \Delta^7Li_{DL-sec}$ (equilibrium isotope fractionation between secondary minerals and solution)

Each flux has its Li isotopic composition

$\delta^7Li_{BR} \bullet S_{BR} = \delta^7Li_{sec} \bullet P_{net} + \delta^7Li_{DL} \bullet F_{DL}$

$\delta^7Li_{BR} \bullet S_{BR} = \delta^7Li_{sec} \bullet (S_{BR}-F_{DL}) + \delta^7Li_{DL} \bullet F_{DL}$

$\delta^7Li_{BR} \bullet S_{BR} = (\delta^7Li_{DL} - \Delta^7Li_{DL-sec}) \bullet (S_{BR}-F_{DL}) + \delta^7Li_{DL} \bullet F_{DL}$

$0 = \delta^7Li_{DL}\bullet S_{BR} - S_{BR}\, \delta^7Li_{BR} \bullet S_{BR} + \Delta^7Li_{DL-sec} \bullet (S_{BR}-F_{DL})$

$0 = \delta^7Li_{DL}\bullet S_{BR} - S_{BR}\, \delta^7Li_{BR} \bullet S_{BR} + \Delta^7Li_{DL-sec} \bullet P$

$-\Delta^7Li_{DL-sec} \bullet P = S_{BR} \bullet (\delta^7Li_{DL}-\delta^7Li_{BR})$

$-\Delta^7Li_{DL-sec} \bullet P/S_{BR} = \delta^7Li_{DL}-\delta^7Li_{BR}$

$-\Delta^7Li_{DL-sec} \bullet f_{sec} = \delta^7Li_{DL}-\delta^7Li_{BR}$

$\delta^7Li_{BR} = \delta^7Li_{DL} -\Delta^7Li_{DL-sec} \bullet f_{sec}$

$\delta^7Li_{BR} = \delta^7Li_{DL} -\Delta^7Li_{DL-sec} \bullet (1-f_{DL})$

$$f_{DL} = 1-\left(\frac{\delta^7Li_{DL} - \delta^7Li_{BR}}{\Delta^7Li_{DL-sec}}\right)$$

S4-11 Lithium isotopes and concentrations in the lake basins and Nama Chu, Lake Bangong catchment
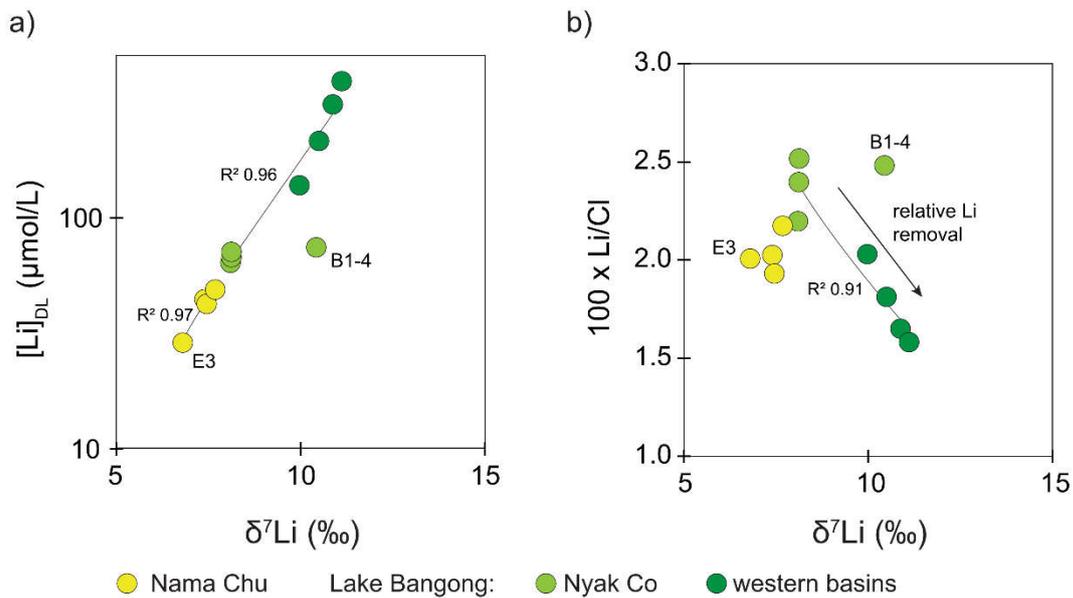
a) Coeval increase of Li concentrations and δ^7Li values in Nama Chu (after location E3 where inflow is almost completely dammed by road constructions) and in the lake basins. b) Relative Li removal and coeval δ^7Li increase westwards in the lake basin chain is indicated.

4.9 ACKNOWLEDGMENTS

Chapter 4: A low δ⁷Li weathering regime on the western Tibetan Plateau – source effect or supply limited weathering under a hyper-arid climate?

CHAPTER 5

CONCLUSIONS AND OUTLOOK

5.1 OVERALL CONCLUSIONS

This chapter summarizes the major findings of the chapters 2 to 4, which represent the scientific achievements of this thesis. The main contribution of this dissertation is the first research on lithium isotope variations across the Tibetan Plateau. On the one hand, it is one of the first studies that performs a detailed investigation of Li isotope variations in lake catchments. On the other hand, it is the first study that investigates the controls on Li isotope variations in large rivers across the Tibetan Plateau and looks for implications on weathering and erosion as well as the interpretation of Li isotope archives. The five main findings regarding to the research goals of section 1-6 are:

I.   Chemical weathering of carbonates determines the ion composition of streams in both lake catchments as well as the upper Huang He, the upper Indus, and the Yarlung Tsangpo. Evaporation accounts for a lake water loss of 55 % in Lake Donggi Cona and 69 % to 86 % in the basins of Lake Bangong as well as substantial water loss in its smallest inflow. Riverine lithium is mainly solubilized from silicates either by chemical weathering reactions in the weathering zone or dissolution by thermal waters in deeper areas. The hydrochemical and oxygen-hydrogen-isotope composition of surface waters in Lake Donggi Cona catchment highlight that the major inflow (Dongqu River) supplies around 90 % and thermal waters around 10 % to the hydrochemical budget of the lake. Similar oxygen and lithium isotope compositions of the modern Lake Donggi Cona water or lake sediments, respectively and oxygen and lithium in archives indicate stable climate and weathering conditions in the area since at least 4300 years.

II. δ^7Li values of streams and the lake are nearly constant around +16.6 ‰ in the Lake Donggi Cona catchment. A small inflow to Lake Donggi Cona displays δ^7Li values of +20.5 ‰, which are the highest reported for the plateau so far. The high content of Na, Cl, Ca, and HCO_3 as well as Li in the stream is mainly of hydrothermal origin. A model reproduces the measured δ^7Li values and Li concentrations in the small inflow. Waters, which solubilize Li from bedrock minerals in the weathering zone (with a δ^7Li around +1.9 ‰), and thermal waters (δ^7Li around +10.5 ‰) are mixed in proportions of around 30 % and 70 %, respectively. Subsequently, around 70 % of Li is incorporated into secondary minerals under a fractionation factor of α ~0.982. The fractionation factor is deduced from areas of the catchment without hydrothermal activity. Thus,

hydrothermally provided Li is not admixed to the surface waters but percolates through the weathering zone where it is processed by chemical weathering.

Thermal waters do not emerge in the catchment of Lake Bangong but high Li/Na ratios identify a hydrothermal contribution on riverine Li concentrations. The ion composition of nearby geothermal fields and Lake Bangong inflows considerably differ. For this reason, it is proposed that hydrothermally provided Li is not admixed to solutions but likewise processed in the weathering zone. A substantial hydrothermal contribution is not reported for the upper Indus and the Yarlung Tsangpo, ions are almost exclusively derived from dissolution of silicates and carbonates. Thus, Li in rivers on the western and southern Tibetan Plateau dominantly reflects silicate weathering.

Processes in the weathering zone and not the source dominate the Li isotope composition in the rivers. The possible large quantity of Li provided by thermal waters does not obscure the use of Li isotopes as weathering tracer on the Tibetan Plateau.

III. Rivers on the Tibetan Plateau display a wide range of δ^7Li values between +6 ‰ and +21 ‰. Nearly constant δ^7Li values around +17 ‰ of hydrothermally uncontaminated streams on the northeastern plateau reflect incorporation of ~85 % of initially solubilized Li in clays. Although soils in the catchment are thin, poor developed, and frozen throughout the winter the weathering reactor is capable to incorporate large quantities of initially solubilized Li into secondary minerals. Nearly constant isotopic fractionation but varying hydraulic conditions and topography at the sample locations imply (nearly) equilibrium fractionation under an α ~0.982 ($\pm$0.002).

Average riverine δ^7Li values in the two major inflows of Lake Bangong are low between +6 ‰ and +9 ‰, which reflects a net-incorporation of only ~25 % and ~40 % Li in secondary minerals. Lithium isotope variations in fluvial sediments correlate with weathering intensity proxies confirming that sedimentary Li isotope variations trace weathering intensity and not the source. δ^7Li values and weathering intensity proxies indicate progressive and relatively intense weathering of river sediments in small floodplains where moisture concentrates.

δ^7Li variations between bedrock, solution, and eroded sediments in both catchments reflect relative differences in the export fluxes from the weathering zone as dissolved Li compared to Li eroded in secondary minerals and rock detritus. For the catchment of Lake Donggi Cona an at least five times higher erosion rate compared to the chemical

weathering flux was calculated for Li. Both fluxes are roughly balanced in the catchment of Lake Bangong. The relative differences in the export fluxes are characteristic for a kinetically-limited weathering regime on the northeastern and a supply limited weathering regime on the western Tibetan Plateau (with respect to Li). The Li isotope composition of dissolved Li and Li in suspended particles in the upper Indus and the Yarlung Tsangpo resemble the low ones from the catchment of Lake Bangong whereas δ^7Li values in the Huang He resemble those of streams in Lake Donggi Cona catchment. In combination with literature data from the Yangtze headwaters a low δ^7Li weathering regime is identified on the western and southern Tibetan Plateau and a high δ^7Li regime in the northeast.

Morphology, relief, and temperatures resemble each other in the catchments of Lake Bangong, Lake Donggi Cona, the upper Indus and Huang He as well as the Yarlung Tsangpo. The difference in weathering and erosion is related to differences in annual precipitation (climate), which causes kinetically-limited silicate weathering in the northeast and facilitates supply-limited silicate weathering in the west and south of the Tibetan Plateau. In sum, Li isotopes on the Tibetan Plateau are controlled by the weathering regime.

IV.   A correlation or dependency between riverine Li isotope compositions and silicate weathering rates on the Tibetan Plateau was not observed. Riverine δ^7Li values are between +6 ‰ and +21 ‰ but silicate weathering rates across the plateau are low around 1 t/km^2/a. Thus, silicate weathering rates have no direct control on riverine Li isotope compositions. However, weathering and denudation rates have an indirect influence on Li isotope compositions: The low silicate weathering rates on the northeastern plateau allow the incorporation of around 85 % of initially solubilized Li although soils are thin, poorly developed, and frozen for half of the year. Further, nearly absent erosion results in long fluvial sediment residence times, which facilitates chemical weathering to overcome the water limitation on the hyper-arid western plateau.

V.   The Li isotope composition of Lake Donggi Cona can be reproduced if the Li isotope composition of the contributors are applied to the identified water balance for the lake. Thus, Li isotopes are not secondarily altered within the lake and the lake water reflects the Li isotope composition of the integrated weathering solutions of the catchment. In contrast, Li isotopes in Lake Bangong are secondary altered due strong evaporation and related mineral transformation in the smallest inflow and the lake basins itself. For this

reason, lake archives on the northeastern plateau would satisfyingly record the weathering history of the catchment whereas the hyper-arid climate obscures weathering induced Li variations in lake archives on the western plateau.

Modern rivers that drain the Tibetan Plateau display low and high riverine δ^7Li values, thus, rivers that drain the plateau do not necessarily increase global riverine δ^7Li values. However, the high riverine δ^7Li values are the result of kinetically-limited weathering reactions. The formation of the steep, high-precipitation mountain belts that border the plateau result in large-scale kinetically-limited weathering, capable to partly create the high δ^7Li values that are on average observed in modern global rivers.

The proposed control of riverine δ^7Li values by the weathering regime in this thesis supports former studies, which explain the rise of the global riverine and related oceanic δ^7Li during the Cenozoic by a weathering regime change. This thesis adds new evidence that the Cenozoic climate change is related to a weathering regime change, which does not necessarily has to come along with a substantial increase in silicate weathering rates.

5.2 OUTLOOK

In this thesis, the oxygen isotope composition of modern surface waters and the lithium isotope composition of modern clays from Lake Donggi Cona catchment were compared with those in old lake sediments. Within 1 ‰ similar $\delta^{18}O$ values identified stable climatic conditions since at least 4300 a (chapter 2) and within 0.5 ‰ similar δ^7Li values of modern clays and old lake or wetland sediments are explained with stable weathering conditions since 7800 a (chapter 3) in the catchment. Differences in the annual amount of precipitation, thus, climate were identified as main driver for the change of the weathering regime and, subsequent, Li isotope variations in rivers and fluvial sediments across the plateau. Recently, studies on Li isotope variations in clays in the Nile basin and Himalayan river basins as well as speleothems in Israel propose a coupling of climate (temperature and precipitation) and Li isotope variations (Dosseto et al., 2015; Bastian et al, 2017; Pogge von Strandmann et al., 2017c). The East Asian monsoon was identified as the dominant moisture source for the catchment of Lake Donggi Cona and the northeastern Tibetan Plateau (chapter 2). Several studies in the catchments of Lake Qinghai (Lister et al., 1991; Henderson et al., 2003; Henderson and Holmes, 2009; An et al., 2012) and Lake Donggi Cona (Mischke et al., 2010; Aichner et al., 2012; Ijmker et al., 2012; Opitz et al., 2012; Dietze et al., 2013; Opitz et al., 2016) identified considerable monsoon intensity fluctuations during the Early Holocene. Lake sediments in the catchment of Lake

Donggi Cona are well characterized, interpreted on climatic variations, and still available for research (Mischke et al., 2010; Aichner et al., 2012; Ijmker et al., 2012; Opitz et al., 2012; Dietze et al., 2013; Opitz et al., 2016). This makes those sediments from lake cores well suited to investigate the possible coupling of Li isotope variations in authigenic carbonates and clays with climate parameters, in particular, annual precipitation. Further, this allows to use the knowledge on modern weathering and erosion patterns and the connection to Li isotope variations in sediments, which is the outcome of this thesis, to infer on variations in the weathering-erosion-style on the northeastern Tibetan Plateau since the last glaciation.

This thesis reveals a shift from low riverine δ^7Li values around +6 ‰ on the western and southern to high riverine δ^7Li around +17 ‰ on the northeastern Tibetan Plateau. The shift in riverine δ^7Li across the plateau resembles the proposed shift for riverine δ^7Li during the Cenozoic, which maybe created the 9 ‰ rise of the seawater δ^7Li. The climate during the Eocene is certainly not comparable with the cold and dry climate on the Tibetan Plateau (Zachos et al., 2001). However, the shift of riverine δ^7Li values across the Tibetan Plateau and throughout the Cenozoic are both attributed to a change from supply- to kinetically-limited weathering (e.g. Misra and Froelich, 2012; Bouchez et al., 2013; Froelich and Misra, 2014; Li and West et al., 2014; Dellinger et al., 2015).

The change of the global weathering regime may affect the atmospheric CO_2 concentration by changing ocean alkalinity because processing of intensely weathered material through the weathering zone will deliver little alkali and earth alkali elements, whereas weathering of feldspar and other primary minerals may deliver a large amount of alkali and earth alkali elements as well as hydrogen carbonate to the ocean. On geological time scales this will shift the ocean alkalinity and related pH and reduce the CO_2 partial pressure of the atmosphere (e.g. Maher and Chamberlain, 2014). This processes may explain the proposed roughly stable weathering fluxes throughout the Cenozoic (e.g. Willenbring and von Blanckenburg; 2010) and is in agreement with the outcome of this thesis that a change of the global silicate weathering rate is not required to explain increasing riverine δ^7Li. For this reason, it is clearly of great interest to validate if the oceanic rise in δ^7Li mirrors a weathering regime change, thus, weathering in the Early Cenozoic created supply-limited weathering with respect to Li. The determination and investigation of Li isotope ratios and variations in weathering products within Eocene fluvial deposits or observed laterites (e.g. Nahon, 2003) would be coherent to test if the hypothesis is valid. River sediments in the supply-limited weathering regime on the western plateau display low δ^7Li down to -4.3 ‰ but clays on the northeastern plateau values

not lower than -1 ‰. The observation of substantially lower δ^7Li values in fine fluvial sediments compared to the bedrock under supply-limited weathering but a small offset under kinetically-limited weathering is supported from investigations on fluvial sediments of large global rivers (Dellinger et al.; 2017). For this reason, low δ^7Li values for Eocene fluvial deposits would provide further evidence for the hypothesis that supply-limited weathering conditions prevailed in the Early Cenozoic and caused the low δ^7Li of rivers and seawater.

REFERENCES

Ahmad, T., Khanna, P.P., Chakrapani, G.J., Balakrishnan, S., 1998. Geochemical characteristics of water and sediment of the Indus river, Trans-Himalaya, India: constraints on weathering and erosion. Journal of Asian Earth Sciences, 16(2–3): 333-346. https://doi.org/10.1016/S0743-9547(98)00016-6

Aichner, B., Herzschuh, U., Wilkes, H., Schulz, H.-M., Wang, Y., Plessen, B., Mischke, S., Diekmann, B., Zhang, C., 2012. Ecological development of Lake Donggi Cona, north-eastern Tibetan Plateau, since the late glacial on basis of organic geochemical proxies and non-pollen palynomorphs. Palaeogeography, Palaeoclimatology, Palaeoecology 313–314, 140-149. doi 10.1016/j.palaeo.2011.10.015

An, Z., Clemens, S.C., Shen, J., Qiang, X., Jin, Z., Sun, Y., Prell, W.L., Luo, J., Wang, S., Xu, H., Cai, Y., Zhou, W., Liu, X., Liu, W., Shi, Z., Yan, L., Xiao, X., Chang, H., Wu, F., Ai, L., Lu, F., 2011. Glacial-Interglacial Indian Summer Monsoon Dynamics. Science 333, 719-723. doi 10.1126/science.1203752

An, Z., Colman, S.M., Zhou, W., Li, X., Brown, E.T., Jull, A.J.T., Cai, Y., Huang, Y., Lu, X., Chang, H., Song, Y., Sun, Y., Xu, H., Liu, W., Jin, Z., Liu, X., Cheng, P., Liu, Y., Ai, L., Li, X., Liu, X., Yan, L., Shi, Z., Wang, X., Wu, F., Qiang, X., Dong, J., Lu, F., Xu, X., 2012. Interplay between the Westerlies and Asian monsoon recorded in Lake Qinghai sediments since 32 ka. Sci. Rep.,

http://www.nature.com/srep/2012/120831/srep00619/abs/srep00619.html#supplementary-information

An, Z., Kutzbach, J.E., Prell, W.L., Porter, S.C., 2001. Evolution of Asian monsoons and phased uplift of the Himalaya-Tibetan plateau since Late Miocene times. Nature (London) 411, 62-66. doi 10.1038/35075035

Anderson, S.P., von Blanckenburg, F., White, A.F., 2007. Physical and Chemical Controls on the Critical Zone. Elements, 3(5): 315-319. 10.2113/gselements.3.5.315

Araguas-Araguas, L., Froehlich, K., Rozanski, K., 1998. Stable isotope composition of precipitation over southeast Asia. Journal of Geophysical Research-Atmospheres 103, 28721-28742. doi

Araoka, D., Kawahata, H., Takagi, T., Watanabe, Y., Nishimura, K., Nishio, Y., 2014. Lithium and strontium isotopic systematics in playas in Nevada, USA: constraints on the origin of lithium. Mineralium Deposita, 49(3): 371-379. 10.1007/s00126-013-0495-y

Aulbach, S., Rudnick, R.L., 2009. Origins of non-equilibrium lithium isotopic fractionation in xenolithic peridotite minerals: Examples from Tanzania. Chemical Geology, 258(1–2): 17-27. http://dx.doi.org/10.1016/j.chemgeo.2008.07.015

Babechuk, M.G., Widdowson, M., Kamber, B.S., 2014. Quantifying chemical weathering intensity and trace element release from two contrasting basalt profiles, Deccan Traps, India. Chemical Geology, 363: 56-75. http://dx.doi.org/10.1016/j.chemgeo.2013.10.027

Bagard, M.-L., West, A.J., Newman, K., Basu, A.K., 2015. Lithium isotope fractionation in the Ganges–Brahmaputra floodplain and implications for groundwater impact on seawater isotopic composition. Earth and Planetary Science Letters. http://dx.doi.org/10.1016/j.epsl.2015.08.036

Bastian, L., Revel, M., Bayon, G., Dufour, A., Vigier, N., 2017. Abrupt response of chemical weathering to Late Quaternary hydroclimate changes in northeast Africa. Scientific Reports, 7: 44231. 10.1038/srep44231

Beaulieu, E., Godderis, Y., Donnadieu, Y., Labat, D., Roelandt, C., 2012. High sensitivity of the continental-weathering carbon dioxide sink to future climate change. Nature Clim. Change, 2(5): 346-349.

Beerling, D.J., Royer, D.L., 2011. Convergent Cenozoic CO2 history. Nature Geosci, 4(7): 418-420.

Benton, L.D., Ryan, J.G., Savov, I.P., 2004. Lithium abundance and isotope systematics of forearc serpentinites, Conical Seamount, Mariana forearc: Insights into the mechanics of slab-mantle exchange during subduction. Geochemistry, Geophysics, Geosystems, 5(8): Q08J12. 10.1029/2004gc000708

Berner, R.A., 1992. Weathering, plants, and the long-term carbon cycle. Geochimica et Cosmochimica Acta, 56(8): 3225-3231. http://dx.doi.org/10.1016/0016-7037(92)90300-8

Berner, R.A., Lasaga, A.C., Garrels, R.M., 1983. The carbonate-silicate geochemical cycle and its effect on atmospheric carbon dioxide over the past 100 million years. American Journal of Science, 283(7): 641-683. 10.2475/ajs.283.7.641

Bershaw, J., Penny, S.M., Garzione, C.N., 2012. Stable isotopes of modern water across the Himalaya and eastern Tibetan Plateau: Implications for estimates of paleoelevation and paleoclimate. Journal of Geophysical Research: Atmospheres, 117(D2): n/a-n/a. 10.1029/2011JD016132

Bouchez, J., Gaillardet, J., France-Lanord, C., Maurice, L., Dutra-Maia, P., 2011. Grain size control of river suspended sediment geochemistry: Clues from Amazon River depth profiles. Geochemistry, Geophysics, Geosystems, 12(3): Q03008. 10.1029/2010GC003380

Bouchez, J., von Blanckenburg, F., Schuessler, J.A., 2013. Modeling novel stable isotope ratios in the weathering zone. American Journal of Science, 313(4): 267-308. 10.2475/04.2013.01

Breitenbach, S.F.M., Adkins, J.F., Meyer, H., Marwan, N., Kumar, K.K., Haug, G.H., 2010. Strong influence of water vapor source dynamics on stable isotopes in precipitation observed in Southern Meghalaya, NE India. Earth and Planetary Science Letters 292, 212-220. doi 10.1016/j.epsl.2010.01.038

Brunet, F., Gaiero, D., Probst, J.L., Depetris, P.J., Gauthier Lafaye, F., Stille, P., 2005. δ13C tracing of dissolved inorganic carbon sources in Patagonian rivers (Argentina). Hydrological Processes 19, 3321-3344. doi 10.1002/hyp.5973

Buggle, B., Glaser, B., Hambach, U., Gerasimenko, N., Marković, S., 2011. An evaluation of geochemical weathering indices in loess–paleosol studies. Quaternary International, 240(1–2): 12-21. http://dx.doi.org/10.1016/j.quaint.2010.07.019

Burton, K.W., Vigier, N., 2012. Lithium Isotopes as Tracers in Marine and Terrestrial Environments. In: Baskaran, M. (Ed.), Handbook of Environmental Isotope Geochemistry: Vol I. Springer Berlin Heidelberg, Berlin, Heidelberg, pp. 41-59.

Caldeira, K., Wickett, M.E., 2003. Oceanography: Anthropogenic carbon and ocean pH. Nature, 425(6956): 365-365.

Cartwright, I., Weaver, T.R., Fulton, S., Nichol, C., Reid, M., Cheng, X., 2004. Hydrogeochemical and isotopic constraints on the origins of dryland salinity, Murray Basin, Victoria, Australia. Applied Geochemistry 19, 1233-1254. doi http://dx.doi.org/10.1016/j.apgeochem.2003.12.006

Caves, J.K., Jost, A.B., Lau, K.V., Maher, K., 2016. Cenozoic carbon cycle imbalances and a variable weathering feedback. Earth and Planetary Science Letters, 450: 152-163. http://dx.doi.org/10.1016/j.epsl.2016.06.035

Caves, J.K., Winnick, M.J., Graham, S.A., Sjostrom, D.J., Mulch, A., Chamberlain, C.P., 2015. Role of the westerlies in Central Asia climate over the Cenozoic. Earth and Planetary Science Letters, 428: 33-43. http://dx.doi.org/10.1016/j.epsl.2015.07.023

Chan, L.-H., Edmond, J.M., Thompson, G., 1993. A lithium isotope study of hot springs and metabasalts from Mid-Ocean Ridge Hydrothermal Systems. Journal of Geophysical Research: Solid Earth, 98(B6): 9653-9659. 10.1029/92jb00840

Chan, L.H., Edmond, J.M., Thompson, G., Gillis, K., 1992. Lithium isotopic composition of submarine basalts: implications for the lithium cycle in the oceans. Earth and Planetary Science Letters, 108(1–3): 151-160. http://dx.doi.org/10.1016/0012-821X(92)90067-6

Clark, I., Fritz, P., 1997. Environmental isotopes in hydrogeology, 2nd ed. CRC Press LLC, Boca Raton, New York, USA.

Clergue, C., Dellinger, M., Buss, H.L., Gaillardet, J., Benedetti, M.F., Dessert, C., 2015. Influence of atmospheric deposits and secondary minerals on Li isotopes budget in a highly weathered catchment, Guadeloupe (Lesser Antilles). Chemical Geology, 414: 28-41. http://dx.doi.org/10.1016/j.chemgeo.2015.08.015

Coogan, L.A., Kasemann, S.A., Chakraborty, S., 2005. Rates of hydrothermal cooling of new oceanic upper crust derived from lithium-geospeedometry. Earth and Planetary Science Letters, 240(2): 415-424. http://dx.doi.org/10.1016/j.epsl.2005.09.020

Coplen, T.B., 2011. Guidelines and recommended terms for expression of stable-isotope-ratio and gas-ratio measurement results. Rapid Communications in Mass Spectrometry, 25(17): 2538-2560. 10.1002/rcm.5129

Craig, H., 1961. Isotopic Variations in Meteoric Waters. Science 133, 1702-1703.

Craig, H., 1963. The isotopic geochemistry of water and carbon in geothermal areas, in: Tongiorgi, E. (Ed.), Nuclear geology in geothermal areas. Consiglio Nazionale della Ricerche, Laboratorio de Geologia Nucleare, Pisa, Italy, pp. 17-53.

Craig, H., Gordon, L.I., 1965. Deuterium and Oxygen l8 Variations in the Ocean and the Marine Atmosphere. Stable Isotopes in Oceanographic Studies and Paleaotemperatures

Craig, J., Absar, A., Bhat, G., Cadel, G., Hafiz, M., Hakhoo, N., Kashkari, R., Moore, J., Ricchiuto, T.E., Thurow, J., Thusu, B., 2013. Hot springs and the geothermal energy potential of Jammu & Kashmir State, N.W. Himalaya, India. Earth-Science Reviews, 126: 156-177. https://doi.org/10.1016/j.earscirev.2013.05.004

Cui, B.-L., Li, X.-Y., 2014. Characteristics of stable isotope and hydrochemistry of the groundwater around Qinghai Lake, NE Qinghai-Tibet Plateau, China. Environ Earth Sci 71, 1159-1167. doi 10.1007/s12665-013-2520-y

Curio, J., Maussion, F., Scherer, D., 2015. A 12-year high-resolution climatology of atmospheric water transport over the Tibetan Plateau. Earth Syst. Dynam., 6(1): 109-124. 10.5194/esd-6-109-2015

Currell, M., Cartwright, I., 2011. Major-ion chemistry, $\delta13C$ and 87Sr/86Sr as indicators of hydrochemical evolution and sources of salinity in groundwater in the Yuncheng Basin, China. Hydrogeol J 19, 835-850. doi 10.1007/s10040-011-0721-6

Deer, W.A., Howie, R.A., Zussman, J., 2012. An Introduction to the Rock-Forming Minerals, 495 pp.

Dellinger, M., Bouchez, J., Gaillardet, J., Faure, L., Moureau, J., 2017. Tracing weathering regimes using the lithium isotope composition of detrital sediments. Geology, 45(5): 411-414. 10.1130/g38671.1

Dellinger, M., Gaillardet, J., Bouchez, J., Calmels, D., Galy, V., Hilton, R.G., Louvat, P., France-Lanord, C., 2014. Lithium isotopes in large rivers reveal the cannibalistic nature of modern continental weathering and erosion. Earth and Planetary Science Letters, 401(0): 359-372.

Dellinger, M., Gaillardet, J., Bouchez, J., Calmels, D., Louvat, P., Dosseto, A., Gorge, C., Alanoca, L., Maurice, L., 2015. Riverine Li isotope fractionation in the Amazon River basin controlled by the weathering regimes. Geochimica et Cosmochimica Acta(0). http://dx.doi.org/10.1016/j.gca.2015.04.042

Dellinger, M., Joshua West, A., Paris, G., Adkins, J.F., Pogge von Strandmann, P., Ullmann, C.V., Eagle, R.A., Freitas, P., Bagard, M.-L., Ries, J.B., Corsetti, F.A., Perez-Huerta, A., Kampf, A.R., 2018. The Li isotope composition of marine biogenic carbonates: Patterns and Mechanisms. Geochimica et Cosmochimica Acta. https://doi.org/10.1016/j.gca.2018.03.014

DePaolo, D.J., 2011. Surface kinetic model for isotopic and trace element fractionation during precipitation of calcite from aqueous solutions. Geochimica et Cosmochimica Acta, 75(4): 1039-1056. http://dx.doi.org/10.1016/j.gca.2010.11.020

Dessert, C., Lajeunesse, E., Lloret, E., Clergue, C., Crispi, O., Gorge, C., Quidelleur, X., 2015. Controls on chemical weathering on a mountainous volcanic tropical island: Guadeloupe (French West Indies). Geochimica et Cosmochimica Acta, 171: 216-237. http://dx.doi.org/10.1016/j.gca.2015.09.009

Dettman, D.L., Kohn, M.J., Quade, J., Ryerson, F.J., Ojha, T.P., Hamidullah, S., 2001. Seasonal stable isotope evidence for a strong Asian monsoon throughout the past 10.7 m.y. Geology 29, 31-34. doi 10.1130/0091-7613(2001)029<0031:ssiefa>2.0.co;2

Diekmann, B., Kuhn, G., Rachold, V., Abelmann, A., Brathauer, U., Fütterer, D.K., Gersonde, R., Grobe, H., 2000. Terrigenous sediment supply in the Scotia Sea (Southern Ocean): response to Late Quaternary ice dynamics in Patagonia and on the Antarctic Peninsula. Palaeogeography, Palaeoclimatology, Palaeoecology, 162(3–4): 357-387.

Dietze, E., Hartmann, K., Diekmann, B., Ijmker, J., Lehmkuhl, F., Opitz, S., Stauch, G., Wünnemann, B., Borchers, A., 2012. An end-member algorithm for deciphering modern detrital processes from lake sediments of Lake Donggi Cona, NE Tibetan Plateau, China. Sedimentary Geology 243–244, 169-180. doi 10.1016/j.sedgeo.2011.09.014

Dietze, E., Wünnemann, B., Diekmann, B., Aichner, B., Hartmann, K., Herzschuh, U., Ijmker, J., Jin, H., Kopsch, C., Lehmkuhl, F., Li, S., Mischke, S., Niessen, F., Opitz, S., Stauch, G., Yang, S., 2010. Basin morphology and seismic stratigraphy of Lake Donggi Cona, north-eastern Tibetan Plateau, China. Quaternary International 218, 131-142. doi http://dx.doi.org/10.1016/j.quaint.2009.11.035

Dietze, E., Wünnemann, B., Hartmann, K., Diekmann, B., Jin, H., Stauch, G., Yang, S., Lehmkuhl, F., 2013. Early to mid-Holocene lake high-stand sediments at Lake Donggi Cona, northeastern Tibetan Plateau, China. Quaternary Research 79, 325-336. doi http://dx.doi.org/10.1016/j.yqres.2012.12.008

Domrös, M., Peng, G., 1988. The climate of China. Springer Berlin Heidelberg.

Dosseto, A., Vigier, N., Joannes-Boyau, R., Moffat, I., Singh, T., Srivastava, P., 2015. Rapid response of silicate weathering rates to climate change in the Himalaya. Geochemical Perspectives Letters, 1(0): 10-19.

Edmond, J.M., Palmer, M.R., Measures, C.I., Grant, B., Stallard, R.F., 1995. The fluvial geochemistry and denudatin rate of the Guayana Shield in Venezuela, Colombia, and Brasil. Geochimica Et Cosmochimica Acta, 59(16): 3301-3325. 10.1016/0016-7037(95)00128-m

Edmunds, W.M., Bath, A.H., Miles, D.L., 1982. Hydrochemical evolution of the East Midlands Triassic sandstone aquifer, England. Geochimica et Cosmochimica Acta 46, 2069-2081. doi http://dx.doi.org/10.1016/0016-7037(82)90186-7

Einsele, G., Ratschbacher, L., Wetzel, A., 1996. The Himalaya-Bengal Fan Denudation-Accumulation System during the past 20 Ma. The Journal of Geology, 104(2): 163-184.

Elderfield, H., Schultz, A., 1996. Mid-ocean ridge hydrothermal fluxes and the chemical composition of the ocean. Annual Review of Earth and Planetary Sciences, 24(1): 191-224. doi:10.1146/annurev.earth.24.1.191

Epstein, S., Mayeda, T., 1953. Variation of O18 content of waters from natural sources. Geochimica et Cosmochimica Acta 4, 213-224.

Fischer-Godde, M., Becker, H., Wombacher, F., 2011. Rhodium, gold and other highly siderophile elements in orogenic peridotites and peridotite xenoliths. Chemical Geology, 280(3-4): 365-383. 10.1016/j.chemgeo.2010.11.024

Fontes, J.C., Gasse, F., Gibert, E., 1996. Holocene environmental changes in Lake Bangong basin (western Tibet) .1. Chronology and stable isotopes of carbonates of a Holocene lacustrine core. Palaeogeography Palaeoclimatology Palaeoecology, 120(1-2): 25-47.

References

Fort, M., van Vliet-Lanoe, B., 2007. Permafrost and periglacial environment of Western Tibet. Landform Analysis, 5: 25-29.

France-Lanord, C., Derry, L.A., 1997. Organic carbon burial forcing of the carbon cycle from Himalayan erosion. Nature, 390(6655): 65-67.

Freeze, R.A., Cherry, J.A., 1979. Groundwater. Prentice Hall, 604 pp.

Froelich, F., Misra, S., 2014. Was the Late Paleocene-Early Eocene Hot Because Earth Was Flat? An Ocean Lithium Isotope View of Mountain Building, Continental Weathering, Carbon Dioxide, and Earth's Cenozoic Climate. Oceanography, 27. 10.5670/oceanog.2014.06

Fröhlich, F., 1960. Beitrag zur Geochemie des Chroms. Geochimica et Cosmochimica Acta, 20(3–4): 215-240. http://dx.doi.org/10.1016/0016-7037(60)90075-2

Fu, B., Awata, Y., 2007. Displacement and timing of left-lateral faulting in the Kunlun Fault Zone, northern Tibet, inferred from geologic and geomorphic features. Journal of Asian Earth Sciences 29, 253-265. doi 10.1016/j.jseaes.2006.03.004

Gaillardet, J., Dupré, B., Allègre, C.J., 1999a. Geochemistry of large river suspended sediments: silicate weathering or recycling tracer? Geochimica et Cosmochimica Acta, 63(23–24): 4037-4051. http://dx.doi.org/10.1016/S0016-7037(99)00307-5

Gaillardet, J., Dupré, B., Louvat, P., Allègre, C.J., 1999b. Global silicate weathering and CO2 consumption rates deduced from the chemistry of large rivers. Chemical Geology, 159(1–4): 3-30. 10.1016/s0009-2541(99)00031-5

Garzione, C.N., 2008. Surface uplift of Tibet and Cenozoic global cooling. Geology, 36(12): 1003-1004. 10.1130/focus122008.1

Garzione, C.N., Quade, J., DeCelles, P.G., English, N.B., 2000. Predicting paleoelevation of Tibet and the Himalaya from $\delta 18O$ vs. altitude gradients in meteoric water across the Nepal Himalaya. Earth and Planetary Science Letters 183, 215-229. doi http://dx.doi.org/10.1016/S0012-821X(00)00252-1

Gasse, F., Fontes, J.C., Van Campo, E., Wei, K., 1996. Holocene environmental changes in Bangong Co basin (Western Tibet). Part 4: Discussion and conclusions. Palaeogeography, Palaeoclimatology, Palaeoecology, 120(1-2): 79-92.

Gat, J.R., 1996. Oxygen and Hydrogen Isotopes in the hydrologic cycle. Annu. Rev. Earth Planet. Sci. 24, 225-262. doi

Gibbs, R.J., 1970. Mechanisms Controlling World Water Chemistry. Science 170, 1088-1090. doi 10.1126/science.170.3962.1088

Gislason, S.R., Arnorsson, S., Armannsson, H., 1996. Chemical weathering of basalt in Southwest Iceland; effects of runoff, age of rocks and vegetative/glacial cover. American Journal of Science, 296(8): 837-907. 10.2475/ajs.296.8.837

Gislason, S.R., Oelkers, E.H., Eiriksdottir, E.S., Kardjilov, M.I., Gisladottir, G., Sigfusson, B., Snorrason, A., Elefsen, S., Hardardottir, J., Torssander, P., Oskarsson, N., 2009. Direct evidence of the feedback between climate and weathering. Earth and Planetary Science Letters, 277(1–2): 213-222. http://dx.doi.org/10.1016/j.epsl.2008.10.018

Goldschmidt, V.M., 1933. Grundlagen der quantitativen Geochemie. Fortschritte der Mineralogie, Kristallographie und Petrographie, 17(2): 112-156.

Gonfiantini, R., 1978. Standards for stable isotope measurements in natural compounds. Nature 271, 534-536.

Gonfiantini, R., 1986. Environmental Isotopes in Lake Studies. Handbook of environmental isotope geochemistry 2, 113-168.

Gourbet, L., Mahéo, G., Leloup, P.H., Paquette, J.-L., Sorrel, P., Henriquet, M., Liu, X., Liu, X., 2017. Western Tibet relief evolution since the Oligo-Miocene. Gondwana Research, 41: 425-437. http://doi.org/10.1016/j.gr.2014.12.003

Grimaud, D., Huang, S., Michard, G., Zheng, K., 1985. Chemical study of geothermal waters of Central Tibet (China). Geothermics, 14(1): 35-48. http://dx.doi.org/10.1016/0375-6505(85)90092-6

Guo, Q., Wang, Y., Liu, W., 2007. Major hydrogeochemical processes in the two reservoirs of the Yangbajing geothermal field, Tibet, China. Journal of Volcanology and Geothermal Research, 166(3–4): 255-268. https://doi.org/10.1016/j.jvolgeores.2007.08.004

Guo, X., Tian, L., Wen, R., Yu, W., Qu, D., 2017. Controls of precipitation $\delta 18O$ on the northwestern Tibetan Plateau: A case study at Ngari station. Atmospheric Research, 189: 141-151. http://doi.org/10.1016/j.atmosres.2017.02.004

Guo, X., Tian, L., Wang, L., Yu, W., Qu, D., 2017b. River recharge sources and the partitioning of catchment evapotranspiration fluxes as revealed by stable isotope signals in a typical high-elevation arid catchment. Journal of Hydrology. http://doi.org/10.1016/j.jhydrol.2017.04.037

Hathorne, E.C., James, R.H., 2006. Temporal record of lithium in seawater: A tracer for silicate weathering? Earth and Planetary Science Letters, 246(3-4): 393-406.

Harris, N., 2006. The elevation history of the Tibetan Plateau and its implications for the Asian monsoon. Palaeogeography, Palaeoclimatology, Palaeoecology 241, 4-15.

Hayes, J.M., Strauss, H., Kaufman, A.J., 1999. The abundance of 13C in marine organic matter and isotopic fractionation in the global biogeochemical cycle of carbon during the past 800 Ma. Chemical Geology, 161(1–3): 103-125.

Henchiri, S., Clergue, C., Dellinger, M., Gaillardet, J., Louvat, P., Bouchez, J., 2014. The Influence of Hydrothermal Activity on the Li Isotopic Signature of Rivers Draining Volcanic Areas. Procedia Earth and Planetary Science, 10: 223-230. http://dx.doi.org/10.1016/j.proeps.2014.08.026

Henchiri, S., Gaillardet, J., Dellinger, M., Bouchez, J., Spencer, R.G.M., 2016. Riverine dissolved lithium isotopic signatures in low-relief central Africa and their link to weathering regimes. Geophysical Research Letters, 43(9): 4391-4399.

Henderson, A.C.G., Holmes, J.A., 2009. Palaeolimnological evidence for environmental change over the past millennium from Lake Qinghai sediments: A review and future research prospective. Quaternary International, 194(1–2): 134-147. http://dx.doi.org/10.1016/j.quaint.2008.09.008

Henderson, A.C.G., Holmes, J.A., Zhang, J., Leng, M.J., Carvalho, L.R., 2003. A carbon- and oxygen-isotope record of recent environmental change from Qinghai Lake, NE Tibetan Plateau. Chinese Science Bulletin, 48(14): 1463-1468. 10.1360/02wd0272

Herold, N., Buzan, J., Seton, M., Goldner, A., Green, J.A.M., Müller, R.D., Markwick, P., Huber, M., 2014. A suite of early Eocene (~ 55 Ma) climate model boundary conditions. Geosci. Model Dev., 7(5): 2077-2090. 10.5194/gmd-7-2077-2014

Herzschuh, U., 2006. Palaeo-moisture evolution in monsoonal Central Asia during the last 50,000 years. Quaternary Science Reviews 25, 163-178. doi 10.1016/j.quascirev.2005.02.006

Heyman, J., Stroeven, A., Harbor, J., Li, Y., Haettestrand, C., 2014. Erosion of the NE Tibetan Plateau based on Be-10 in river sediments. EGU abstract.

Hochstein, M.P., Regenauer-Lieb, K., 1998. Heat generation associated with collision of two plates: the Himalayan geothermal belt. Journal of Volcanology and Geothermal Research, 83(1–2): 75-92. https://doi.org/10.1016/S0377-0273(98)00018-3

Hoefs, J., Sywall, M., 1997. Lithium isotope composition of quaternary and tertiary biogene carbonates and a global lithium isotope balance. Geochimica et Cosmochimica Acta, 61(13): 2679-2690.

Hoke, L., Lamb, S., Hilton, D.R., Poreda, R.J., 2000. Southern limit of mantle-derived geothermal helium emissions in Tibet: implications for lithospheric structure. Earth and Planetary Science Letters, 180(3–4): 297-308. https://doi.org/10.1016/S0012-821X(00)00174-6

Hren, M.T., Bookhagen, B., Blisniuk, P.M., Booth, A.L., Chamberlain, C.P., 2009. δ18O and δD of streamwaters across the Himalaya and Tibetan Plateau: Implications for moisture sources and paleoelevation reconstructions. Earth and Planetary Science Letters 288, 20-32. doi

Hren, M.T., Chamberlain, C.P., Hilley, G.E., Blisniuk, P.M., Bookhagen, B., 2007. Major ion chemistry of the Yarlung Tsangpo-Brahmaputra river: Chemical weathering, erosion, and CO2 consumption in the southern Tibetan plateau and eastern syntaxis of the Himalaya. Geochimica et Cosmochimica Acta, 71(12): 2907-2935.

Huang, K.-F., You, C.-F., Liu, Y.-H., Wang, R.-M., Lin, P.-Y., Chung, C.-H., 2010. Low-memory, small sample size, accurate and high-precision determinations of lithium isotopic ratios in natural materials by MC-ICP-MS. Journal of Analytical Atomic Spectrometry, 25(7): 1019-1024.

Huh, Y., Chan, L.-H., Edmond, J.M., 2001. Lithium isotopes as a probe of weathering processes: Orinoco River. Earth and Planetary Science Letters, 194(1–2): 189-199. http://dx.doi.org/10.1016/S0012-821X(01)00523-4

Huh, Y., Chan, L.-H., Zhang, L., Edmond, J.M., 1998. Lithium and its isotopes in major world rivers: implications for weathering and the oceanic budget. Geochimica et Cosmochimica Acta, 62(12): 2039-2051.

Ijmker, J., Stauch, G., Dietze, E., Hartmann, K., Diekmann, B., Lockot, G., Opitz, S., Wünnemann, B., Lehmkuhl, F., 2012a. Characterisation of transport processes and sedimentary deposits by statistical end-member mixing analysis of terrestrial sediments in the Donggi Cona lake catchment, NE Tibetan Plateau. Sedimentary Geology 281, 166-179. doi http://dx.doi.org/10.1016/j.sedgeo.2012.09.006

Ijmker, J., Stauch, G., Hartmann, K., Diekmann, B., Dietze, E., Opitz, S., Wünnemann, B., Lehmkuhl, F., 2012b. Environmental conditions in the Donggi Cona lake catchment, NE Tibetan Plateau, based on factor analysis of geochemical data. Journal of Asian Earth Sciences 44, 176-188. doi 10.1016/j.jseaes.2011.04.021

Ijmker, J., Stauch, G., Pötsch, S., Diekmann, B., Wünnemann, B., Lehmkuhl, F., 2012c. Dry periods on the NE Tibetan Plateau during the late Quaternary. Palaeogeography, Palaeoclimatology, Palaeoecology 346–347, 108-119. doi http://dx.doi.org/10.1016/j.palaeo.2012.06.005

Immerzeel, W.W., van Beek, L.P.H., Bierkens, M.F.P., 2010. Climate Change Will Affect the Asian Water Towers. Science 328, 1382-1385. doi 10.1126/science.1183188

Jeffcoate, A.B., Elliott, T., Kasemann, S.A., Ionov, D., Cooper, K., Brooker, R., 2007. Li isotope fractionation in peridotites and mafic melts. Geochimica et Cosmochimica Acta, 71(1): 202-218. http://dx.doi.org/10.1016/j.gca.2006.06.1611

Jeffcoate, A.B., Elliott, T., Thomas, A., Bouman, C., 2004. Precise, small sample size determinations of lithium isotopic compositions of geological reference materials and modern seawater by MC-ICP-MS. Geostandards and Geoanalytical Research, 28(1): 161-172. 10.1111/j.1751-908X.2004.tb01053.x

Jiang, L., Yao, Z., Wang, R., Liu, Z., Wang, L., Wu, S., 2015. Hydrochemistry of the middle and upper reaches of the Yarlung Tsangpo River system: weathering processes and CO2 consumption. Environmental Earth Sciences, 74(3): 2369-2379. 10.1007/s12665-015-4237-6

Jin, Z., You, C.-F., Wang, Y., Shi, Y., 2010. Hydrological and solute budgets of Lake Qinghai, the largest lake on the Tibetan Plateau. Quaternary International 218, 151-156. doi http://dx.doi.org/10.1016/j.quaint.2009.11.024

Jonell, T.N., Carter, A., Böning, P., Pahnke, K., Clift, P.D., 2017. Climatic and glacial impact on erosion patterns and sediment provenance in the Himalayan rain shadow, Zanskar River, NW India. GSA Bulletin, 129(7-8): 820-836. 10.1130/B31573.1

References

Karim, A., Veizer, J., 2000. Weathering processes in the Indus River Basin: implications from riverine carbon, sulfur, oxygen, and strontium isotopes. Chemical Geology, 170(1–4): 153-177. http://dx.doi.org/10.1016/S0009-2541(99)00246-6

Kerrick, D.M., 2001. Present and past nonanthropogenic CO2 degassing from the solid earth. Reviews of Geophysics, 39(4): 565-585. 10.1029/2001RG000105

Kisakurek, B., James, R.H., Harris, N.B.W., 2005. Li and delta Li-7 in Himalayan rivers: Proxies for silicate weathering? Earth and Planetary Science Letters, 237(3-4): 387-401. 10.1016/j.epsl.2005.07.019

Kisakurek, B., Widdowson, M., James, R.H., 2004. Behaviour of Li isotopes during continental weathering: the Bidar laterite profile, India. Chemical Geology, 212(1-2): 27-44. 10.1016/j.chemgeo.2004.08.027

Konstantinovskaia, E.A., Brunel, M., Malavieille, J., 2003. Discovery of the Paleo-Tethys residual peridotites along the Anyemaqen–KunLun suture zone (North Tibet). Comptes Rendus Geoscience, 335(8): 709-719. http://dx.doi.org/10.1016/S1631-0713(03)00118-4

Kump, L.R., Arthur, M.A., 1999. Interpreting carbon-isotope excursions: carbonates and organic matter. Chemical Geology, 161(1–3): 181-198.

Kump, L.R., Arthur, M.A., 1997. Global Chemical Erosion during the Cenozoic: Weatherability Balances the Budgets. In: Ruddiman, W.F. (Ed.), Tectonic Uplift and Climate Change. Springer US, Boston, MA, pp. 399-426.

Kump, L.R., Casting, J.F., Crane, R.G., 2003. The Earth System. Prentice Hall, 432 pp.

Kutzbach, J.E., Prell, W.L., Ruddiman, W.F., 1993. Sensitivity of Eurasian Climate to Surface Uplift of the Tibetan Plateau. The Journal of Geology, 101(2): 177-190.

Kürschner, H., Herzschuh, U., Wagner, D., 2005. Phytosociological studies in the north-eastern Tibetan Plateau (NW China) — A first contribution to the subalpine scrub and alpine meadow vegetation. Botanische Jahrbücher, 126(3): 273-315. 10.1127/0006-8152/2005/0126-0273

Lal, D., Harris, N.B.W., Sharma, K.K., Gu, Z., Ding, L., Liu, T., Dong, W., Caffee, M.W., Jull, A.J.T., 2003. Erosion history of the Tibetan Plateau since the last interglacial: constraints from the first studies of cosmogenic 10Be from Tibetan bedrock. Earth and Planetary Science Letters, 217(1–2): 33-42. http://dx.doi.org/10.1016/S0012-821X(03)00600-9

Lambs, L., Balakrishna, K., Brunet, F., Probst, J.L., 2005. Oxygen and hydrogen isotopic composition of major Indian rivers: a first global assessment. Hydrological Processes 19, 3345-3355.

Lechler, A.R., Niemi, N.A., 2011. Controls on the Spatial Variability of Modern Meteoric δ18O: Empirical Constraints from the Western U.S. and East Asia and Implications for Stable Isotope Studies. American Journal of Science, 311(8): 664-700. 10.2475/08.2011.02

Lefebvre, V., Donnadieu, Y., Goddéris, Y., Fluteau, F., Hubert-Théou, L., 2013. Was the Antarctic glaciation delayed by a high degassing rate during the early Cenozoic? Earth and Planetary Science Letters, 371–372: 203-211. http://dx.doi.org/10.1016/j.epsl.2013.03.049

Lehmkuhl, F., Haselein, F., 2000. Quaternary paleoenvironmental change on the Tibetan Plateau and adjacent areas (Western China and Western Mongolia). Quaternary International, 65–66(0): 121-145. http://dx.doi.org/10.1016/S1040-6182(99)00040-3

Lemarchand, E., Chabaux, F., Vigier, N., Millot, R., Pierret, M.C., 2010. Lithium isotope systematics in a forested granitic catchment (Strengbach, Vosges Mountains, France). Geochimica et Cosmochimica Acta, 74(16): 4612-4628. 10.1016/j.gca.2010.04.057

Leng, M.J., Marshall, J.D., 2004. Palaeoclimate interpretation of stable isotope data from lake sediment archives. Quaternary Science Reviews 23, 811-831.

Li, G., Elderfield, H., 2013. Evolution of carbon cycle over the past 100 million years. Geochimica et Cosmochimica Acta, 103: 11-25. http://dx.doi.org/10.1016/j.gca.2012.10.014

Li, Y., Li, D., Liu, G., Harbor, J., Caffee, M., Stroeven, A.P., 2014b. Patterns of landscape evolution on the central and northern Tibetan Plateau investigated using in-situ produced 10Be concentrations from river sediments. Earth and Planetary Science Letters, 398(0): 77-89.

Li, G., West, A.J., 2014. Evolution of Cenozoic seawater lithium isotopes: Coupling of global denudation regime and shifting seawater sinks. Earth and Planetary Science Letters, 401(0): 284-293. http://dx.doi.org/10.1016/j.epsl.2014.06.011

Lister, G.S., Kelts, K., Zao, C.K., Yu, J.Q., Niessen, F., 1991. Lake Qinghai, China - closed-basin lake levels and the oxygen isootpe record for ostracoda since the last Pleistocene. Palaeogeography Palaeoclimatology Palaeoecology 84, 141-162. doi 10.1016/0031-0182(91)90041-o

Liu, C.-Q., Zhao, Z.-Q., Wang, Q., Gao, B., 2011. Isotope compositions of dissolved lithium in the rivers Jinshajiang, Lancangjiang, and Nujiang: Implications for weathering in Qinghai-Tibet Plateau. Applied Geochemistry, 26, Supplement(0): S357-S359. http://dx.doi.org/10.1016/j.apgeochem.2011.03.059

Liu, D., Huang, Q., Fan, S., Zhang, L., Shi, R., Ding, L., 2014. Subduction of the Bangong–Nujiang Ocean: constraints from granites in the Bangong Co area, Tibet. Geological Journal, 49(2): 188-206. 10.1002/gj.2510

Liu, X., Yin, Z.-Y., 2002a. Sensitivity of East Asian monsoon climate to the uplift of the Tibetan Plateau. Palaeogeography, Palaeoclimatology, Palaeoecology 183, 223-245. doi http://dx.doi.org/10.1016/S0031-0182(01)00488-6

Liu, X.-M., Rudnick, R.L., McDonough, W.F., Cummings, M.L., 2013. Influence of chemical weathering on the composition of the continental crust: Insights from Li and Nd isotopes in bauxite profiles developed on Columbia River Basalts. Geochimica et Cosmochimica Acta, 115(0): 73-91. http://dx.doi.org/10.1016/j.gca.2013.03.043

Liu, X.-M., Wanner, C., Rudnick, R.L., McDonough, W.F., 2015. Processes controlling δ^7Li in rivers illuminated by study of streams and groundwaters draining basalts. Earth and Planetary Science Letters, 409(0): 212-224. http://dx.doi.org/10.1016/j.epsl.2014.10.032

Liu, X.M., Rudnick, R.L., 2011. Constraints on continental crustal mass loss via chemical weathering using lithium and its isotopes. Proceedings of the National Academy of Sciences of the United States of America, 108(52): 20873-20880. 10.1073/pnas.1115671108

Liu, X.D., Yin, Z.Y., 2002b. Sensitivity of East Asian monsoon climate to the uplift of the Tibetan Plateau. Palaeogeography Palaeoclimatology Palaeoecology 183, 223-245.

Liu, Z., Tian, L., Yao, T., Yu, W., 2010. Characterization of precipitation $\delta^{18}O$ variation in Nagqu, central Tibetan Plateau and its climatic controls Theoretical and Applied Climatology 99, 95-104.

Lupker, M., France-Lanord, C., Lavé, J., Bouchez, J., Galy, V., Métivier, F., Gaillardet, J., Lartiges, B., Mugnier, J.-L., 2011. A Rouse-based method to integrate the chemical composition of river sediments: Application to the Ganga basin. Journal of Geophysical Research: Earth Surface, 116(F4): 10.1029/2010jf001947

Magna, T., Wiechert, U., Grove, T.L., Halliday, A.N., 2006. Lithium isotope fractionation in the southern Cascadia subduction zone. Earth and Planetary Science Letters, 250(3-4): 428-443. 10.1016/j.epsl.2006.08.019

Magna, T., Wiechert, U.H., Halliday, A.N., 2004. Low-blank isotope ratio measurement of small samples of lithium using multiple-collector ICPMS. International Journal of Mass Spectrometry, 239(1): 67-76. 10.1016/j.ijms.2004.09.008

Maher, K., Chamberlain, C.P., 2014. Hydrologic Regulation of Chemical Weathering and the Geologic Carbon Cycle. Science, 343(6178): 1502-1504.

Majoube, M., 1971. fractionment en oxygene-18 et en deutirium entre l'ean et sa vapor. Journal de Chimie et de Physique 68, 1428-1436.

Marschall, H.R., Wanless, V.D., Shimizu, N., Pogge von Strandmann, P.A.E., Elliott, T., Monteleone, B.D., 2017. The boron and lithium isotopic composition of mid-ocean ridge basalts and the mantle. Geochimica et Cosmochimica Acta, 207: 102-138. https://doi.org/10.1016/j.gca.2017.03.028

Maussion, F., Scherer, D., Mölg, T., Collier, E., Curio, J., Finkelnburg, R., 2014. Precipitation Seasonality and Variability over the Tibetan Plateau as Resolved by the High Asia Reanalysis. Journal of Climate, 27(5): 1910-1927. 10.1175/jcli-d-13-00282.1

Meunier, A., Velde, B., 2004. Illite. Springer Verlag Berlin Heidelberg.

Meybeck, M., 1987. Global chemical -weathering of surficial rocks estimated from river dissolved loads. American Journal of Science 287, 401-428.

Miehe, G., Kaiser, K., Co, S., Liu, L., 2008. Geo-ecological transect studies in northeast Tibet (Qinghai, China) reveal human-made mid-holocene environmental changes in the upper Yello River catchment changing forrest to grassland. Erdkunde, 62(3): 187-199.

Millot, R., Girard, J.P., 2007. Lithium isotope fractionation during adsorption onto mineral surfaces, Clay in Natural & Engineered Barriers for Radioactive Waste Confinement: 3red international meeting, Lille.

Millot, R., Guerrot, C., Innocent, C., Négrel, P., Sanjuan, B., 2011. Chemical, multi-isotopic (Li–B–Sr–U–H–O) and thermal characterization of Triassic formation waters from the Paris Basin. Chemical Geology, 283(3–4): 226-241. http://dx.doi.org/10.1016/j.chemgeo.2011.01.020

Millot, R., Hegan, A., Négrel, P., 2012. Geothermal waters from the Taupo Volcanic Zone, New Zealand: Li, B and Sr isotopes characterization. Applied Geochemistry, 27(3): 677-688.

Millot, R., Négrel, P., 2007. Multi-isotopic tracing (δ7Li, δ11B, 87Sr/86Sr) and chemical geothermometry: evidence from hydro-geothermal systems in France. Chemical Geology, 244(3–4): 664-678.

Millot, R., Négrel, P., Petelet-Giraud, E., 2007. Multi-isotopic (Li, B, Sr, Nd) approach for geothermal reservoir characterization in the Limagne Basin (Massif Central, France). Applied Geochemistry, 22(11): 2307-2325.

Millot, R., Petelet-Giraud, E., Guerrot, C., Négrel, P., 2010a. Multi-isotopic composition (δ7Li–δ11B–δD–δ18O) of rainwaters in France: Origin and spatio-temporal characterization. Applied Geochemistry, 25(10): 1510-1524. http://dx.doi.org/10.1016/j.apgeochem.2010.08.002

Millot, R., Scaillet, B., Sanjuan, B., 2010b. Lithium isotopes in island arc geothermal systems: Guadeloupe, Martinique (French West Indies) and experimental approach. Geochimica et Cosmochimica Acta, 74(6): 1852-1871. http://dx.doi.org/10.1016/j.gca.2009.12.007

Millot, R., Vigier, N., Gaillardet, J., 2010c. Behaviour of lithium and its isotopes during weathering in the Mackenzie Basin, Canada. Geochimica et Cosmochimica Acta, 74(14): 3897-3912. 10.1016/j.gca.2010.04.025

Mischke, S., Aichner, B., Diekmann, B., Herzschuh, U., Plessen, B., Wünnemann, B., Zhang, C., 2010a. Ostracods and stable isotopes of a late glacial and Holocene lake record from the NE Tibetan Plateau. Chem. Geol. 276, 95-103. doi 10.1016/j.chemgeo.2010.06.003

Mischke, S., Boessneck, U., Diekmann, B., Herzschuh, U., Jin, H., Kramer, A., Wuennemann, B., Zhang, C., 2010b. Quantitative relationship between water-depth and sub-fossil ostracod assemblages in Lake Donggi Cona, Qinghai Province, China. Journal of Paleolimnology 43, 589-608. doi 10.1007/s10933-009-9355-2

Mischke, S., Kramer, M., Zhang, C., Shang, H., Herzschuh, U., Erzinger, J., 2008. Reduced early Holocene moisture availability in the Bayan Har Mountains, northeastern Tibetan Plateau,

inferred from a multi-proxy lake record. Palaeogeography, Palaeoclimatology, Palaeoecology 267, 59-76. doi http://dx.doi.org/10.1016/j.palaeo.2008.06.002

Mischke, S., Weynell, M., Zhang, C., Wiechert, U., 2013. Spatial variability of 14C reservoir effects in Tibetan Plateau lakes. Quaternary International. doi http://dx.doi.org/10.1016/j.quaint.2013.01.030

Mischke, S., Zhang, C., Börner, A., Herzschuh, U., 2010c. Lateglacial and Holocene variation in aeolian sediment flux over the northeastern Tibetan Plateau recorded by laminated sediments of a saline meromictic lake. Journal of Quaternary Science, 25(2): 162-177. 10.1002/jqs.1288

Mischke, S., Zhang, C., Fan, R., 2015. Early to mid-Holocene lake high-stand sediments at Lake Donggi Cona, northeastern Tibetan Plateau, China — Comment to the paper published by Dietze et al., Quaternary Research 79 (2013), 325-336. Quaternary Research 83, 256-258. doi http://dx.doi.org/10.1016/j.yqres.2014.06.005

Misra, S., Froelich, P.N., 2012. Lithium Isotope History of Cenozoic Seawater: Changes in Silicate Weathering and Reverse Weathering. Science, 335(6070): 818-823. 10.1126/science.1214697

Molnar, P., Boos, W.R., Battisti, D.S., 2010. Orographic Controls on Climate and Paleoclimate of Asia: Thermal and Mechanical Roles for the Tibetan Plateau. Annual Review of Earth and Planetary Sciences, Vol 38 38, 77-102. doi 10.1146/annurev-earth-040809-152456

Moon, S., Chamberlain, C.P., Hilley, G.E., 2014. New estimates of silicate weathering rates and their uncertainties in global rivers. Geochimica et Cosmochimica Acta, 134: 257-274. http://dx.doi.org/10.1016/j.gca.2014.02.033

Morrill, C., Overpeck, J.T., Cole, J.E., 2003. A synthesis of abrupt changes in the Asian summer monsoon since the last deglaciation. Holocene 13, 465-476. doi 10.1191/0959683603hl639ft

Morrill, C., Overpeck, J.T., Cole, J.E., Liu, K.-b., Shen, C., Tang, L., 2006. Holocene variations in the Asian monsoon inferred from the geochemistry of lake sediments in central Tibet. Quaternary Research 65, 232-243. doi http://dx.doi.org/10.1016/j.yqres.2005.02.014

Mukhopadhyay, B., Dutta, A., 2010. A Stream Water Availability Model of Upper Indus Basin Based on a Topologic Model and Global Climatic Datasets. Water Resources Management, 24(15): 4403-4443. 10.1007/s11269-010-9666-0

Munack, H., Korup, O., Resentini, A., Limonta, M., Garzanti, E., Blöthe, J.H., Scherler, D., Wittmann, H., Kubik, P.W., 2014. Postglacial denudation of western Tibetan Plateau margin outpaced by long-term exhumation. GSA Bulletin, 126(11-12): 1580-1594. 10.1130/B30979.1

Nahon, D., 2003. Altérations dans la zone tropicale. Signification à travers les mécanismes anciens et/ou encore actuels. Comptes Rendus Geoscience, 335(16): 1109-1119. http://dx.doi.org/10.1016/j.crte.2003.10.008

Négrel, P., Allègre, C.J., Dupré, B., Lewin, E., 1993. Erosion sources determined by inversion of major and trace element ratios and strontium isotopic ratios in river water: The Congo Basin case. Earth and Planetary Science Letters 120, 59-76. doi http://dx.doi.org/10.1016/0012-821X(93)90023-3

Négrel, P., Millot, R., Brenot, A., Bertin, C., 2010. Lithium isotopes as tracers of groundwater circulation in a peat land. Chemical Geology, 276(1–2): 119-127. http://dx.doi.org/10.1016/j.chemgeo.2010.06.008

Oliver, L., Harris, N., Bickle, M., Chapman, H., Dise, N., Horstwood, M., 2003. Silicate weathering rates decoupled from the 87Sr/86Sr ratio of the dissolved load during Himalayan erosion. Chemical Geology, 201(1–2): 119-139. http://dx.doi.org/10.1016/S0009-2541(03)00236-5

O'Neil, J.R., Clayton, R.N., Mayeda, T.K., 1969. Oxygen Isotope Fractionation in Divalent Metal Carbonates. The Journal of Chemical Physics 51, 5547-5558. doi doi:http://dx.doi.org/10.1063/1.1671982

Opitz, S., Ramisch, A., Ijmker, J., Lehmkuhl, F., Mischke, S., Stauch, G., Wünnemann, B., Zhang, Y., Diekmann, B., 2016. Spatio-temporal pattern of detrital clay-mineral supply to a lake system on

the north-eastern Tibetan Plateau, and its relation ship to late Quaternary paleoenvironmental changes. Catena, 137: 203-218. doi:10.1016/j.catena.2015.09.003

Opitz, S., Wünnemann, B., Aichner, B., Dietze, E., Hartmann, K., Herzschuh, U., Ijmker, J., Lehmkuhl, F., Li, S., Mischke, S., Plotzki, A., Stauch, G., Diekmann, B., 2012. Late Glacial and Holocene development of Lake Donggi Cona, north-eastern Tibetan Plateau, inferred from sedimentological analysis. Palaeogeography, Palaeoclimatology, Palaeoecology 337–338, 159-176. doi 10.1016/j.palaeo.2012.04.013

Otto-Bliesner, B.L., 1995. Continental drift, runoff, and weathering feedbacks: Implications from climate model experiments. Journal of Geophysical Research: Atmospheres, 100(D6): 11537-11548. 10.1029/95JD00591

Pagani, M., Caldeira, K., Berner, R., Beerling, D.J., 2009. The role of terrestrial plants in limiting atmospheric CO2 decline over the past 24 million years. Nature, 460: 85. 10.1038/nature08133

Pang, Z., Kong, Y., Froehlich, K., Huang, T., Yuan, L., Li, Z., Wang, F., 2011. Processes affecting isotopes in precipitation of an arid region. Tellus B 63, 352-359. doi 10.1111/j.1600-0889.2011.00532.x

Pearson, P.N., Palmer, M.R., 2000. Atmospheric carbon dioxide concentrations over the past 60 million years. Nature, 406: 695. 10.1038/35021000

Peucker-Ehrenbrink, B., Ravizza, G., 2000. The marine osmium isotope record. Terra Nova, 12(5): 205-219. 10.1046/j.1365-3121.2000.00295.x

Phan, V.H., Lindenbergh, R.C., Menenti, M., 2013. Geometric dependency of Tibetan lakes on glacial runoff. Hydrol. Earth Syst. Sci., 17(10): 4061-4077. 10.5194/hess-17-4061-2013

Pistiner, J.S., Henderson, G.M., 2003. Lithium-isotope fractionation during continental weathering processes. Earth and Planetary Science Letters, 214(1–2): 327-339. 10.1016/s0012-821x(03)00348-0

Pogge von Strandmann, P.A.E., Burton, K.W., James, R.H., van Calsteren, P., Gislason, S.R., 2010. Assessing the role of climate on uranium and lithium isotope behaviour in rivers draining a basaltic terrain. Chemical Geology, 270(1-4): 227-239. 10.1016/j.chemgeo.2009.12.002

Pogge von Strandmann, P.A.E., Burton, K.W., James, R.H., van Calsteren, P., Gíslason, S.R., Mokadem, F., 2006. Riverine behaviour of uranium and lithium isotopes in an actively glaciated basaltic terrain. Earth and Planetary Science Letters, 251(1–2): 134-147. http://dx.doi.org/10.1016/j.epsl.2006.09.001

Pogge von Strandmann, P.A.E., Burton, K.W., Opfergelt, S., Eiríksdóttir, E.S., Murphy, M.J., Einarsson, A., Gislason, S.R., 2016. The effect of hydrothermal spring weathering processes and primary productivity on lithium isotopes: Lake Myvatn, Iceland. Chemical Geology. http://dx.doi.org/10.1016/j.chemgeo.2016.02.026

Pogge von Strandmann, P.A.E., Desrochers, A., Murphy, M.J., Finlay, A.J., Selby, D., Lenton, T.M., 2017b. Global climate stabilisation by chemical weathering during the Hirnantian glaciation. Geochemical Perspectives Letters, 3(2): 230-237. http://dx.doi.org/10.7185/geochemlet.1726

Pogge von Strandmann, P.A.E., Frings, P.J., Murphy, M.J., 2017. Lithium isotope behaviour during weathering in the Ganges Alluvial Plain. Geochimica et Cosmochimica Acta, 198: 17-31. http://dx.doi.org/10.1016/j.gca.2016.11.017

Pogge von Strandmann, P.A.E., Henderson, G.M., 2015. The Li isotope response to mountain uplift. Geology. 10.1130/g36162.1

Pogge von Strandmann, P.A.E., James, R.H., van Calsteren, P., Gislason, S.R., Burton, K.W., 2008. Lithium, magnesium and uranium isotope behaviour in the estuarine environment of basaltic islands. Earth and Planetary Science Letters, 274(3-4): 462-471. 10.1016/j.epsl.2008.07.041

Pogge von Strandmann, P.A.E., Jenkyns, H.C., Woodfine, R.G., 2013. Lithium isotope evidence for enhanced weathering during Oceanic Anoxic Event 2. Nature Geosci, 6(8): 668-672. 10.1038/ngeo1875

Pogge von Strandmann, P.A.E., Opfergelt, S., Lai, Y.-J., Sigfússon, B., Gislason, S.R., Burton, K.W., 2012. Lithium, magnesium and silicon isotope behaviour accompanying weathering in a basaltic soil and pore water profile in Iceland. Earth and Planetary Science Letters, 339–340(0): 11-23. http://dx.doi.org/10.1016/j.epsl.2012.05.035

Pogge von Strandmann, P.A.E., Porcelli, D., James, R.H., van Calsteren, P., Schaefer, B., Cartwright, I., Reynolds, B.C., Burton, K.W., 2014. Chemical weathering processes in the Great Artesian Basin: Evidence from lithium and silicon isotopes. Earth and Planetary Science Letters, 406(0): 24-36.

Pogge von Strandmann, P.A.E., Vaks, A., Bar-Matthews, M., Ayalon, A., Jacob, E., Henderson, G.M., 2017c. Lithium isotopes in speleothems: Temperature-controlled variation in silicate weathering during glacial cycles. Earth and Planetary Science Letters, 469: 64-74. http://dx.doi.org/10.1016/j.epsl.2017.04.014

Pye, K., 1987. Aeolian Dust and Dust Deposits. Academic Press, pp. 118-141.

Qiu, L., Rudnick, R.L., McDonough, W.F., Merriman, R.J., 2009. Li and δ7Li in mudrocks from the British Caledonides: Metamorphism and source influences. Geochimica et Cosmochimica Acta, 73(24): 7325-7340. https://doi.org/10.1016/j.gca.2009.08.017

Rad, S., Rivé, K., Vittecoq, B., Cerdan, O., Allègre, C.J., 2013. Chemical weathering and erosion rates in the Lesser Antilles: An overview in Guadeloupe, Martinique and Dominica. Journal of South American Earth Sciences, 45: 331-344. http://dx.doi.org/10.1016/j.jsames.2013.03.004

Raymo, M.E., Ruddiman, W.F., 1992. Tectonic forcing of late Cenozoic climate. Nature, 359(6391): 117-122.

Ren, W., Yao, T., Yang, X., Joswiak, D.R., 2013. Implications of variations in δ18O and δD in precipitation at Madoi in the eastern Tibetan Plateau. Quaternary International 313–314, 56-61. doi http://dx.doi.org/10.1016/j.quaint.2013.05.026

Riebe, C.S., Kirchner, J.W., Finkel, R.C., 2003. Long-term rates of chemical weathering and physical erosion from cosmogenic nuclides and geochemical mass balance. Geochimica et Cosmochimica Acta, 67(22): 4411-4427. http://dx.doi.org/10.1016/S0016-7037(03)00382-X

Riebe, C.S., Kirchner, J.W., Finkel, R.C., 2004. Erosional and climatic effects on long-term chemical weathering rates in granitic landscapes spanning diverse climate regimes. Earth and Planetary Science Letters, 224(3-4): 547-562. 10.1016/j.epsl.2004.05.019

Roberts, J., Kaczmarek, K., Langer, G., Skinner, L.C., Bijma, J., Bradbury, H., Turchyn, A.V., Lamy, F., Misra, S., 2018. Lithium isotopic composition of benthic foraminifera: A new proxy for paleo-pH reconstruction. Geochimica et Cosmochimica Acta. https://doi.org/10.1016/j.gca.2018.02.038

Rowley, D.B., 2002. Rate of plate creation and destruction: 180 Ma to present. Bulletin of the Geological Society of America, 114(8): 927-933. 10.1130/0016-7606(2002)114<0927:ROPCAD>2.0.CO;2

Rowley, D.B., Pierrehumbert, R.T., Currie, B.S., 2001. A new approach to stable isotope-based paleoaltimetry: implications for paleoaltimetry and paleohypsometry of the High Himalaya since the Late Miocene. Earth and Planetary Science Letters 188, 253-268. doi 10.1016/s0012-821x(01)00324-7

Royden, L.H., Burchfiel, B.C., van der Hilst, R.D., 2008. The Geological Evolution of the Tibetan Plateau. Science 321, 1054-1058. doi 10.1126/science.1155371

Royer, D.L., Berner, R.A., Montañez, I.P., Tabor, N.J., Beerling, D.J., 2004. CO2 as a primary driver of Phanerozoic climate. GSA Today, 14(3): 4-9.

Rudnick, R.L., Tomascak, P.B., Njo, H.B., Gardner, L.R., 2004. Extreme lithium isotopic fractionation during continental weathering revealed in saprolites from South Carolina. Chemical Geology, 212: 45-57.

Ryan, W.B.F., S.M. Carbotte, J.O. Coplan, S. O'Hara, A. Melkonian, R. Arko, R.A. Weissel, V. Ferrini, A. Goodwillie, F. Nitsche, J. Bonczkowski, and R. Zemsky (2009), Global Multi-Resolution Topography synthesis, Geochem. Geophys. Geosyst., 10, Q03014, doi:10.1029/2008GC002332

Sauzéat, L., Rudnick, R.L., Chauvel, C., Garçon, M., Tang, M., 2015. New perspectives on the Li isotopic composition of the upper continental crust and its weathering signature. Earth and Planetary Science Letters, 428: 181-192. http://dx.doi.org/10.1016/j.epsl.2015.07.032

Schaller, M.F., Fung, M.K., Wright, J.D., Katz, M.E., Kent, D.V., 2016. Impact ejecta at the Paleocene-Eocene boundary. Science, 354(6309): 225-229. 10.1126/science.aaf5466

Schmitt, A.-D., Vigier, N., Lemarchand, D., Millot, R., Stille, P., Chabaux, F., 2012. Processes controlling the stable isotope compositions of Li, B, Mg and Ca in plants, soils and waters: A review. Comptes Rendus Geoscience, 344(11–12): 704-722. http://dx.doi.org/10.1016/j.crte.2012.10.002

Schnug, E., Haneklaus, S., 1996. A rapid method for the indirect determination of the clay content by x-ray fluorescence spectroscopic analysis of rubidium in soils. Communications in Soil Science and Plant Analysis, 27(5-8): 1707-1719. 10.1080/00103629609369664

Schuessler, J.A., Schoenberg, R., Sigmarsson, O., 2009. Iron and lithium isotope systematics of the Hekla volcano, Iceland — Evidence for Fe isotope fractionation during magma differentiation. Chemical Geology, 258(1–2): 78-91. http://dx.doi.org/10.1016/j.chemgeo.2008.06.021

Schulte, P., van Geldern, R., Freitag, H., Karim, A., Négrel, P., Petelet-Giraud, E., Probst, A., Probst, J.-L., Telmer, K., Veizer, J., Barth, J.A.C., 2011. Applications of stable water and carbon isotopes in watershed research: Weathering, carbon cycling, and water balances. Earth-Science Reviews 109, 20-31. doi http://dx.doi.org/10.1016/j.earscirev.2011.07.003

Sengupta, S., Sarkar, A., 2006. Stable isotope evidence of dual (Arabian Sea and Bay of Bengal) vapour sources in monsoonal precipitation over north India. Earth and Planetary Science Letters 250, 511-521. doi

Sharma, P.V., 1997. Environmental and Engineering Geophysics. Cambridge University Press, Cambridge.

Sharp, Z., 2007. Principles of stable isotope geochemistry. Pearson Education Upper Saddle River, NJ.

Shi, R., Yang, J., Xu, Z., Qi, X., 2008. The Bangong Lake ophiolite (NW Tibet) and its bearing on the tectonic evolution of the Bangong–Nujiang suture zone. Journal of Asian Earth Sciences, 32(5–6): 438-457. http://dx.doi.org/10.1016/j.jseaes.2007.11.011

Shen, L., Wu, K., Xiao, Q., Yuan, D., 2011. Carbon dioxide degassing flux from two geothermal fields in Tibet, China. Chinese Science Bulletin, 56(35): 3783-3793. 10.1007/s11434-011-4352-z

Spötl, C., 2005. A robust and fast method of sampling and analysis of δ13C of dissolved inorganic carbon in ground waters. Isotopes in Environmental and Health Studies, 41(3): 217-221. 10.1080/10256010500230023

Sprenger, C., Parimala Renganayaki, S., Schneider, M., Elango, L., 2014. Hydrochemistry and stable isotopes during salinity ingress and refreshment in surface- and groundwater from the Arani–Koratallai (A–K) basin north of Chennai (India). Environ Earth Sci, 1-12. doi 10.1007/s12665-014-3269-7

Stallard, R.F., Edmond, J.M., 1983. Geochemistry of the Amazon: 2. The influence of geology and weathering environment on the dissolved load. Journal of Geophysical Research: Oceans, 88(C14): 9671-9688. 10.1029/JC088iC14p09671

Stauch, G., Ijmker, J., Pötsch, S., Zhao, H., Hilgers, A., Diekmann, B., Dietze, E., Hartmann, K., Opitz, S., Wünnemann, B., Lehmkuhl, F., 2012. Aeolian sediments on the north-eastern Tibetan Plateau. Quaternary Science Reviews 57, 71-84. doi http://dx.doi.org/10.1016/j.quascirev.2012.10.001

Stauch, G., Pötsch, S., Zhao, H., Lehmkuhl, F., 2014. Interaction of geomorphological processes on the north-eastern Tibetan Plateau during the Holocene, an example from a sub-catchment of Lake Donggi Cona. Geomorphology 210, 23-35. doi http://dx.doi.org/10.1016/j.geomorph.2013.12.014

Stroeven, A.P., Hättestrand, C., Heyman, J., Harbor, J., Li, Y.K., Zhou, L.P., Caffee, M.W., Alexanderson, H., Kleman, J., Ma, H.Z., Liu, G.N., 2009. Landscape analysis of the Huang He headwaters, NE Tibetan Plateau — Patterns of glacial and fluvial erosion. Geomorphology 103, 212-226. doi http://dx.doi.org/10.1016/j.geomorph.2008.04.024

Sun, H., Xiao, Y., Gao, Y., Zhang, G., Casey, J.F., Shen, Y., 2018. Rapid enhancement of chemical weathering recorded by extremely light seawater lithium isotopes at the Permian–Triassic boundary. Proceedings of the National Academy of Sciences, 115(15): 3782-3787. 10.1073/pnas.1711862115

Sun, J., Li, S.-H., Muhs, D.R., Li, B., 2007. Loess sedimentation in Tibet: provenance, processes, and link with Quaternary glaciations. Quaternary Science Reviews, 26(17–18): 2265-2280. http://dx.doi.org/10.1016/j.quascirev.2007.05.003

Sun, Q., Colin, C., 2014. Paleoclimate and Paleoenvironment of Gonghe Basin, Qinghai-Tibet Plateau, During the Lastdeglacial: Weathering, Erosion and Vegetation Cover Affect Clay Mineral Formation. Acta Geologica Sinica - English Edition, 88(2): 647-660. 10.1111/1755-6724.12220

Szramek, K., Walter, L.M., McCall, P., 2004. Arsenic mobility in groundwater/surface water systems in carbonate-rich Pleistocene glacial drift aquifers (Michigan). Applied Geochemistry 19, 1137-1155. doi http://dx.doi.org/10.1016/j.apgeochem.2004.01.012

Taft, L., Wiechert, U., Riedel, F., Weynell, M., Zhang, H., 2012. Sub-seasonal oxygen and carbon isotope variations in shells of modern Radix sp. (Gastropoda) from the Tibetan Plateau: potential of a new archive for palaeoclimatic studies. Quaternary Science Reviews 34, 44-56. doi http://dx.doi.org/10.1016/j.quascirev.2011.12.006

Taft, L., Wiechert, U., Zhang, H., Lei, G., Mischke, S., Plessen, B., Weynell, M., Winkler, A., Riedel, F., 2013. Oxygen and carbon isotope patterns archived in shells of the aquatic gastropod Radix: Hydrologic and climatic signals across the Tibetan Plateau in sub-monthly resolution. Quaternary International. doi http://dx.doi.org/10.1016/j.quaint.2012.10.031

Tan, H.B., Chen, J., Rao, W.B., Zhang, W.J., Zhou, H.F., 2012. Geothermal constraints on enrichment of boron and lithium in salt lakes: An example from a river-salt lake system on the northern slope of the eastern Kunlun Mountains, China. Journal of Asian Earth Sciences, 51: 21-29. 10.1016/j.jseaes.2012.03.002

Tapponnier, P., Zhiqin, X., Roger, F., Meyer, B., Arnaud, N., Wittlinger, G., Jingsui, Y., 2001. Oblique Stepwise Rise and Growth of the Tibet Plateau. Science, 294(5547): 1671-1677. 10.1126/science.105978

Taylor, S.R., McLennan, S.M., McCulloch, M.T., 1983. Geochemistry of loess, continental crustal composition and crustal model ages. Geochimica et Cosmochimica Acta, 47(11): 1897-1905.

Teng, F.-Z., Rudnick, R.L., McDonough, W.F., Wu, F.-Y., 2009. Lithium isotopic systematics of A-type granites and their mafic enclaves: Further constraints on the Li isotopic composition of the continental crust. Chemical Geology, 262(3-4): 370-379. 10.1016/j.chemgeo.2009.02.009

Teng, F.Z., McDonough, W.F., Rudnick, R.L., Dalpé, C., Tomascak, P.B., Chappell, B.W., Gao, S., 2004. Lithium isotopic composition and concentration of the upper continental crust. Geochimica et Cosmochimica Acta, 68(20): 4167-4178. 10.1016/j.gca.2004.03.031

Tian, L., Ma, L., Yu, W., Liu, Z., Yin, C., Zhao, Z., Tang, W., Wang, Y., 2008b. Seasonal variations of stable isotope in precipitation and moisture transport at Yushu, eastern Tibetan Plateau Sci. China Ser. D-Earth Sci. 51, 1121-1128. doi

Tian, L., Yao, T., MacClune, K., White, J.W.C., Schilla, A., Vaughn, B., Vachon, R., Ichiyanagi, K., 2007. Stable isotopic variations in west China: A consideration of moisture sources. J. Geophys. Res. 112. doi 10.1029/2006jd007718

Tian, L., Yao, T., Schuster, P.F., White, J.W.C., Ichiyanagi, K., Pendall, E., Pu, J., Yu, W., 2003. Oxygen-18 concentrations in recent precipitation and ice cores on the Tibetan Plateau. J. Geophys. Res. 108, 4293. doi 10.1029/2002jd002173

Tian, S., Hou, Z., Tian, Y., Zhao, Y., Hou, K., Li, X., Zhang, Y., Hu, W., Mo, X., Yang, Z., Li, Z., Zhao, M., 2018. Lithium content and isotopic composition of the juvenile lower crust in southern Tibet. Gondwana Research. https://doi.org/10.1016/j.gr.2018.02.011

Tian, S., Zhao, Y., Hou, Z., Tian, Y., Hou, K., Li, X., Yang, Z., Hu, W., Mo, X., Zheng, Y., 2017. Lithium isotopic composition and concentration of Himalayan leucogranites and the Indian lower continental crust. Lithos, 284: 416-428. http://dx.doi.org/10.1016/j.lithos.2017.05.001

Tomascak, P.B., 2004. Developments in the understanding and application of lithium isotopes in the earth and planetary sciences. In: Johnson, C.M., Beard, B.L., Albarede, F. (Eds.), Geochemistry of Non-Traditional Stable Isotopes. Reviews in Mineralogy & Geochemistry, pp. 153-195.

Tomascak, P.B., Hemming, N.G., Hemming, S.R., 2003. The lithium isotopic composition of waters of the Mono Basin, California. Geochimica et Cosmochimica Acta, 67(4): 601-611. http://dx.doi.org/10.1016/S0016-7037(02)01132-8

Tomascak, P.B., Magna, T., Dohmen, R., 2016. Advances in Lithium Isotope Geochemistry, 1. Springer International Publishing, 195 pp.

Torres, M.A., West, A.J., Li, G., 2014. Sulphide oxidation and carbonate dissolution as a source of CO2 over geological timescales. Nature, 507(7492): 346-349. 10.1038/nature13030

Tranter, M., Wadham, J.L., 2014. 7.5 - Geochemical Weathering in Glacial and Proglacial Environments A2 - Holland, Heinrich D. In: Turekian, K.K. (Ed.), Treatise on Geochemistry. Pergamon, Oxford, pp. 157-173.

Tsai, P.-H., You, C.-F., Huang, K.-F., Chung, C.-H., Sun, Y.-B., 2014. Lithium distribution and isotopic fractionation during chemical weathering and soil formation in a loess profile. Journal of Asian Earth Sciences, 87(0): 1-10. http://dx.doi.org/10.1016/j.jseaes.2014.02.001

Van Der Meer, D.G., Zeebe, R.E., van Hinsbergen, D.J.J., Sluijs, A., Spakman, W., Torsvik, T.H., 2014. Plate tectonic controls on atmospheric CO2 levels since the Triassic. Proceedings of the National Academy of Sciences, 111(12): 4380-4385. 10.1073/pnas.1315657111

VanCampo, E., Cour, P., Hang, S.X., 1996. Holocene environmental changes in Bangong Co basin (western Tibet) .2. The pollen record. Palaeogeography Palaeoclimatology Palaeoecology, 120(1-2): 49-63.

Van Der Woerd, J., Tapponnier, P., Ryerson, F.J., Meriaux, A.S., Meyer, B., Gaudemer, Y., Finkel, R.C., Caffee, M.W., Zhao, G.G., Xu, Z.Q., 2002. Uniform postglacial slip-rate along the central 600 km of the Kunlun Fault (Tibet), from Al-26, Be-10, and C-14 dating of riser offsets, and climatic origin of the regional morphology. Geophysical Journal International 148, 356-388. doi 10.1046/j.1365-246x.2002.01556.x

Verney-Carron, A., Vigier, N., Millot, R., 2011. Experimental determination of the role of diffusion on Li isotope fractionation during basaltic glass weathering. Geochimica et Cosmochimica Acta, 75(12): 3452-3468.

Verney-Carron, A., Vigier, N., Millot, R., Hardarson, B.S., 2015. Lithium isotopes in hydrothermally altered basalts from Hengill (SW Iceland). Earth and Planetary Science Letters, 411(0): 62-71. http://dx.doi.org/10.1016/j.epsl.2014.11.047

Vigier, N., Decarreau, A., Millot, R., Carignan, J., Petit, S., France-Lanord, C., 2008. Quantifying Li isotope fractionation during smectite formation and implications for the Li cycle. Geochimica et Cosmochimica Acta, 72(3): 780-792. 10.1016/j.gca.2007.11.011

Vigier, N., Gislason, S.R., Burton, K.W., Millot, R., Mokadem, F., 2009. The relationship between riverine lithium isotope composition and silicate weathering rates in Iceland. Earth and Planetary Science Letters, 287(3-4): 434-441. 10.1016/j.epsl.2009.08.026

Vigier, N., Goddéris, Y., 2015. A new approach for modeling Cenozoic oceanic lithium isotope paleo-variations: the key role of climate. Clim. Past, 11(4): 635-645. 10.5194/cp-11-635-2015

Vigier, N., Rollion-Bard, C., Levenson, Y., Erez, J., 2015. Lithium isotopes in foraminifera shells as a novel proxy for the ocean dissolved inorganic carbon (DIC). Comptes Rendus Geoscience(0). http://dx.doi.org/10.1016/j.crte.2014.12.001

Vlastélic, I., Koga, K., Chauvel, C., Jacques, G., Télouk, P., 2009. Survival of lithium isotopic heterogeneities in the mantle supported by HIMU-lavas from Rurutu Island, Austral Chain. Earth and Planetary Science Letters, 286(3–4): 456-466. http://dx.doi.org/10.1016/j.epsl.2009.07.013

Vogel, S., Märker, M., Rellini, I., Hoelzmann, P., Wulf, S., Robinson, M., Steinhübel, L., Di Maio, G., Imperatore, C., Kastenmeier, P., Liebmann, L., Esposito, D., Seiler, F., 2015. From a stratigraphic sequence to a landscape evolution model: Late Pleistocene and Holocene volcanism, soil formation and land use in the shade of Mount Vesuvius (Italy). Quaternary International. http://dx.doi.org/10.1016/j.quaint.2015.02.033

von Blanckenburg, F., Bouchez, J., Ibarra, D.E., Maher, K., 2015. Stable runoff and weathering fluxes into the oceans over Quaternary climate cycles. Nature Geosci, 8(7): 538-542. 10.1038/ngeo2452

von Blanckenburg, F., Hewawasam, T., Kubik, P.W., 2004. Cosmogenic nuclide evidence for low weathering and denudation in the wet, tropical highlands of Sri Lanka. Journal of Geophysical Research: Earth Surface, 109(F3): n/a-n/a.

von Oheimb, P.V., Albrecht, C., Riedel, F., Du, L., Yang, J., Aldridge, D.C., BÃ¶ÃŸneck, U., Zhang, H., Wilke, T., 2011. Freshwater Biogeography and Limnological Evolution of the Tibetan Plateau - Insights from a Plateau-Wide Distributed Gastropod Taxon. PLoS ONE 6, e26307. doi

Walker, J.C.G., Hays, P.B., Kasting, J.F., 1981. A negative feedback mechanism for the long-term stabilization of Earth's surface temperature. Journal of Geophysical Research: Oceans, 86(C10): 9776-9782. 10.1029/JC086iC10p09776

Wang, Q.-L., Chetelat, B., Zhao, Z.-Q., Ding, H., Li, S.-L., Wang, B.-L., Li, J., Liu, X.-L., 2015. Behavior of lithium isotopes in the Changjiang River system: Sources effects and response to weathering and erosion. Geochimica et Cosmochimica Acta, 151(0): 117-132. http://dx.doi.org/10.1016/j.gca.2014.12.015

Wang, Y., Herzschuh, U., Shumilovskikh, L.S., Mischke, S., Birks, H.J.B., Wischnewski, J., Böhner, J., Schlütz, F., Lehmkuhl, F., Diekmann, B., Wünnemann, B., Zhang, C., 2014. Quantitative reconstruction of precipitation changes on the NE Tibetan Plateau since the Last Glacial Maximum – extending the concept of pollen source area to pollen-based climate reconstructions from large lakes. Clim. Past, 10(1): 21-39. 10.5194/cp-10-21-2014

Wang, Y., Xu, G., Lin, Q., Gong, S., 2001. Depositional model of Early Permian reef-island ocean in Eastern Kunlun. Sci. China Ser. D-Earth Sci. 44, 808-815. doi 10.1007/bf02907093

Wang, Y.B., Yang, H., 2004. Middle Permian palaeobiogeography study in East Kunlun, A'nyemaqen and Bayan Har. Science in China Series D-Earth Sciences 47, 1120-1126. doi 10.1360/02yd0450

Wanner, C., Sonnenthal, E.L., Liu, X.-M., 2014. Seawater δ7Li: A direct proxy for global CO2 consumption by continental silicate weathering? Chemical Geology, 381(0): 154-167. http://dx.doi.org/10.1016/j.chemgeo.2014.05.005

Wassenaar, L.I., Athanasopoulos, P., Hendry, M.J., 2011. Isotope hydrology of precipitation, surface and ground waters in the Okanagan Valley, British Columbia, Canada. Journal of Hydrology 411, 37-48. doi http://dx.doi.org/10.1016/j.jhydrol.2011.09.032

Wei, G., Li, X.-H., Liu, Y., Shao, L., Liang, X., 2006. Geochemical record of chemical weathering and monsoon climate change since the early Miocene in the South China Sea. Paleoceanography, 21(4): n/a-n/a. 10.1029/2006PA001300

Wen, R., Tian, L., Liu, F., Qu, D., 2016. Lake water isotope variation linked with the in-lake water cycle of the alpine Bangong Co, arid western Tibetan Plateau. Arctic, Antarctic, and Alpine Research, 0(0): null. doi:10.1657/AAAR0015-028

West, A.J., Galy, A., Bickle, M., 2005. Tectonic and climatic controls on silicate weathering. Earth and Planetary Science Letters, 235(1–2): 211-228. http://dx.doi.org/10.1016/j.epsl.2005.03.020

Weynell, M., Wiechert, U., Schuessler, J.A., 2017. Lithium isotopes and implications on chemical weathering in the catchment of Lake Donggi Cona, northeastern Tibetan Plateau. Geochimica et Cosmochimica Acta, 213: 155-177. https://doi.org/10.1016/j.gca.2017.06.026

Weynell, M., Wiechert, U., Zhang, C., 2016. Chemical and isotopic (O, H, C) composition of surface waters in the catchment of Lake Donggi Cona (NW China) and implications for paleoenvironmental reconstructions. Chemical Geology. http://dx.doi.org/10.1016/j.chemgeo.2016.04.012

Willenbring, J.K., von Blanckenburg, F., 2010. Long-term stability of global erosion rates and weathering during late-Cenozoic cooling. Nature, 465(7295): 211-214. http://www.nature.com/nature/journal/v465/n7295/suppinfo/nature09044_S1.html

Williams, L.B., Hervig, R.L., 2005. Lithium and boron isotopes in illite-smectite: The importance of crystal size. Geochimica et Cosmochimica Acta, 69(24): 5705-5716. http://dx.doi.org/10.1016/j.gca.2005.08.005

Wilson, G.C., Long, J.V.P., 1983. The distribution of lithium in some Cornish minerals: ion microprobe measurements Mineralogical Magazine, 47: 191-199.

Wimpenny, J., Gislason, S.R., James, R.H., Gannoun, A., Pogge Von Strandmann, P.A.E., Burton, K.W., 2010a. The behaviour of Li and Mg isotopes during primary phase dissolution and secondary mineral formation in basalt. Geochimica et Cosmochimica Acta, 74(18): 5259-5279. 10.1016/j.gca.2010.06.028

Wimpenny, J., James, R.H., Burton, K.W., Gannoun, A., Mokadem, F., Gíslason, S.R., 2010b. Glacial effects on weathering processes: New insights from the elemental and lithium isotopic composition of West Greenland rivers. Earth and Planetary Science Letters, 290(3–4): 427-437. http://dx.doi.org/10.1016/j.epsl.2009.12.042

Wimpenny, J., Colla, C.A., Yu, P., Yin, Q.-Z., Rustad, J.R., Casey, W.H., 2015. Lithium isotope fractionation during uptake by gibbsite. Geochimica et Cosmochimica Acta, 168: 133-150.

Wu, L., Huh, Y., Qin, J., Du, G., van Der Lee, S., 2005. Chemical weathering in the Upper Huang He (Yellow River) draining the eastern Qinghai-Tibet Plateau. Geochimica et Cosmochimica Acta, 69(22): 5279-5294. http://dx.doi.org/10.1016/j.gca.2005.07.001

Wu, Y., Cui, Z., Liu, G., Ge, D., Yin, J., Xu, Q., Pang, Q., 2001. Quaternary geomorphological evolution of the Kunlun Pass area and uplift of the Qinghai-Xizang (Tibet) Plateau. Geomorphology 36, 203-216. doi http://dx.doi.org/10.1016/S0169-555X(00)00057-X

Wu, W., Xu, S., Yang, J., Yin, H., 2008a. Silicate weathering and CO2 consumption deduced from the seven Chinese rivers originating in the Qinghai-Tibet Plateau. Chemical Geology, 249(3–4): 307-320. https://doi.org/10.1016/j.chemgeo.2008.01.025

Wu, W., Yang, J., Xu, S., Yin, H., 2008. Geochemistry of the headwaters of the Yangtze River, Tongtian He and Jinsha Jiang: Silicate weathering and CO2 consumption. Applied Geochemistry, 23(12): 3712-3727.

Xu, H., Hou, Z.H., Ai, L., Tan, L.C., 2007. Precipitation at Lake Qinghai, NE Qinghai–Tibet Plateau, and its relation to Asian summer monsoons on decadal/interdecadal scales during the past 500 years. Palaeogeography, Palaeoclimatology, Palaeoecology 254, 541-549. doi 10.1016/j.palaeo.2007.07.007

Yao, T., Masson-Delmotte, V., Gao, J., Yu, W., Yang, X., Risi, C., Sturm, C., Werner, M., Zhao, H., He, Y., Ren, W., Tian, L., Shi, C., Hou, S., 2013. A review of climatic controls on $\delta18O$ in precipitation over the Tibetan Plateau: Observations and simulations. Reviews of Geophysics 51, 2012RG000427. doi 10.1002/rog.20023

Yin, A., Harrison, T.M., 2000. Geologic evolution of the Himalayan-Tibetan orogen. Annual Review of Earth and Planetary Sciences, 28: 211-280.

Yu, J., Gao, C., Cheng, A., Liu, Y., Zhang, L., He, X., 2013. Geomorphic, hydroclimatic and hydrothermal controls on the formation of lithium brine deposits in the Qaidam Basin, northern Tibetan Plateau, China. Ore Geology Reviews 50, 171-183. doi http://dx.doi.org/10.1016/j.oregeorev.2012.11.001

Zachos, J.C., Dickens, G.R., Zeebe, R.E., 2008. An early Cenozoic perspective on greenhouse warming and carbon-cycle dynamics. Nature, 451(7176): 279-283.

Zachos, J., Pagani, M., Sloan, L., Thomas, E., Billups, K., 2001. Trends, Rhythms, and Aberrations in Global Climate 65 Ma to Present. Science, 292(5517): 686-693. 10.1126/science.1059412

Zeebe, R.E., 2012. History of Seawater Carbonate Chemistry, Atmospheric CO2, and Ocean Acidification. Annual Review of Earth and Planetary Sciences, 40(1): 141-165. doi:10.1146/annurev-earth-042711-105521

Zeng, M., Song, Y., An, Z., Chang, H., Li, Y., 2014. Clay mineral records of the Erlangjian drill core sediments from the Lake Qinghai Basin, China. Science China Earth Sciences, 57(8): 1846-1859. 10.1007/s11430-013-4817-9

Zhang, C., Mischke, S., 2009. A Lateglacial and Holocene lake record from the Nianbaoyeze Mountains and inferences of lake, glacier and climate evolution on the eastern Tibetan Plateau. Quaternary Science Reviews, 28(19–20): 1970-1983. http://dx.doi.org/10.1016/j.quascirev.2009.03.007

Zhang, F., Jin, Z., Hu, G., Li, F., Shi, Y., 2009. Seasonally chemical weathering and CO2 consumption flux of Lake Qinghai river system in the northeastern Tibetan Plateau. Environmental Earth Sciences, 59(2): 297-313. 10.1007/s12665-009-0027-3

Zhang, F., Jin, Z., Li, F., Yu, J., Xiao, J., 2013. Controls on seasonal variations of silicate weathering and CO2 consumption in two river catchments on the NE Tibetan Plateau. Journal of Asian Earth Sciences, 62(0): 547-560. http://dx.doi.org/10.1016/j.jseaes.2012.11.004

Zhang, J., Quay, P.D., Wilbur, D.O., 1995. Carbon isotope fractionation during gas-water exchange and dissolution of CO2. Geochimica et Cosmochimica Acta 59, 107-114. doi http://dx.doi.org/10.1016/0016-7037(95)91550-D

Zhang, R., Jiang, D., Zhang, Z., Yu, E., 2015a. The impact of regional uplift of the Tibetan Plateau on the Asian monsoon climate. Palaeogeography, Palaeoclimatology, Palaeoecology, 417: 137-150. http://dx.doi.org/10.1016/j.palaeo.2014.10.030

Zhang, Y.F., Tan, H.B., Zhang, W.J., Huang, J.Z., Zhang, Q., 2015b. A new geochemical perspective on hydrochemical evolution of the Tibetan geothermal system. Geochemistry International, 53(12): 1090-1106. 10.1134/s0016702915120125

Zhao, P., Dor, J., Liang, T., Jin, J., Zhang, H., 1998. Characteristics of gas geochemistry in Yangbajing geothermal field, Tibet. Chinese Science Bulletin, 43(21): 1770-1777. 10.1007/bf02883369

Zhao, Y., Yu, Z., Chen, F., Ito, E., Zhao, C., 2007. Holocene vegetation and climate history at Hurleg Lake in the Qaidam Basin, northwest China. Review of Palaeobotany and Palynology, 145(3–4): 275-288. http://dx.doi.org/10.1016/j.revpalbo.2006.12.002

Zheng, H., Powell, C.M., An, Z., Zhou, J., Dong, G., 2000. Pliocene uplift of the northern Tibetan Plateau. Geology 28, 715-718. doi 10.1130/0091-7613(2000)28<715:puotnt>2.0.co;2

Zheng, M., 1997. An Introduction to Saline Lakes on the Qinghai—Tibet Plateau. Springer Netherlands.

Zhou, W.J., Donahue, D.J., Porter, S.C., Jull, T.A., Li, X.Q., Stuiver, M., An, Z.S., Matsumoto, E., Dong, G.G., 1996. Variability of monsoon climate in East Asia at the end of the last glaciation. Quaternary Research 46, 219-229.

CURRICULUM VITAE

For reasons of data protection,

the curriculum vitae is not included in the online version